

MOLDING, STRUCTURE AND MECHANICAL PROPERTIES
OF SHORT GLASS FIBER-REINFORCED THERMOPLASTIC COMPOSITES

by

© Shailesh R. Doshi

A thesis submitted to the Faculty of Graduate Studies and Research
in partial fulfillment of the requirements for the degree of
Master of Engineering.

Department of Chemical Engineering,
McGill University,
Montreal, Canada.

© March, 1983.

To, my Parents

ABSTRACT

This study is intended towards a better understanding of the structure - property relationships of short glass fiber-filled thermoplastic composites. A review of various approaches for predicting the elastic and ultimate properties of fiber composite materials is presented. The theories for predicting elastic properties are considered in greater details and used to examine the effect of two very important structural parameters, namely, fiber length distribution and non-homogeneous fiber orientation distribution on the overall composite properties. Moldings of short glass fiber-filled composites based on Polystyrene and Polyethylene matrices with varying fiber content were prepared so as to obtain a preferential fiber orientation in a given direction. The mechanical anisotropy of these systems is characterized by measuring various elastic and ultimate properties in both static and impact modes. Elastic properties are analyzed in terms of the theoretical model and a discussion of the structure and, in particular, the fiber orientation resulting from the flow of molten composites is presented.

RESUME

Cette étude vise à mieux comprendre les relations entre structure et propriétés pour des composites thermoplastiques à fibres de verre courtes. Une revue des différentes méthodes de prédiction des propriétés élastiques et à la rupture pour des composites à fibres est présentée. Les théories prédisant les propriétés élastiques sont considérées en plus grand détail et utilisées pour examiner l'effet de deux paramètres de structure importants soit la distribution de la longueur des fibres et la non-homogénéité de la distribution de l'orientation des fibres sur les propriétés globales des composites. Des moulages de composites à fibres de verre courtes basées sur des matrices de polystyrène ou de polyéthylène avec des taux de verre variables ont été préparés de façon à obtenir une orientation préférentielle dans une direction. L'anisotropie mécanique de ces systèmes est caractérisée par la mesure de plusieurs propriétés élastiques ou à la rupture en modes statiques ou dynamiques. Les propriétés élastiques sont analysées à la lumière du modèle théorique et une discussion de la structure et en particulier de l'orientation des fibres résultant de l'écoulement du composite fondu est présentée.

ACKNOWLEDGEMENTS

I wish to express my sincere gratitude to all the people and organizations who contributed to this study.

In particular, I am greatly indebted to my research director, Professor J.-M. Charrier, for his constant guidance and encouragement throughout the duration of this work.

In addition, I wish to sincerely thank:

- Mr. J. Dumont, for his excellent services and assistance;
- Mr. A. Krish and the staff of the Chemical Engineering machinshop for their help in the design and construction of some of the equipment parts and useful suggestions;
- Industrial Material Research Institute, National Research Council of Canada, notably Mr. F. Hamel for assistance in carrying out a majority of mechanical testing;
- Fiberglas Canada (Guelph, Ontario) and Fiberfil (Evansville, Indiana) for supplying the materials;
- Mr. T. Mutel for helpful discussions and Mr. K. Kant for his encouragement;
- Mrs. P. Hyland for her perseverance and conscientious efforts in typing this manuscript;

- National Research Council of Canada for financial support for the project;

- finally, all my friends and colleagues and the Department of Chemical Engineering, McGill University, for making my work an enjoyable and memorable experience.

LIST OF FIGURES

<u>Figure</u>	<u>Caption</u>	<u>Page No.</u>
4.1	Unidirectional Fiber Composite and its Elastic Constants.	40
4.2	Parallel Model for Unidirectional Composite with a Fiber Length Distribution. (a) Composite, (b) Element.	43
4.3	Series Model for Unidirectional Composite with a Fiber Length Distribution. (a) Elements in Series in L Direction, (b) Elements in Series in T Direction.	43
4.4	(a) Variation of E_L with Fiber Aspect Ratio for Monodisperse Systems ($V_f = 0.2$). (b) Variation of E_T with Fiber Aspect Ratio for Monodisperse Systems ($V_f = 0.2$).	49 50
4.5	Variation of \bar{E}_L and \bar{E}_T with V_f for Polydisperse Systems ($E_f/E_m = 100$, $(\bar{z}/d) = 30$).	53
4.6	(a) Variation of \bar{E}_L and \bar{E}_T with V_f for Polydisperse Systems ($E_f/E_m = 20$, $(\bar{z}/d) = 30$).	54
4.7	Systems used in Model for Elastic Moduli. (a) Unidirectional Composite. (b) Reference Direction at Angle θ to the Fiber Direction of Unidirectional Composite. (c) Symmetrical System with Equal Number of Fibers at $+\theta$ and $-\theta$.	56

<u>Figure</u>	<u>Caption</u>	<u>Page No.</u>
4.8	Non-homogeneous Structure in Molded Parts.	64
4.9	Variation of C_{ℓ} across the Thickness for Model.	64
4.10	Strain Distribution across the Cross-section in: (a) Flexure, (b) Tension.	64
4.11	Variation of \bar{E}_{ℓ} and \bar{E}_t across the Thickness for Variation of $C_{\ell} = 1$ to $C_{\ell M} = 2$ ($E_f/E_m = 50$, $V_f = 0.2$, $(\bar{z}/d) = 30$).	70
4.12	Variation of $(E^f/E^t)_{\ell}$ and $(E^f/E^t)_t$ with V_f for Variation of $C_{\ell} = 1$ to $C_{\ell M} = 2$.	72
5.1	A Half of the Premolding Device with a Premolding.	76
5.2	Assembled Premolding Device.	78
5.3	Premolding.	78
5.4	A Half of the Shearing Device.	80
5.5	Arrangement for Changing Gap Width in the Shearing Device.	81
5.6	Assembled Shearing Device.	82
5.7	Sheared Molding.	84
5.8	(a) Spring and Stopper Arrangement for Lower Piston.	85
	(b) Hydraulic Control System.	85

<u>Figure</u>	<u>Caption</u>	<u>Page No.</u>
5.9	Modified Lower Piston Assembly.	88.
5.10	"Equivalent Premolding" made in Shearing Device.	92
5.11	Three-Point Bending Test. (a) Schematic Diagram. (b) Three-point Bending Device.	99
5.12	(a) Pattern for Cutting Flexural Test-pieces from 1.6 mm (1/16 in.) Thick Plates. (b) Actual Dimensions of 1.6 mm (1/16 in.) Thick Flexural Test-pieces.	101 101
5.13	(a) Pattern for Cutting Flexural Test-pieces from 3.2 mm (1/8 in.) Thick Plates. (b) Actual Dimensions of 3.2 mm (1/8 in.) Thick Flexural Test-pieces.	102 102
5.14	Schematic Diagram of Tensile Modulus Measurement.	107
5.15	Actual Dimensions of Tensile Modulus Test-pieces.	107
5.16	Schematic Diagram showing Machining of Dumbbell Shaped Test-pieces. (a) Top View. (b) Side View.	108

<u>Figure</u>	<u>Caption</u>	<u>Page No.</u>
5.17	(a) Actual Dimensions of 1.6 mm (1/16 in.) Thick Tensile Strength Test-pieces.	110
	(b) 1.6 mm (1/16 in.) Thick Tensile Strength Test-piece held in Grips.	110
5.18	Typical Load-Deflection Curves.	112
5.19	Schematic Diagram of Izod Impact Testing.	114
5.20	(a) Pattern of Cutting Test-pieces for Izod-type Testing.	115
	(b) Actual Dimensions of Izod-type Impact Test-pieces.	115
5.21	(a) Holding the Test-piece in Standard Izod Impact Test.	116
	(b) Schematic Diagram of Izod-type Test carried out in this Study.	116
5.22	(a) Actual Dimensions of Tensile Impact Test-piece.	118
	(b) Break under Tensile Impact at the End.	118
	(c) Modified Tensile Impact Test-piece.	118
5.23	Schematic Diagrams of Tensile Impact Testing.	119
	(a) View along Pendulum Arm.	
	(b) Holding the Test-piece.	
6.1	Variation of Flexural Moduli of PS Composites with Fiber Content. (a) 1.6 mm Thickness,	124
	(b) 3.2 mm Thickness.	

<u>Figure</u>	<u>Caption</u>	<u>Page No.</u>
6.2	Identification of Specimen Location for Table (6.2).	125
6.3	Variation of Flexural Moduli of PE Composites with Fiber Content. (a) 1.6 mm Thickness, (b) 3.2 mm Thickness.	130
6.4	Variation of Tensile Moduli with Fiber Content. (a) PS Composites, (b) PE Composites.	134
6.5	Variation of Tensile Strengths of PS Composites with Fiber Content. (a) 1.6 mm Thickness, (b) 3.2 mm Thickness.	137
6.6	Variation of Tensile Strengths of PE Composites with Fiber Content. (a) 1.6 mm Thickness, (b) 3.2 mm Thickness.	140
6.7	Variation of Izod-type Impact Energies of PS Composites with Fiber Content. (a) 1.6 mm Thickness, (b) 3.2 mm Thickness.	144
6.8	Variation of Izod-type Impact Energies of PE Composites with Fiber Content. (a) 1.6 mm Thickness, (b) 3.2 mm Thickness.	146
6.9	Variation of Tensile Impact Energies of PS Composites with Fiber Content. (a) 1.6 mm Thickness, (b) 3.2 mm Thickness.	149
6.10	Variation of Tensile Impact Energies of PE Composites with Fiber Content. (a) 1.6 mm Thickness, (b) 3.2 mm Thickness.	151

<u>Figure</u>	<u>Caption</u>	<u>Page No.</u>
6.11	Comparison of Experimental Results with Theoretical Predictions for PS Composites. (a) PS + 20% (wt.) Fibers. (b) PS + 40% (wt.) Fibers.	158
6.12	Comparison of Experimental Results with Theoretical Predictions for PE Composites. (a) PE + 20% (wt.) Fibers. (b) PE + 30% (wt.) Fibers.	162
6.13	Velocity Profiles for Poiseuille Flow in a Slit (Schematic). (a) For Less Viscous Material (PE). (b) For More Viscous Material (PS).	167
B.1	Cross-head Bounce Correction Factor for Tensile Impact Testing.	B.4

LIST OF TABLES

<u>Table</u>	<u>Caption</u>	<u>Page No.</u>
4.1	Values of Parameters used in Computations for Studying the Effect of Fiber Length on Composite Moduli.	47
4.2	Comparison of the Results obtained by Different Methods of Summation.	52
4.3	Values of Parameters used in Computations of Overall Moduli of Composites with Non-homogeneous Orientation Distribution.	69
4.4	Values of C_{LM} used in Computations of Section 4.3.	69
4.5	Comparison of Ratios $(E^f/E^t)_l$ and $(E^f/E^t)_t$ for Various Values of C_{LM} for $V_f = 0.2$.	73
5.1	Details on Matrix Materials.	97
5.2	Slopes of Load versus Deflection Curves for Deflection of Three-Point Bending Devices. (a) 25 mm Span, (b) 50 mm Span.	105
6.1	Flexural Moduli for Test-pieces cut from a given 1.6 mm thick PS Plate. (a) Longitudinal, (b) Transverse.	125
6.2	Flexural Moduli for Test-pieces cut from Plates made from a given Pair of Reservoir Blocks. (a) Longitudinal, (b) Transverse.	127

<u>Table</u>	<u>Caption</u>	<u>Page No.</u>
6.3	Mean Flexural Moduli of PS Composites.	128
6.4	Mean Flexural Moduli of PE Composites.	131
6.5	Tensile Moduli of PS Composites.	135
6.6	Tensile Moduli of PE Composites.	135
6.7	Mean Tensile Strengths of PS Composites.	138
6.8	Mean Tensile Strengths of PE Composites.	141
6.9	Mean Izod-type Impact Energies of PS Composites.	147
6.10	Mean Izod-type Impact Energies of PE Composites.	147
6.11	Mean Tensile Impact Energies of PS Composites.	152
6.12	Mean Tensile Impact Energies of PE Composites.	152
6.13	Values of various Parameters used in the Theoretical Analysis of the Experimental Results. (a) PS Composites, (b) PE Composites.	156
6.14	Values of C_2 and (\bar{z}/d) for PS Composites.	160
6.15	Values of C_2 and (\bar{z}/d) for PE Composites.	165

TABLE OF CONTENTS

	<u>Page</u>
ABSTRACT	i
RESUME	ii
ACKNOWLEDGEMENTS	iii
LIST OF FIGURES	v
LIST OF TABLES	xi
TABLE OF CONTENTS	xiii
CHAPTER I	INTRODUCTION
	1
1.1	Definition of Composite Materials
	1
1.2	Short Fiber-Reinforced Thermoplastics
	2
1.2.1	Structure of SF RTP
	3
1.2.1.1	Fiber Content
	3
1.2.1.2	Fiber Dimensions
	4
1.2.1.3	Fiber Arrangement
	5
1.2.1.4	Fiber-Matrix Interface
	6
1.2.1.5	Aggregates and Voids
	6
1.2.2	Effect of Processing on Structural Parameters
	6
CHAPTER II	REVIEW OF LITERATURE
	8
2.1	Prediction of Mechanical Properties of SF RTP Materials
	8
2.1.1	Composite Stiffness Prediction
	9
2.1.2	Composite Strength Prediction
	20
2.2	Experimental Studies on Structure- Processing Relationships
	27
2.3	Some Aspects of Testing of Composite Materials
	29
CHAPTER III	SCOPE AND PROJECT OBJECTIVES
	32
3.1	Review of Previous Studies in the Group
	32
3.2	Project Objectives
	34
3.2.1	Theoretical
	34
3.2.2	Experimental
	35

		<u>Page</u>
CHAPTER	IV	THEORETICAL STUDY ON STRUCTURE - PROPERTY RELATIONSHIPS
		37
	4.1	Unidirectional Composites with Fiber Length Distribution
		38
	4.1.1	Fiber Length Distribution Function
		38
	4.1.2	Relations for Elastic Constants of Unidirectional Composites
		39
	4.1.3	Moduli of Unidirectional Composites with a Fiber Length Distribution
		42
	4.1.4	Results of Computations and Discussion
		46
	4.2	Review of Model for Evaluating Elastic Constants of Composite with Fiber Orientation Distribution
		55
	4.3	Elastic Constants of Composite with Non-Uniform Fiber Orientation Distri- bution Across Thickness
		62
	4.3.1	Model for Non-Uniform Fiber Orientation Distribution
		63
	4.3.2	Results and Discussion
		68
CHAPTER	V	EXPERIMENTAL PROGRAMME
		74
	5.1	Molding Operation
		75
	5.1.1	Review of the Procedure used by Previous Researchers
		75
	5.1.1.1	Premolding Device
		75
	5.1.1.2	Shearing Device
		77
	5.1.2	Modifications of Shearing Device and Molding Procedure
		86
	5.1.2.1	Modification in Lower Piston Assembly
		86
	5.1.2.1.1	Reasons for Modification
		87
	5.1.2.1.2	Operation of Modified Lower Piston Assembly
		87
	5.1.2.2	Modification in Molding Procedure
		89
	5.1.2.2.1	Reasons for Modification
		89
	5.1.2.2.2	Modified Procedure
		90
	5.2	Materials Used
		95
	5.3	Testing Procedures
		98
	5.3.1	Flexural Modulus
		98
	5.3.2	Tensile Modulus
		106
	5.3.3	Tensile Strength
		109
	5.3.4	Izod Impact Strength
		111
	5.3.5	Tensile Impact Strength
		117

			<u>Page</u>
CHAPTER	VI	EXPERIMENTAL RESULTS	122
	6.1	Results of Mechanical Testing	122
	6.1.1	Flexural Modulus	123
	6.1.2	Tensile Modulus	133
	6.1.3	Tensile Strength	136
	6.1.4	Izod Impact Strength	143
	6.1.5	Tensile Impact Strength	148
	6.2	Analysis of the Experimental Results in Terms of the Theoretical Predictions	153
CHAPTER	VII	CONCLUSION	169
	7.1	Suggestions for Future Work	171
APPENDIX	A		A.1
	A.1	Method of Incorporating Correction for Device Deflection in Three- Point Bending Test	A.1
	A.2	Deflection of Steel Bar used for Determining Correction Factor	A.2
APPENDIX	B	DETERMINATION OF CROSSHEAD BOUNCE CORRECTION FACTOR IN TENSILE IMPACT TESTING	B.1
APPENDIX	C	COMPUTER PROGRAMS USED FOR NUMERICAL CALCULATIONS	C.1
	C.1	Moduli for Unidirectional Composites with Log-normal Fiber Length Distribution	C.1
	C.2	Moduli for Composites with Non-homo- geneous Fiber Orientation Distribution	C.5
	C.3	Key to Major Symbols used in Com- puter Programs	C.10
NOMENCLATURE			N.1
REFERENCES			R.1

CHAPTER I

INTRODUCTION

With the advances in technology, the need for stiffer, stronger and tougher materials with longer life in adverse environments has also grown. Plastics have emerged as alternatives to metals in many respects as they are lighter and, largely through processing advantages, often cost less. They frequently, however, lack the necessary mechanical properties to be fully acceptable substitutes to metals in many mechanical applications. However, reinforcement of plastics by fibers or other inclusions can lead to mechanical properties comparable to those of metals. Since such composite materials can retain the advantages of ease of processing, lower cost and lower weight, they are gaining credibility as potential structural materials.

1.1 Definition of Composite Materials

In simple terms, a composite material can be defined as a combination of several distinct materials designed to enhance or modify a set of properties of one or several of the phases (Charrier (1)). One of the components forms a continuous phase and is called matrix; while the remaining components constitute discrete phases.

1.2 Short Fiber-Reinforced Thermoplastics

In the case of reinforced plastic composites, the polymer forms the continuous or matrix phase. The discrete phase may consist of short or continuous fibers of glass, graphite or metal or particles like mica, chalk or some other fillers (Titow and Lanham (2)).

The cheaper utility thermoplastics like Polyethylene, Polypropylene, Polystyrene, etc., when reinforced by short glass fibers can become valuable structural materials (Santrach (3)) with characteristics like:

- (1) higher modulus,
- (2) higher strength,
- (3) better heat resistance,
- (4) higher impact strength (brittle polymers),
- (5) better creep resistance,
- (6) lower cost / performance,
- (7) resin conservation,
- (8) higher surface hardness,
- (9) reduced thermal expansion,
- (10) reduced shrinkage.

However, properties of these short fiber reinforced thermoplastics (often referred to as SF RTP) are strongly dependent on many parameters. The main factors influencing the most common mechanical pro-

properties like stiffness and strength of the composite materials are:

- (1) type of polymer matrix,
- (2) type of fiber material,
- (3) fiber content of the composite,
- (4) fiber shape and dimensions,
- (5) spatial arrangement of fibers,
- (6) fiber-matrix adhesion and interface,
- (7) presence of aggregates and voids.

While the first two factors essentially represent the component properties of SF RTP, the remaining parameters may be referred to as structural parameters.

1.2.1 Structure of SF RTP

For a given composite system, the properties are essentially determined by the structural parameters and hence each of them needs a somewhat detailed discussion.

1.2.1.1 Fiber Content

Fiber content of the SF RTP material is the most important structural parameter. It is usually specified as the mass fraction M_f

of the fibers in the composite, the mass fraction of the polymer matrix being given by

$$M_m = 1 - M_f \quad (1.1)$$

However, for the theories of prediction of composite properties, it is more appropriate to represent the fiber content by volume fraction V_f (Charrier (1)). It is related to M_f in terms of fiber and matrix densities ρ_f and ρ_m respectively, as

$$V_f = \frac{M_f / \rho_f}{M_f / \rho_f + M_m / \rho_m} \quad (1.2)$$

In general, increasing the volume fraction of fibers increases composite stiffness and strength. However, these improvements can be achieved only up to a certain point. A very high fiber content can result into insufficient continuity in the matrix material resulting into poor bonding and hence a weaker material.

1.2.1.2 Fiber Dimensions

For the short glass fibers of finite length, the most important dimensions are fiber length z and diameter d . The aspect ratio, defined as the ratio of a major to a minor dimension of the particle (z / d in the case of short fibers), is often considered more appropriate for theoretical treatment than individual dimensions.

In general, stiffness and strength of the SFRTF increase with an increase in fiber aspect ratio, in a given direction. However, there is a complex interaction of several parameters that determine the composite properties and hence it is difficult to isolate the effect of a single parameter like aspect ratio.

1.2.1.3 Fiber Arrangement

The spatial arrangement of fibers in the composite is another important factor. The cylindrical particles like short glass fibers can be oriented in a random fashion so that the fraction of fibers lying parallel to any given direction is the same or they may be uniformly oriented so that all the fibers are perfectly aligned in a given direction. In fact, for a real composite, the fiber orientation can be anywhere between the random and the perfectly aligned cases.

The degree of orientation determines the degree of anisotropy in the composite properties. Since the fibers impart a much higher reinforcement in the direction of their axes than in the direction normal to their axes, composites with preferentially aligned fibers exhibit higher stiffness and strength in the direction of fiber alignment compared to the direction normal to it. On the other hand, a random composite will have equal degree of reinforcement in all directions and may be expected to be isotropic, on large scale.

1.2.1.4 Fiber-Matrix Interface

Fiber-matrix adhesion is not considered as important in the determination of SF RTP stiffness, as in the determination of composite strength. In general, better fiber-matrix adhesion is desirable for high strength.

1.2.1.5 Aggregates and Voids.

The agglomeration or bundling of fibers can have a strong effect on the mechanical properties. Most theories for predicting composite properties assume a uniform spatial distribution of individual particles. But in most cases, it is difficult to achieve in highly viscous non-Newtonian polymeric melts.

Presence of aggregates can result in measured properties that are higher or lower than those expected for the given fiber content depending on the mechanical strength of the aggregates themselves and test conditions.

Presence of voids and air bubbles in SF RTP usually result in a weaker material.

1.2.2 Effect of Processing on Structural Parameters

Though most of the processing techniques may not signifi-

cantly influence the properties of the individual components of SF RTP , the structural parameters are greatly affected.

SF RTP can be processed by a variety of common molding techniques, but injection molding remains the most attractive practice. During molding, the material is subjected to high stresses and flows through complex geometries. Both of these result into changes in fiber aspect ratio due to attrition and a complex fiber orientation distribution.

It is desirable to characterize the structural parameters of the molded SF RTP parts in order to be able to predict their properties at the molding stage. Since the resulting flow-induced structure necessarily determines the solid state properties, it is also desirable to study the flow behavior and the solid state mechanical behavior of SF RTP and correlate them in the hope of improving the processing techniques and fully extracting the advantages of short fiber reinforcement.

CHAPTER II

REVIEW OF LITERATURE

As has been seen in the Introduction, several parameters can influence the properties of fiber composite materials. A detailed review of various approaches for predicting the composite mechanical properties is presented in Section 2.1. This is followed by a review of the work directed towards experimental structural characterization and some aspects of mechanical testing of fiber composites in Sections 2.2 and 2.3 respectively.

2.1 Prediction of Mechanical Properties of SF RTP Materials

Stiffness and strength are often the most important properties required in the designing procedures. Hence, various approaches developed to model the mechanical behavior of fiber composites almost exclusively concentrate on predicting these two properties.

It must be pointed out that though the factors going into the determination of fiber reinforcement for stiffness and strength are superficially identical, their relative importance is not so due to the differences in the mechanism of reinforcement.

Composite stiffness essentially reflects sharing of the applied load between the discrete and continuous phases below the limit of

elasticity. Fiber-matrix interface and fiber length, beyond a certain value are of relatively minor importance. Strength determination, on the other hand, must identify a fracture mechanism and mode of stress transfer at the interface. Consequently, both the fiber-matrix adhesion and fiber length are of significant importance, of course, in addition to the fiber and matrix properties.

In the following, Section 2.1.1 concentrates on the composite stiffness while Section 2.1.2 concerns the composite strength.

2.1.1 Composite Stiffness Prediction

The simplest but rather crude approximation to the composite modulus E_c has been provided by the so-called "Law of Mixture" equation that represents an upper bound to the composite property in terms of fiber and matrix moduli E_f and E_m respectively and fiber volume fraction V_f (Ashton et. al. (4)). It is obtained by assuming equal strains in the two phases (parallel model)

$$E_c = (1 - V_f) E_m + V_f E_f \quad (2.1)$$

An assumption of equal stresses in the two components yields the lower bound (series model)

$$E_c = \left(\frac{1 - V_f}{E_m} + \frac{V_f}{E_f} \right)^{-1} \quad (2.2)$$

The first equation is closely valid for the perfectly aligned or unidirectional continuous fiber composites in the direction of fiber alignment.

Takayanagi et. al. (5) combined equations (2.1) and (2.2) to propose a two parameter series-parallel model

$$E_c = \left(\frac{\psi}{\chi E_m + (1 - \psi) E_f} + \frac{1 - \psi}{E_f} \right)^{-1} \quad (2.3)$$

where $1 - \psi \chi = V_f$.

The basic problem is to determine each of ψ and χ .

Weng and Sun (6) have used the concepts of series and parallel models to obtain the following equation for the unidirectional short fiber composites, in the fiber direction:

$$E_c = \frac{(1 + R)^2 V_f E_f}{1 + R \frac{E_f}{E_m}} + [1 - (1 + R) V_f] E_m \quad (2.4)$$

where R is a parameter characterizing the fiber length. E_c increases from the lower bound given by equation (2.2) to the upper bound represented by equation (2.1), as R decreases from V_m / V_f to zero.

A simple approach towards modifying equation (2.1) for short fiber-reinforced composites is to include a fiber length efficiency factor

η_l ,

$$E_c = (1 - V_f) E_m + \eta_1 V_f E_f \quad (2.5)$$

Cox (7), using shear-lag analysis for fiber-fiber transfer of the tensile stresses in the direction of their axes by shear, derived the following expression for η_1 ,

$$\eta_1 = 1 - \frac{\tanh(\beta z/2)}{(\beta z/2)} \quad (2.6)$$

where z is the fiber length
and β is related to the matrix shear modulus, fiber stiffness and system geometry.

η_1 is high for larger values of β , but approaches zero as $\beta z/2$ approaches zero.

A rigorous approach to predict the elastic constants has been provided by Hill's "self-consistent method" (8). This analysis models the composite as an inclusion embedded in an infinite homogeneous medium that is subjected to a uniform stress and the resulting strain field in the inclusion is solved to obtain the composite elastic constants. Halpin et. al. (9) reduced Herman's (10) solution of an equivalent approach to obtain the so-called "Halpin-Tsai equations",

$$\frac{p}{p_m} = \frac{1 + \epsilon_j \eta V_f}{1 - \eta V_f} \quad (2.7)$$

where

$$\eta = \frac{p_f/p_m - 1}{p_f/p_m + \epsilon_j}$$

In this equation, \bar{p} is a composite modulus, p_f and p_m are the corresponding fiber and matrix moduli respectively and ϵ_j depends on the reinforcement geometry and the loading conditions.

Nielsen (11) has modified these equations to account for the maximum filler packing fraction in terms of a parameter B as

$$\frac{\bar{p}}{p_m} = \frac{1 + \epsilon_j \cdot \eta \cdot V_f}{1 - \eta \cdot B \cdot V_f} \quad (2.8)$$

The self-consistent approach has also been used in a more rigorous manner to obtain the composite properties through numerical solutions (e.g., Chou et. al. (12)), but for sufficiently long fibers it has been shown that the semi-empirical solutions of Halpin and Tsai are reasonably close to the exact solutions.

Another form of relationships has been suggested by Puck and used by Manera (13). For the transverse Young's modulus, E_T ,

$$E_T = \frac{E_m}{1 - G_m^2} \cdot \frac{1 + 0.85 V_f^2}{(1 - V_f)^{1.25} + \frac{E_m}{E_f} \frac{V_f}{1 - G_m^2}} \quad (2.9)$$

where G_m is the matrix shear modulus. Manera has also suggested some simplifications to these equations which do not seem to be globally applicable.

It has been shown that the classical Rayleigh and Maxwell relationships for spherical and continuous fiber inclusions can be put into a generalized form and made applicable to a variety of composite properties including mechanical properties (Carrier (1)). The longitudinal and transverse elastic moduli, E_L and E_T respectively, for the case of the unidirectional short cylindrical inclusions of length z and diameter d are given as,

$$E_L = E_m \left[1 + \frac{(2 \frac{z}{d} + 1) (\frac{E_f}{E_m} - 1) V_f}{(\frac{E_f}{E_m} + 2 \frac{z}{d}) - (\frac{E_f}{E_m} - 1) V_f} \right] \quad (2.10a)$$

$$E_T = E_m \left[1 + \frac{(\frac{d}{z} + 2) (\frac{E_f}{E_m} - 1) V_f}{(\frac{E_f}{E_m} + 1 + \frac{d}{z}) - (\frac{E_f}{E_m} - 1) V_f} \right] \quad (2.10b)$$

Recently Chow (14) has derived a general theory for the elastic moduli of the fiber composite materials on the basis of Eshelby's

approach (15) of ellipsoidal inclusions at dilute concentration. He took into account particle-particle interaction for finite concentrations yielding for a unidirectional structure, equations of the type

$$E_L = E_m \left[1 + \frac{(k_f/k_m - 1) G_1 + 2(\mu_f/\mu_m - 1) K_1}{2K_1 G_3 - G_1 K_3} v_f \right] \quad (2.11)$$

where k and μ are the bulk and shear moduli respectively,

$$K_i = 1 + (k_f/k_m - 1)(1 - v_f) \alpha_i$$

$$G_i = 1 + (\mu_f/\mu_m - 1)(1 - v_f) \beta_i$$

and α_i and β_i are related to the fiber aspect ratio and the matrix Poisson's ratio.

Similar expressions have also been presented for transverse Young's, bulk and shear moduli.

Since the real composites have neither uniform fiber length nor uniform degree of orientation, it is desirable to incorporate the distribution of each of these parameters for a given system.

(a) Fiber Orientation

In a real composite, the fiber orientation can correspond to anywhere from a random to a unidirectional structure.

An early attempt to incorporate the effect of fiber misalignment has been reported by Cook (16), and Knibbs and Morris (17).

They suggested that for low angles of misorientation, an average angle of orientation should be sufficient to account for the orientation distribution.

Krenchel (18) proposed that the effect of fiber orientation can be taken into account by including a fiber orientation efficiency factor, η_0 , in the law of mixture equation (2.5)

$$E_L = (1 - V_f) E_m + \eta_0 \eta_1 V_f E_f \quad (2.12a)$$

where

$$\eta_0 = \sum_{k=1}^m a_k \cos^4 \theta_k \quad (2.12b)$$

a_k is fiber fraction at orientation angle θ_k with respect to the direction of symmetry, and

m is number of angle intervals into which fiber orientation distribution is divided.

This requires an experimental determination of the fiber orientation distribution.

Fukuda and Kawata (19) represented the fiber orientation distribution in terms of an arbitrary function $g(\theta)$. They calculated composite moduli for several mathematical forms of this function, but were unable to correlate any of them to the physical process of composite formation.

Several attempts have been made to correlate the fiber orientation distribution in SF RTP materials to the deformation involved in the process of making the composites, like molding or extrusion. The basis for these correlations is the affine deformation of the material.

Eisenberg (20) has presented an analysis of partial alignment of SF RTP during compression molding of an initially random composite. A similar analysis has been presented by Nicolais et. al. (21) for extrusion and drawing of SF RTP. Curtis et. al. (22) have also reported that the degree of fiber orientation in uniaxial extension of an initially random composite specimen can be described in terms of an extension ratio. A more complete analysis of this nature has been presented by Charrier and Tran (23) (also Sudlow (24)). Both two and three dimensional cases are considered. For the planar case, with an initially random composite,

$$dV(\theta) = \frac{d\theta}{\pi \left(\frac{\cos^2 \theta}{C_l^2} - C_l^2 \sin^2 \theta \right)} \quad (2.13)$$

represents the fraction of the fibers oriented in the interval $\theta \pm d\theta/2$ and C_l is an orientation parameter related to the degree of deformation.

For the spatial case,

$$dV(\theta, \phi) = \frac{d\theta d\phi}{2\pi \left(\frac{\cos^2 \theta}{C_l^2} - \frac{\sin^2 \theta \cos^2 \phi}{C_t^2} - C_l^2 C_t^2 \sin^2 \theta \sin^2 \phi \right)^{3/2}} \quad (2.14)$$

where $dV(\theta, \phi)$ is the fraction of the fibers oriented in the interval characterized by $\theta \pm d\theta/2$ and $\phi \pm d\phi/2$ and C_l and C_t are the orientation parameters.

(b) Fiber Length Distribution

In SF RTP, there is always a fiber length distribution that can be affected by processing. The simplest measure of fiber length is the mean or average length \bar{z} . This can be a weight-average or a number-average value. It should be noted that a large number of short fibers has a more significant effect on the number-average than the weight-average. Though it is not very clear as to which average should be considered more appropriate for use in the theoretical predictions, over-estimates might result for the weight-average.

Charrier et. al. (25) have shown that the actual fiber length distribution can be represented quite well by a log-normal distribution function $f(X)$ given as,

$$f(X) = \frac{1}{S_X \sqrt{2\pi}} \exp \left(- \frac{(X - \bar{X})^2}{2 S_X^2} \right) \quad (2.15)$$

where X is the natural logarithm of the fiber length, and \bar{X} and S_X are related to the mean and standard deviation of an experimentally determined fiber length distribution.

(c) Prediction of Composite Stiffness with Fiber Orientation and Length Distribution

Christensen and Waals (26) have presented a method for determining the moduli of fiber composites with planar and spatial random fiber orientations from those of the unidirectional composites transferred to the direction of loading ($E(\theta)$ or $E(\theta, \phi)$) as

$$\bar{E} = \int_0^{\pi} E(\theta) d\theta \quad \text{(planar)} \quad (2.16)$$

and

$$\bar{E} = \int_0^{\pi} \int_0^{\pi} E(\theta, \phi) d\theta d\phi \quad \text{(spatial)} \quad (2.17)$$

An analogous approach has been postulated by Halpin and Pagano (27) in their well-known laminate analogy. This treatment models a planar composite as being made up of several laminae each containing fibers in a given direction. For the random fiber composite, the fraction of fibers in any given direction is the same while for an oriented specimen the fraction of fibers in the direction of preference is higher.

Recently, this laminate analogy has been extended by Loughlin et. al. (28) to take into account the length distribution in addition to the orientation distribution. Here, each lamina with fibers in a given direction is further modelled as being made up of sub-laminae each containing fibers of a given aspect ratio. The lamina stiffness is given by summing up the sub-laminae stiffnesses weighted by an experimen-

tally determined fiber length distribution f_i ,

$$E_j^L = \sum_{i=1}^N E_i^{SL} f_i \quad (2.18)$$

where E_j^L is the stiffness of the j th lamina,

and E_i^{SL} is the stiffness of the sub-lamina with fiber aspect ratio corresponding to the i th interval.

The composite stiffness E_c is obtained by transferring the lamina stiffness E_j^L in the direction of loading (\bar{E}_j^L) and carrying out a summation weighted by an experimentally characterized fiber orientation distribution g_j ,

$$E_c = \sum \bar{E}_j^L g_j \quad (2.19)$$

A comparison with the experimental results of Darlington et. al. (29) showed a relatively small deviation.

The summing-up procedure over the composite elements - laminae or sub-laminae has been explored to a greater depth by Charrier et. al. (30). The authors point out that a parallel laminate model has been tacitly assumed by almost all the workers. However, a series model can represent an equivalent arrangement. The choice is unclear at least for a three dimensional arrangement and led them use a logarithmic addition

procedure yielding answers intermediate between those obtained by the series and parallel additions.

Composite properties have also been calculated by numerical solutions of the theory of elasticity (e.g., Cohen and Romualdi (31), Zybert et. al. (32)). However, certain simplifying assumptions appear to be unavoidable reducing the generality and global applicability of the solutions.

2.1.2 Composite Strength Prediction

Theoretical analysis of the composite strength has not been pursued as extensively as that of the elastic moduli (Hashin (33)). The basic reason is that any model for prediction requires a definition of a failure criteria. In case of the fiber composites, the mode of failure is not yet clearly understood. In case of the elastic moduli, the material undergoes a process throughout which phase stress-strain relationships and phase geometry do not change. While for strength, the process continues until the failure occurs, which implies fundamental changes in the material behavior. Since modes of failure can be different under different loading conditions, the material behavior under combined loading is also difficult to appreciate.

In analogy with the elastic moduli for unidirectional continuous fiber composites, the strength σ_c of the composite in the fiber

direction can be represented in terms of fiber strength σ_f and matrix strength σ_m by the "law of mixtures" equation,

$$\sigma_c = (1 - V_f) \sigma_m + V_f \sigma_f \quad (2.20)$$

For short fibers, a simple modification is the introduction of a length efficiency factor for strength, K_l ,

$$\sigma_c = (1 - V_f) \sigma_m + K_l V_f \sigma_f \quad (2.21)$$

The basis for the determination of the fiber length efficiency factor lies in the shear-lag analysis of Kelly and Tyson (34).

They suggested that the load applied to a composite is transferred from the matrix to the embedded particles by shear stresses along the interface. For a uniaxial tensile stress in the fiber direction, the force balance over the interface led to the equation:

$$\frac{\sigma_f}{z} = \frac{2\tau}{d} \quad (2.22)$$

where σ_f is the stress in the fiber

and τ is the shear stress along the fiber-matrix interface.

Near the fiber end, the shear stress is maximum and decreases along its length, while the tensile stress is zero near the ends and increases to a constant value along the length.

This has led to the concept of a critical fiber length z_c , which is defined as the minimum fiber length necessary for tensile stress in the fiber to reach the ultimate fiber strength σ_{fu} .

$$z_c = \frac{\sigma_{fu} d}{2\tau} = \frac{E_f \epsilon_c d}{2\tau} \quad (2.23)$$

where ϵ_c is the composite strain at break. Fibers with length smaller than z_c can never be loaded to their ultimate strength. The average tensile stress $\bar{\sigma}_f$ in a fiber with $z < z_c$ is given as

$$\bar{\sigma}_f = \frac{z\tau}{d} \quad (2.24a)$$

and that in a fiber with $z > z_c$ is given as

$$\bar{\sigma}_f = E_f \epsilon_c \left(1 - \frac{E_f \epsilon_c d}{4z\tau}\right) \quad (2.24b)$$

Extending these arguments, Bowyer and Bader (35) suggested that for any value of composite strain, there is a corresponding critical fiber length. For a composite containing a spectrum of fiber lengths, the fiber length efficiency factor can be represented as

$$K_l = \sum_i \tau \frac{z_i}{d} \frac{V_i}{V_f} + \sum_j \left(1 - \frac{E_f \epsilon_c d}{4z_j \tau}\right) \frac{V_j}{V_f} \quad (2.25)$$

where the first term represents the contribution of sub-critical and the second term represents that of supercritical fibers, V_i and V_j being the corresponding fiber volume fractions.

In the case of misaligned fibers an orientation factor K_0 can be incorporated, thus giving the composite strength as:

$$\sigma_c = K_0 \left[\sum_i \tau \frac{z_i}{d} V_i - \sum_j \left(1 - \frac{E_f \epsilon_c d}{4z_j \tau} \right) V_j \right] V_f + (1 - V_f) \epsilon_c E_m \quad (2.26)$$

The above model requires determination of the interfacial shear strength τ and the orientation parameter K_0 .

Bader and Bowyer (36) used stress-strain curve for a given sample along with the fiber length distribution data for determining τ and assumed that it is constant for all the composite strains up to failure.

The method of Ramsteiner and Theysohn (37) is based on a linear relationship between composite strength and fiber volume fraction for aligned fiber composites.

Recently, Gupta and Mittal (38) suggested that the interfacial shear strength, τ , cannot be assumed to be constant at all strains. Instead, they assumed τ to vary linearly with the applied load.

A more general treatment of the Shear-lag analysis has recently been presented by Chen and Sun (39). They determined the tensile

and shear stress distribution along the length of a short fiber embedded in a matrix phase subjected to uniaxial stress at an angle to fiber axis. The model does not consider fiber-fiber interaction, when in an actual case, the stress field around a fiber is significantly affected by neighboring fibers.

An important observation concerning the short fiber composite strength is the fact that unlike the stiffness, the strength does not asymptotically approach the value for the continuous fiber composite (Chen (40)). This has been recognized as a consequence of the stress concentration around the fiber ends (Barker and McLaughlin (41)). Based on Chen's experimental data, Halpin and Kardos (42) suggested the following empirical correlation for a strength reduction factor (SRF) :

$$\frac{(SRF) - (SRF)_0}{(SRF)_\infty - (SRF)_0} = 1 - \exp(-15\beta^{0.95}) \quad (2.27)$$

The factor β is the ratio of the actual to the critical fiber aspect ratio, $(SRF)_0$ and $(SRF)_\infty$ are strength reduction factors as the aspect ratio approaches unity and infinity, respectively. The generality of the equation parameters should be examined using a broad range of experimental data.

(a) Strength of Random Fiber Composites

Failure mechanism in a random fiber composite can be very different from that in an aligned fiber composite.

Lees (43) has suggested a method for predicting strength of random fiber composites using a failure model described by Jackson and Cratchley (44). Three failure mechanisms are considered and the corresponding composite strengths are given as:

- (1) Fiber failure in tension:

$$\sigma_c = \frac{\sigma_L}{\cos^2 \theta} \quad \text{for } 0 \leq \theta \leq \theta_1 \quad (2.28)$$

$$\text{where } \theta_1 = \tan^{-1} \frac{\sigma_L}{\tau}$$

- (2) Shear failure at interface:

$$\sigma_c = \frac{\tau}{\sin \theta \cos \theta} \quad \text{for } \theta_1 \leq \theta \leq \theta_2 \quad (2.29)$$

$$\text{where } \theta_2 = \tan^{-1} \frac{\sigma_T}{\tau}$$

- (3) Matrix failure in tension:

$$\sigma_c = \frac{\sigma_T}{\sin^2 \theta} \quad \text{for } \theta_2 \leq \theta \leq \pi / 2 \quad (2.30)$$

Here σ_L and σ_T are the longitudinal and transverse strengths of an equivalent unidirectional composite. Integration in the thickness direction from $\theta = 0$ to $\theta = \pi / 2$ led to the equation,

$$\sigma_c \text{ (random)} = \frac{2\tau}{\pi} \left(1 + \frac{\sigma_T}{\sigma_m} + \ln \frac{\sigma_T \sigma_m}{\tau^2} \right) \quad (2.31)$$

Chen (40) used a finite-element analysis for strength of unidirectional composite. Using this in conjunction with a method similar to that of Lees led to the following equation,

$$\sigma'_c \text{ (random)} = \frac{2\tau}{\pi} \left(1 + \ln \frac{\epsilon_j \sigma'_c \sigma_m}{\tau^2} \right) \quad (2.32)$$

where ϵ_j is a strength efficiency factor

and σ'_c is the composite strength according to the law of mixture equation (2.20).

(b) Strength of Composite with Fiber Orientation Distribution

Halpin and Kardos (42) have suggested a laminate analogy for the composite strength. A maximum strain theory of Petit and Wad-doup (45) has been employed to define a failure criterion of lamina and repetitive calculation procedure till all the laminae have failed yields the composite strength.

Loughlin et. al. (28) have used a similar approach but with a maximum stress criterion for composite failure.

In general, however, the status of the theory for the fiber composite strength is not as well developed as that for the stiffness.

2.2 Experimental Studies on Structure-Processing Relationships

It is clear that the properties of fiber composite materials are strongly dependent on the structure. Several investigations have been carried out for correlating the structure to the processing conditions.

The mass scale production techniques like injection molding involve flow of materials in complex geometries. Inclusion of fibers results in a melt structure that has significant influence on rheological characteristics (e.g., Chen et. al. (46), Chan et. al. (47)) which in turn influences fiber orientation. Theoretical studies on flow of suspensions with non-Newtonian matrices have not been very successful, (Leal (48)) and hence it becomes essential to revert to the experimental observations.

One of the earlier studies on the orientation of short fiber composites has been reported by Bell (49). He observed that in circular converging channels, the fibers tended to get aligned in the direction of flow, however no further orientation could be achieved along the channel length. Also, the angle of convergence of the channel did not have a significant influence on the degree of fiber alignment.

Lee and George (50) have further confirmed Bell's observations in their flow visualization experiments. They concluded that the extensional flow in the vicinity of convergent section plays a dominant role in aligning the fibers.

Takano (51), using convergent flat plate rectangular channels, observed that fiber orientation is strongly dependent on resin viscosity, fiber loading, angle of convergence and flow rate.

A quantitative characterization of the experimentally observed flow induced orientation has been attempted by Goettler (52). Using a variety of flow geometries in transfer molding experiments, he concluded that strong fiber alignment occurred during the convergent flow in the runner at the entrance and also by shear along its length. Higher viscosity and low flow rates tended to preserve this orientation at the mold surface while the core had transversely oriented fibers due to divergent decelerating flow from the gate to the mold cavity.

The main problem associated with the quantitative characterization of the fiber length and orientation distribution has been the visualization of 10 μm diameter fibers less than 1 mm in length. Fuccella (53) has reviewed various simple techniques for characterization of the fiber orientation distribution. Charrier et. al. (23) have used sectioning and metallographic polishing techniques. On reviewing various methods, Darlington et. al. (54) concluded that the Contact Microradiography [CMR] was the most promising method.

Using CMR technique, Bright and Darlington (55) found that both matrix characteristics and molding conditions can have a significant influence on the fiber orientation in the injection molded parts.

Various mold geometries and gate types suggested that usually the injection molded parts consist of a partially transversely oriented core surrounded by random or partially aligned skins. The relative thickness, which determines the overall degree of anisotropy of the cross-section is dependent on the injection speed, rheological characteristics of matrix and part thickness (Bright et. al. (56), Folkes (57)).

Recently, Xavier et. al. (58) reported that, in addition, injection pressure and temperature can also influence the relative core to skin thickness and hence mechanical properties.

2.3 Some Aspects of Testing of Composite Materials

The methods of testing homogeneous, isotropic materials are not satisfactory for fiber reinforced composites because of their anisotropic nature. For the most common properties of tensile modulus and strength, end-gated injection molded dumbbell shaped bars have been used (Titow and Lanham (2)). However, it has been verified that results may prove misleading due to preferential fiber alignment.

Dunn and Turner (59) have suggested the use of three types of specimens:

- (i) injection molded ASTM bar (69),
- (ii) specimens cut from injection molded edge-gated circular discs, both in the direction of flow and direction normal to it,

- (iii) specimens cut from injection molded flush-gated square plaques in directions at various angles to the major flow direction.

Results indicated that the ASTM bars corresponded to a strong "along-flow" orientation while the disc showed a relatively weak "cross-flow" orientation. For thin plaques, the property deteriorated as the angle between the direction of testing and that of the flow increased. It should, however, be remembered that the injection molded specimens may result in a skin and core structure, the relative thicknesses of which are strongly dependent on several parameters. It is not uncommon to find for a given gate type and flow geometry that the direction of overall reinforcement can change from the flow direction to the transverse direction (Bright et. al. (55)).

Taggart and Pipes (60) have also pointed out that standard test methods cannot account for the heterogeneous fiber orientation distribution resulting from mold flow conditions. They attributed failures in the gripping region of tensile specimen and excessive flexural strength measurements in their testing to such non-homogenities. They concluded that standard ASTM test methods could not be employed for quality control, specification values or component design.

Stephenson et. al. (61) have suggested testing of the entire molded plaques instead of cut-specimens to give gross scale average properties which can prove more appropriate for use in the designing applications.

It appears that universal testing procedures are yet to be developed. The best way to characterize the composite properties would be to measure them for each gate type, flow geometry and specimen thickness for a given resin-fiber system. However, this would prove both time consuming and expensive.

CHAPTER III

SCOPE AND PROJECT OBJECTIVES

This project is a part of a comprehensive programme for studying the processing-structure-property relationships of polymer based composite materials.

3.1 Review of Previous Studies in the Group

The essential aim of the programme is to understand the processing characteristics of composite materials, analyze the structure of the resulting products and determine their properties. The resulting knowledge of inter-relationship of these three factors can be of considerable importance in the optimization of the process itself as well as product properties.

As one of the phases of the programme, study of short glass fiber-reinforced thermoplastics has been undertaken. The research has been carried out along two directions: rheological characterization in molten state and mechanical and structural characterization in solid state, with an aim to ultimately correlate the results (Charrier and Skatchkov (62)).

For rheological studies, a special piston and channel type rheometer has been designed and built (Tran (63)), Padmanabhan (64)).

The rheometer is used in conjunction with an Instron tester as a drive mechanism to obtain an adjustable flow rate and hence the shear rate. Channels are of two types: circular cross-section and thin rectangular cross-section, with variable diameters or thicknesses and lengths. This rheometer has been used to obtain flow data for a variety of glass fiber-thermoplastic systems (Chan et. al. (47, 65)).

For studies of mechanical properties in solid state, two molding devices have been designed and built to produce plates of desired thickness and a fiber orientation that can be either random ("random" plates) or preferential in a given direction ("oriented" plates). The "random" plates are made by a compression molding device that allows application of positive pressure on the material during cooling so as to minimize the inclusion of voids (Pouliot (66)). The "oriented" plates are made using the so-called "preforming" and "shearing" devices in conjunction. Details on their mode of operation are provided in Chapter V.

§ Test pieces could be cut from these molded plates, so as to test them for mechanical properties. The essential properties of interest, till now had been elastic moduli in flexion and tension and static tensile strength.

For structural characterization, reliable techniques for the determination of involved parameters, viz., fiber content, fiber length distribution and fiber orientation distribution have been developed

(Tran (63), Padmanabhan (64)). These distributions have also been mathematically expressed for their ready incorporation in a theoretical correlation (Charrier et. al. (25)).

Attempts directed towards theoretically studying the solid state mechanical behavior of composite materials have resulted in the development of a model for predicting elastic properties of composite materials. This procedure has been reviewed in Chapter IV .

3.2 Project Objectives

The present work is intended mainly as a contribution towards the development of a comprehensive experimental method for generating data on mechanical properties of composite materials for use in the assessment of the structure-property relationships (Charrier and Doshi (67)).

Specific objectives can be divided in two classes, theoretical and experimental, with a major emphasis on the experimental work.

3.2.1 Theoretical

Theoretical objective was to consider relatively simple theories for prediction of mechanical properties of composite materials.

The essential aim was to extend further the model built up so far as a step towards the development of a realistic theory for the global prediction of composite properties. It was decided to consider the theories for elastic properties in some depth and just review those for ultimate properties (cf. Chapter II). This review can be of importance in further studies for developing a generalized method of prediction.

3.2.2 Experimental

The experimental objectives were:

- (1) To mold plates of selected composite systems with preferential fiber orientation.
- (2) To carry out mechanical testing for chosen properties.

First of all, it was necessary to mold plates of selected short fiber - thermoplastic composite systems. Options were either to use the injection molding procedure or the shearing device. It was decided to use the shearing device because it offered a simple flow geometry so as to minimize fiber degradation. Furthermore, it allowed an isothermal operation that could result in a more uniform structure, that is homogeneous on a large scale, as against that of an injection molded specimen (Darlington et. al. (29)).

The molded plates were to be tested for various mechanical properties for characterization of anisotropy induced by the fibers. Though previous studies emphasized only static properties (modulus and strength) (Sudlow (24), Pouliot (66)), for this project, it was decided to study the impact behavior of molded plates in addition to the properties measured at low rates.

CHAPTER IVTHEORETICAL STUDY ON STRUCTURE-PROPERTY RELATIONSHIPS

In spite of the technological importance of the SFRTIP materials, a perfect and realistic theory of composite properties remains to be developed. Complications arise due to multitude of parameters, their individual variations and complex interactions. The essential structural parameters for a given system are fiber length and fiber orientation.

Results presented in this chapter attempt to quantitatively explain the influence of these parameters on composite properties. Section 4.1 deals with the influence of fiber length distribution on composite stiffness for the special case of unidirectional fiber composites. Section 4.2 presents a review of the model developed by the group for predicting composite elastic moduli and referred to in Chapter III. Finally, Section 4.3 uses this procedure for a case of non-uniform fiber orientation distribution.

It must be pointed out that the theoretical work reported in this chapter is viewed as a forward but not the final step in developing a realistic theory for predicting the composite properties for given processing conditions. Consequently it was not considered worthwhile to attempt a detailed comparison of the experimental results with those predicted by the theory at this stage. The theory is used to throw light on the general behavior of model composite systems.

4.1 Unidirectional Composites with Fiber Length Distribution

Fiber degradation during processing and handling leads to a length distribution, and an average length concept may not give a realistic representation. Hence, it is desirable to mathematically express the fiber length distribution and incorporate it in the prediction procedure.

4.1.1 Fiber Length Distribution Function

Fiber length measurements in molded parts after burning off resin has shown that the length distribution can be reasonably well represented by the following log-normal distribution function (Tran (63) and Padmanabhan (64))

$$f(z) = \frac{1}{S_X \sqrt{2\pi}} \exp \left(- \frac{(\ln z - \bar{X})^2}{2 S_X^2} \right) \quad (4.1)$$

where $f(z)$ represents the frequency corresponding to length z and $f(z) dz$ represents the fraction of fibers in the interval $z \pm dz / 2$. The equation has two parameters, \bar{X} and S_X . \bar{X} is the average of $\ln z$ and S_X is the standard deviation of $\ln z$. \bar{X} and S_X are related to measured average fiber length \bar{z} and standard deviation s_z as

$$\bar{X} = \ln \left[\frac{\bar{z}}{\left(1 + \frac{s_z^2}{\bar{z}^2}\right)^{1/2}} \right] \quad (4.2)$$

and

$$S_X = \left[\ln \left(1 + \left(\frac{S_Z}{\bar{Z}} \right)^2 \right) \right]^{1/2} \quad (4.3)$$

\bar{z} and s_z can be readily obtained from experimental data on fiber length measurements, \bar{X} and S_X can then be calculated using equations (4.2) and (4.3) and the corresponding log-normal distribution function can then be generated using equation (4.1).

4.1.2 Relationships for Elastic Constants of Unidirectional Composites

Fiber reinforced composites can be highly anisotropic in nature and require more than two independent material elastic constants for describing their mechanical behavior. A completely anisotropic material (one with no planes of symmetry) under three dimensional state of stress would require 36 elastic constants. However, some simplification is possible when symmetries exist such as in the case of unidirectional or aligned fiber composites.

A unidirectional fiber composite is the one in which all the fibers are aligned in a given direction. (See Figure (4.1)). Such a material is orthotropic, that is, it has three mutually perpendicular planes of symmetry. Furthermore, if one can assume that the material is homogeneous on large scale, then for a two-dimensional state of stress in the plane represented in Figure (4.1) (quite representative for plastic components) one requires only four elastic constants, namely the Young's moduli E_L

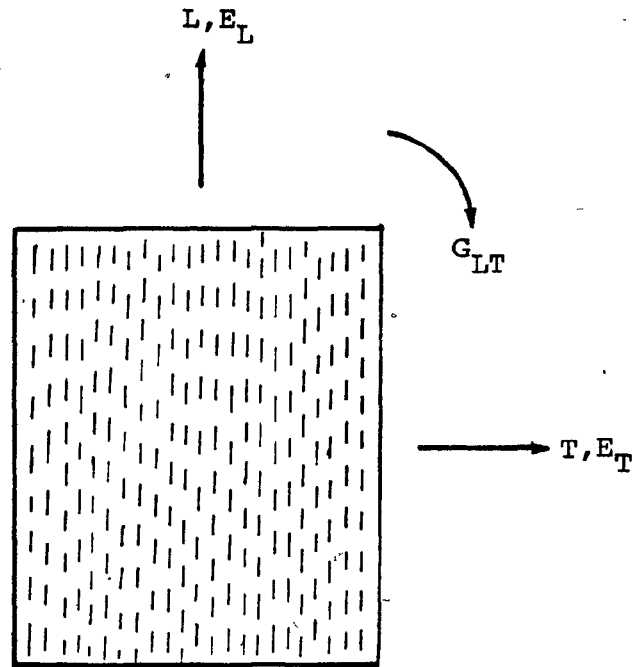


Figure (4.1). Unidirectional Fiber Composite and its Elastic Constants.

and E_T in the direction of fiber orientation L and transverse direction T , the shear modulus G_{LT} for stresses in the plane of the figure and Poisson's ratio μ_{LT} , for the constitutive relationships.

As has been reviewed in Chapter II, there are several relationships proposed to relate composite properties to component properties. However, for our purpose, it is essential to have a relationship that incorporates fiber aspect ratio as a parameter. Rayleigh-Maxwell relationships in their generalized form have been used in this study (Charrier (1)). Three of the four composite elastic constants are thus given as

$$E_L = E_m \left[1 + \frac{(2 \frac{z}{d} + 1) (\frac{E_f}{E_m} - 1) V_f}{(\frac{E_f}{E_m} + 2 \frac{z}{d}) - (\frac{E_f}{E_m} - 1) V_f} \right] \quad (2.10a)$$

$$E_T = E_m \left[1 + \frac{(\frac{d}{z} + 2) (\frac{E_f}{E_m} - 1) V_f}{(\frac{E_f}{E_m} + 1 + \frac{d}{z}) - (\frac{E_f}{E_m} - 1) V_f} \right] \quad (2.10b)$$

$$G_{LT} = G_m \left[1 + \frac{(\frac{d}{z} + 2) (\frac{G_f}{G_m} - 1) V_f}{(\frac{G_f}{G_m} + 1 + \frac{d}{z}) - (\frac{G_f}{G_m} - 1) V_f} \right] \quad (4.4)$$

G_f and G_m being the fiber and matrix shear moduli in equation (4.4).

The fourth elastic constant μ_{LT} is most commonly expressed in terms of the fiber and matrix Poisson's ratios μ_f and μ_m respectively through the law of mixture equation,

$$\mu_{LT} = (1 - V_f) \mu_m + V_f \mu_f \quad (4.5)$$

The anisotropy of the unidirectional composites is easily reflected in the values of E_L and E_T , and hence the subsequent discussion is confined to these two elastic constants.

4.1.3 Moduli of Unidirectional Composites with a Fiber Length Distribution

In a composite with fiber length distribution, fibers of various aspect ratios are distributed in a random manner and mixed intimately. In order to predict the overall moduli, it is convenient to model the composites as being made up of several elements each containing fibers of a given aspect ratio.

Several equivalent approaches can be considered. In the "parallel approach", the different elements with fibers of different aspect ratios are assumed to be arranged in parallel like laminates as shown in Figure (4.2a). Each layer contains fibers of a given length z . The volume fraction of the fibers in each layer is uniform and equal to the overall fiber volume fraction in the composite, however, the thickness of each layer is proportional to the fraction of the fibers of length z , i.e., $f(z) \Delta z$.

Since each layer has aligned fibers of a given specific length, the elastic constants $E_L(z)$ and $E_T(z)$ for the layer can be

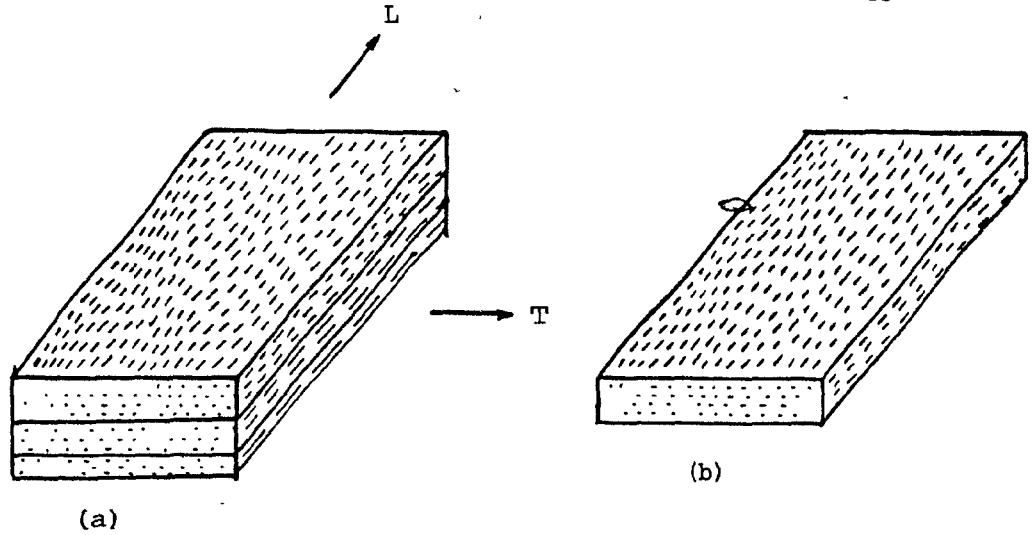


Figure (4.2). Parallel Model for Unidirectional Composite with a Fiber Length Distribution.
(a) Composite, (b) Element.

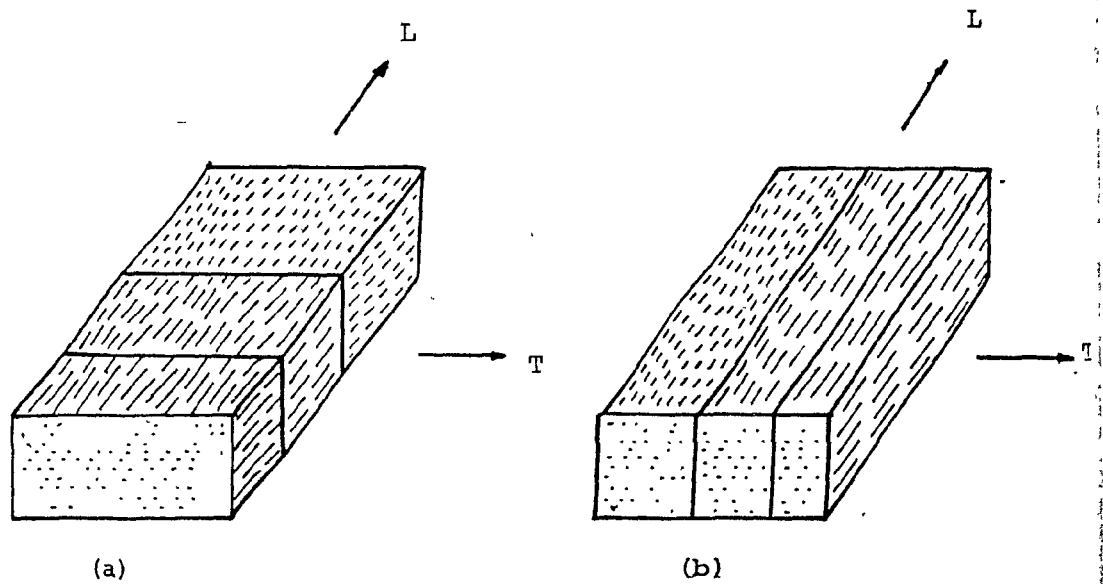


Figure (4.3). Series Models for Unidirectional Composite in
(a) L Direction, (b) T Direction.

determined by the direct application of equations (2.10a) and (2.10b).

The overall composite moduli \bar{E}_L and \bar{E}_T can be determined as follows. Since the various layers are sharing the load in parallel in either L or T direction, the strains in all the layers are equal if one assumes perfect bonding between them. The composite stress on the other hand is equal to the sum of the stresses in the individual layers.

$$\bar{E}_L \epsilon_L = \sum E_L(z) \epsilon_L f(z) \Delta z \quad (4.6)$$

where ϵ_L is the composite or layer strain. Hence

$$\bar{E}_L = \sum E_L(z) f(z) \Delta z \quad (4.7)$$

For a continuous fiber length distribution described, for instance, by the log-normal distribution function, the summation sign can be replaced by an integral sign,

$$\bar{E}_L = \int_0^{\infty} E_L(z) f(z) dz \quad (4.8)$$

and for the T direction, the corresponding equation is

$$\bar{E}_T = \int_0^{\infty} E_T(z) f(z) dz \quad (4.9)$$

However, an alternative approach can be to consider the arrangement shown in Figure (4.3a). Here various elements are in series with each other and hence this is referred as the "series model". For this case, the length of each serial segment is proportional to the fraction of fibers of the corresponding length z , i.e., $f(z) \Delta z$. For the load applied in the direction of fiber orientation, the stresses in various elements are equal, while the composite strain is given by sum of the elemental strains.

$$\frac{\sigma_L}{E_L} = \sum \frac{\sigma_L}{E_L(z)} f(z) \Delta z \quad (4.10)$$

where σ_L is the composite or elemental stress in the fiber direction.

Hence

$$\frac{1}{E_L} = \sum \frac{1}{E_L(z)} f(z) \Delta z \quad (4.11)$$

Again for a continuous distribution, the summation sign can be replaced by an integral sign giving,

$$\frac{1}{E_L} = \int_0^{\infty} \frac{1}{E_L(z)} f(z) dz \quad (4.12)$$

Also, a similar situation arises for the T direction if one considers the arrangement shown in Figure (4.3b), giving

$$\frac{1}{\bar{E}_T} = \int_0^{\infty} \frac{1}{E_T(z)} f(z) dz \quad (4.13)$$

There does not seem to be strong logic in selecting the parallel arrangement in preference to the series model or vice versa, particularly, for a system with fibers of different aspect ratios mixed intimately. Hence a logarithmic summation procedure given by

$$\ln \bar{E}_L = \int_0^{\infty} \ln E_L(z) f(z) dz \quad (4.14)$$

and

$$\ln \bar{E}_T = \int_0^{\infty} \ln E_T(z) f(z) dz \quad (4.15)$$

providing answers intermediate between those given by the above two approaches was considered (Charrier and Sudlow (30)) for getting overall composite moduli.

4.1.4 Results of Computations and Discussion

The main objective here was to study the effect of considering a fiber length distribution as against assuming a uniform length represented by an average value on the predictions of SFRTIP moduli.

Table (4.1) shows the specific values of E_m , E_f , S_z and (\bar{z}/d) used in this study. Values of E_m were chosen to cover the range

TABLE (4.1)

VALUES OF PARAMETERS USED IN COMPUTATIONS
FOR STUDYING THE EFFECT OF FIBER LENGTH ON COMPOSITE MODULI

PARAMETER	VALUE OR RANGE OF VALUES
E_f	68.9 GPa (10^7 psi)
E_m	0.689 - 3.445 GPa (1×10^5 - 5×10^5 psi)
S_z (polydisperse)	0.25 , 0.45
(\bar{z}/d)	30
V_f	0 - 1

of properties of the utility thermoplastic matrices, while values of s_z and (\bar{z}/d) were chosen to represent typical fiber length distributions found in extruded or injection molded parts (Tran (63), Padmanabhan (64)). Computations were done for $V_f = 0$ to $V_f = 1$ for the sake of completeness, though for a real SFRTF, V_f would seldom exceed 0.3.

Figures (4.4a and b) show the variations of E_L and E_T for composites with uniform fiber aspect ratio ("monodisperse") as the latter increases for various values of E_f / E_m and $V_f = 0.2$. Both E 's are reduced by E_m , the moduli that would correspond to composites with infinitely long fibers ($z/d = \infty$). It is seen that the effect of aspect ratio on E_T is insignificant, while in the L direction, the reinforcement efficiency of the fibers increases rapidly with (z/d) . However, this increase is dependent on the matrix and fiber properties. For soft matrices, the increase in E_L is much slower than for stiffer matrices. Hence for a composite with a stiff matrix, the fiber length may not be of significant importance, provided most of the fibers are above a certain minimum length. Whereas for a soft matrix, as long fibers as possible would be desirable for better reinforcement.

The overall composite moduli for the log-normal fiber length distribution were determined using all the three approaches, viz., series, parallel and logarithmic. As expected, it was found that the logarithmic summation always gave predictions intermediate between those given by the other two procedures. The differences between the results

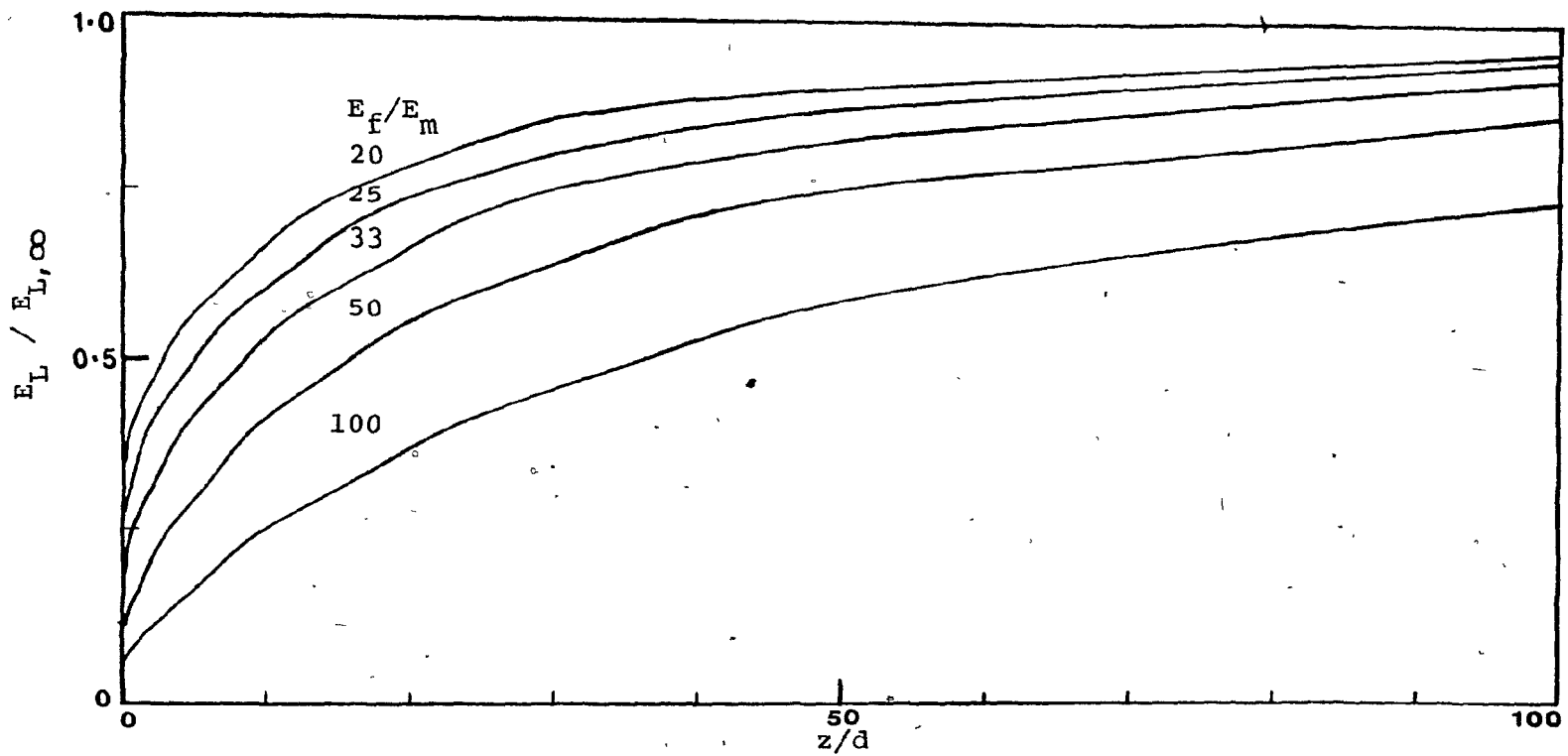


Figure (4.4a). Variation of E_L with Fiber Aspect Ratio for Monodisperse Systems
 $(v_f = 0.2)$.

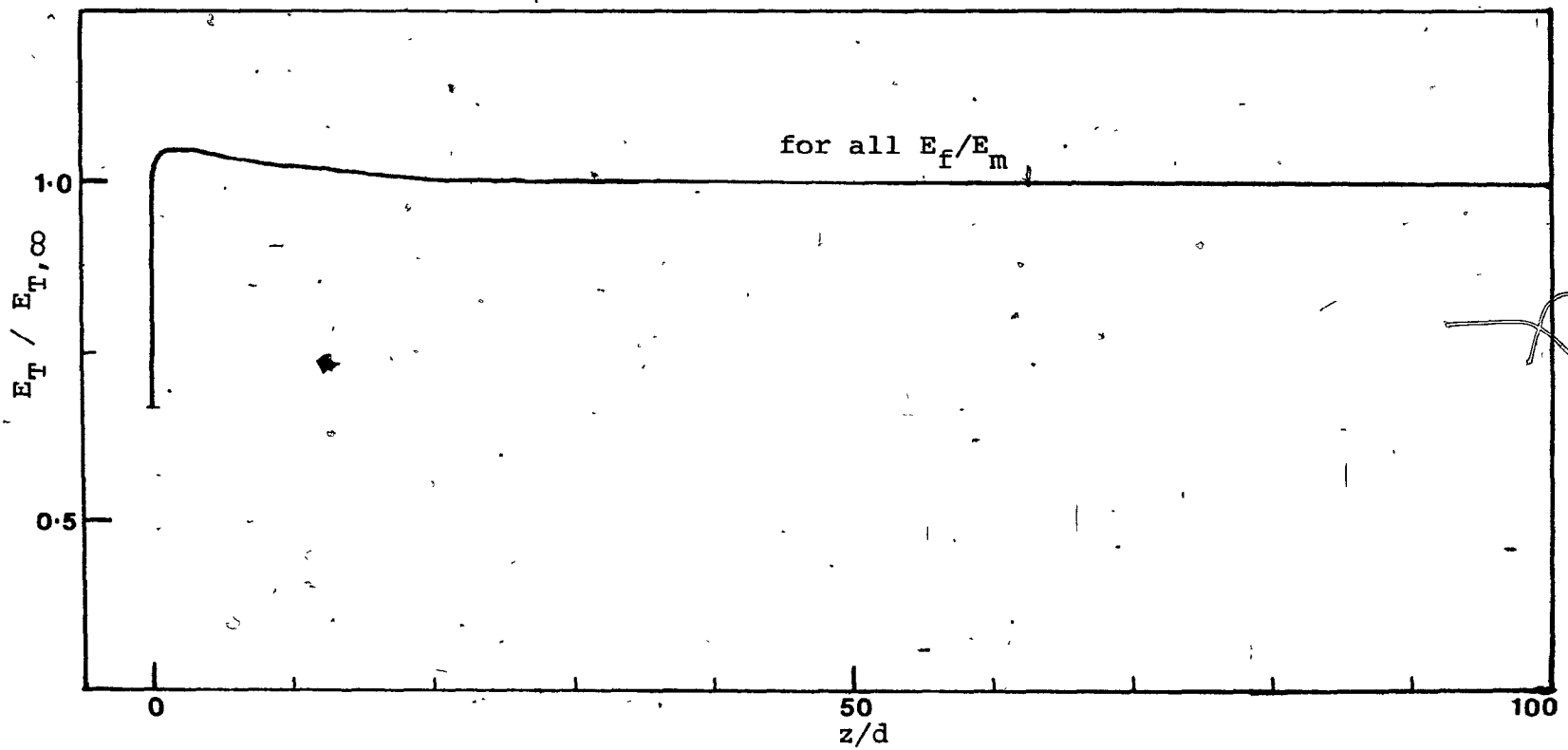


Figure (4.4b). Variation of E_T with Fiber Aspect Ratio for Monodisperse Systems ($V_f = 0.2$).

are relatively large for \bar{E}_L as compared to those for \bar{E}_T as illustrated in Table (4.2) for $E_f / E_m = 100$, $V_f = 0.2$ and $s_z = 0.25$. Henceforth, only the results obtained by the logarithmic summation are considered.

Figure (4.5) show the variations of \bar{E}_L and \bar{E}_T with the fiber volume fraction for various values of s_z for $E_f / E_m = 100$ ($E_m = 0.689$ GPa or 100,000 psi) representing a soft matrix like polyethylene. Figures (4.6) show the similar results for $E_f / E_m = 20$ ($E_m = 3.445$ GPa or 5000,000 psi) which would correspond to a stiff matrix like Polystyrene. In both figures, the composite moduli are reduced by E_m . It is seen from the plots for \bar{E}_L that the broader the length distribution the lower is the value of the composite modulus relative to that predicted assuming a monodisperse fiber composite. However, differences are not as large in the case of a stiffer matrix composite as in the case of a softer matrix composite.

Hence, it may be concluded that the assumption of uniform aspect ratio represented by a mean value may lead to an over prediction of composite stiffness in the fiber direction of a unidirectional composite, though the error may not be very serious in the case of a stiff matrix composite with a relatively narrow fiber length distribution. However, it must be remembered that for partially aligned fibers, influence of fiber length distribution may be stronger, particularly when longer fibers have greater or lower tendency to get oriented in a major direction than shorter fibers during processing of SFRTF.

TABLE (4.2)

COMPARISON OF RESULTS OBTAINED
BY DIFFERENT METHODS OF SUMMATION

Method of Summation	\bar{E}_L (GPa)	\bar{E}_T (GPa)
Parallel	5.825	1.037
Logarithmic	5.458	1.034
Series	5.061	1.034
Uniform ($\bar{z}/d = 30$)	6.624	1.030

$$E_f/E_m = 100$$

$$V_f = 0.2$$

$$S_z = 0.25$$

$$(\bar{z}/d) = 30$$

(polydisperse)

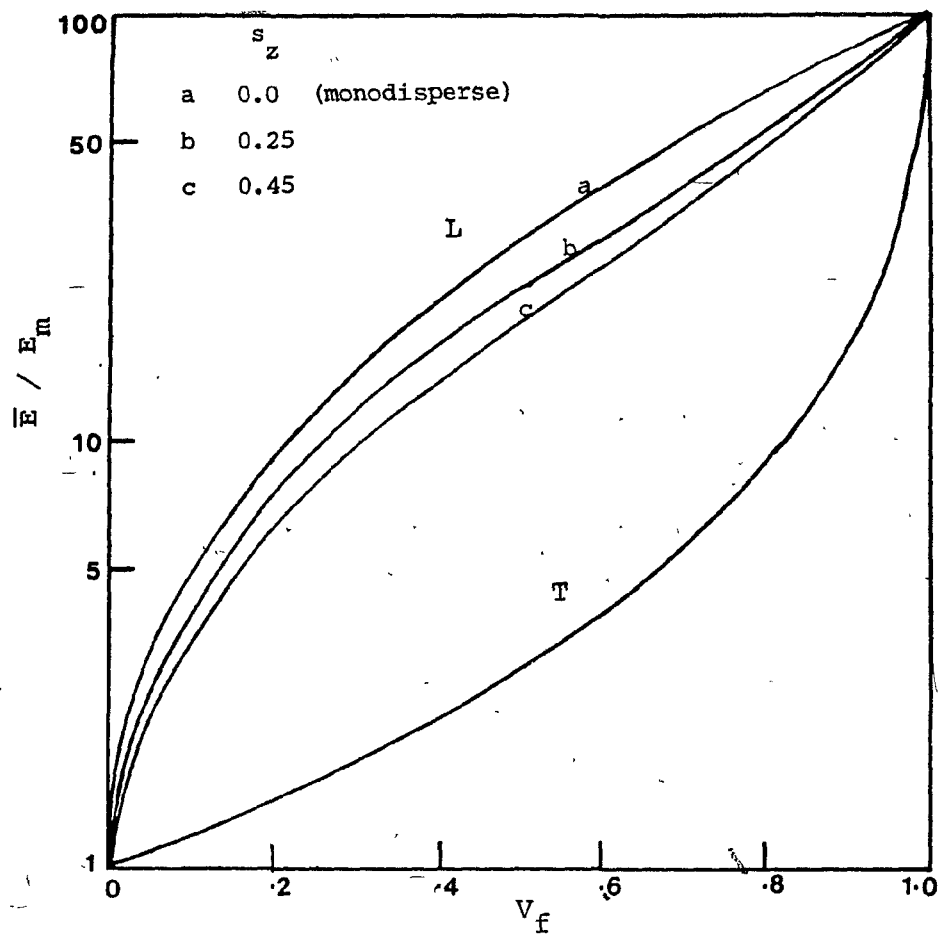


Figure (4.5). Variation of \bar{E}_L and \bar{E}_T with V_f for Polydisperse Systems ($E_f/E_m = 100$, $(\bar{z}/d) = 30$).

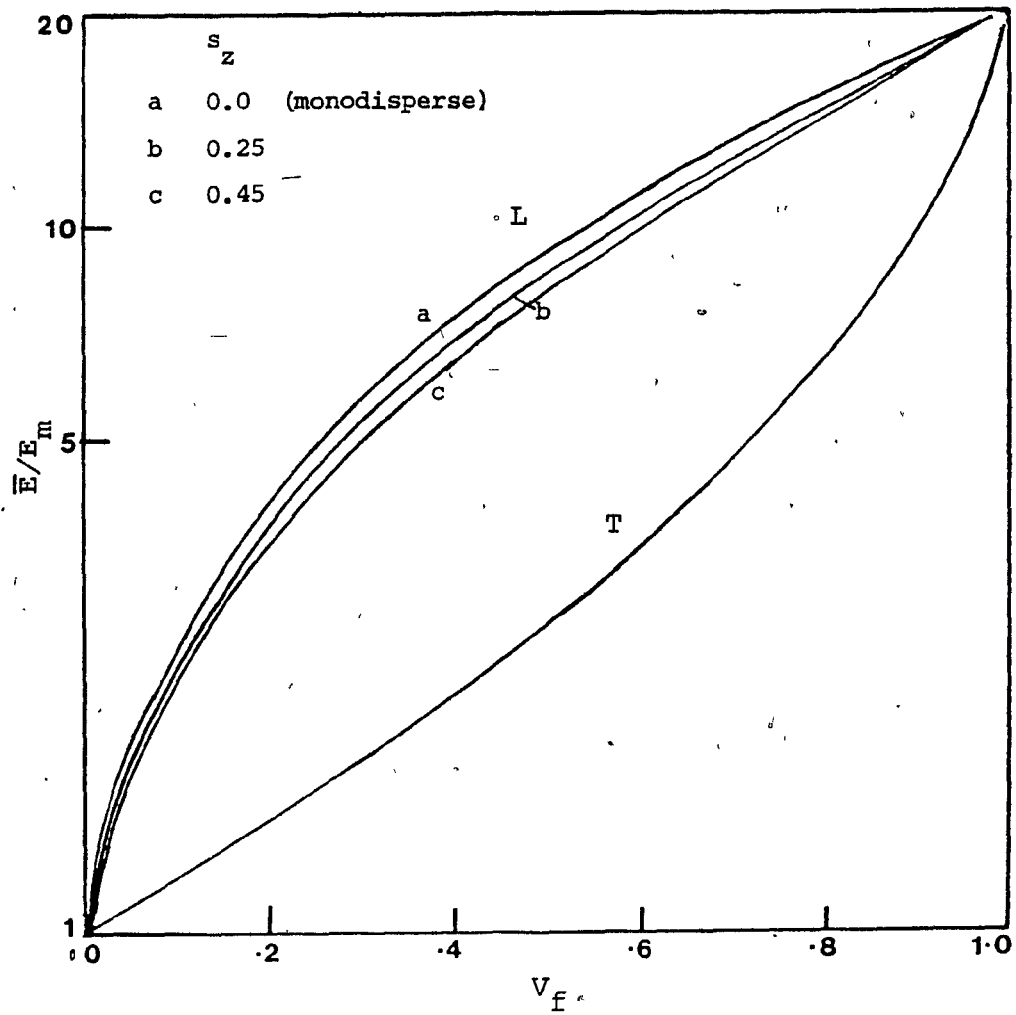


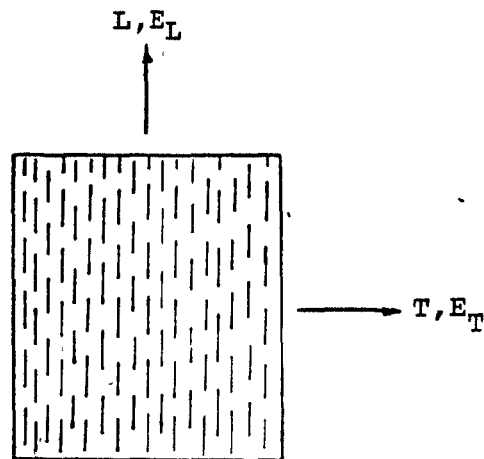
Figure (4.6). Variation of \bar{E}_L and \bar{E}_T with V_f for Polydisperse Systems ($E_f/E_m = 20$, $(\bar{z}/d) = 30$).

There is an additional point to be noted. The value of the average aspect ratio used in the above computations is close to the number average value determined experimentally in molded samples (Tran (63)). A seemingly easier experimental method would involve the determination of a weight-average value by screening analysis. When just the mean aspect ratio is used in theoretical predictions assuming a monodisperse system, it becomes rather ambiguous as to which average is appropriate to use. It must be emphasized that since the weight average can be significantly higher than the number average depending on the overall distribution, so would be the corresponding predicted properties. However, while using a distribution function of the type used in the above analysis, such an ambiguity is removed.

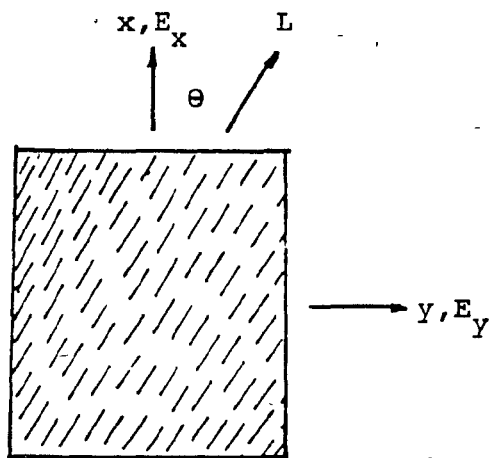
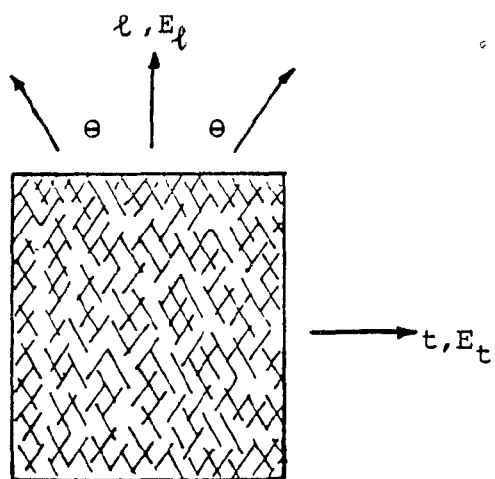
4.2 Review of Model for Evaluating Elastic Constants of Composite with Fiber Orientation Distribution

A model has been developed by the group for computing elastic constants of composite with a fiber orientation distribution in a plane or in space, but with a monodisperse fiber length represented by an average value. It has been discussed in detail by Sudlow (24).

The first stage is the evaluation of the four elastic constants for planar stresses in terms of material constants of the two phases for the unidirectional SFRTF composite, the reference direction being the direction of fiber orientation (see Figure (4.7a)). Rayleigh-Maxwell



(a) Unidirectional Composite

(b) Reference Directional at angle θ to that of Fiber Orientation

(c) Symmetrical System

Figure (4.7). Systems Used in Model for Elastic Moduli

equations (2.10a and b) and (4.4) are employed for evaluating E_L , E_T and G_{LT} and law of mixture equation (4.5) for μ_{LT} .

The next step is to compute elastic constants for the unidirectional composite, reference direction being at an angle θ to the direction of fiber orientation (see Figure (4.7b)). For planar stresses, the stress-strain relationship can be represented as

$$\begin{bmatrix} \epsilon_x \\ \epsilon_y \\ \gamma_{xy} \end{bmatrix} = \begin{bmatrix} C_{11}^{xy} & C_{12}^{xy} & C_{16}^{xy} \\ C_{21}^{xy} & C_{22}^{xy} & C_{26}^{xy} \\ C_{61}^{xy} & C_{62}^{xy} & C_{66}^{xy} \end{bmatrix} \begin{bmatrix} \sigma_x \\ \sigma_y \\ \tau_{xy} \end{bmatrix} \quad (4.16)$$

where C_{11}^{xy} etc. are components of the compliance matrix. Application of the theory of elasticity gives

$$\begin{aligned}
C_{11}^{xy} &= \frac{\cos^4 \theta}{E_L} + \frac{\sin^4 \theta}{E_T} + \frac{\sin^2 2\theta}{4} \left[\frac{1}{G_{LT}} - \frac{2\mu_{LT}}{E_L} \right] \\
C_{22}^{xy} &= \frac{\sin^4 \theta}{E_L} + \frac{\cos^4 \theta}{E_T} + \frac{\sin^2 2\theta}{4} \left[\frac{1}{G_{LT}} - \frac{2\mu_{LT}}{E_L} \right] \\
C_{66}^{xy} &= \frac{1}{E_L} + \frac{2\mu_{LT}}{E_L} + \frac{1}{E_T} - \cos^2 2\theta \left[\frac{1}{E_L} + \frac{2\mu_{LT}}{E_L} + \frac{1}{E_T} - \frac{1}{G_{LT}} \right] \\
C_{12}^{xy} &= C_{21}^{xy} = \frac{1}{E_L} \left[\frac{\sin^2 2\theta}{4} (1 + 2\mu_{LT} + \frac{E_L}{E_T} - \frac{E_L}{G_{LT}} - \mu_{LT}) \right] \\
C_{16}^{xy} &= C_{61}^{xy} = \frac{\sin 2\theta}{E_L} \left[1 + \mu_{LT} - \frac{E_L}{2G_{LT}} \right. \\
&\quad \left. - \sin^2 \theta (1 + 2\mu_{LT} + \frac{E_L}{E_T} - \frac{E_L}{G_{LT}}) \right] \\
C_{62}^{xy} &= C_{26}^{xy} = \frac{\sin 2\theta}{E_L} \left[1 + \mu_{LT} - \frac{E_L}{2G_{LT}} \right. \\
&\quad \left. - \cos^2 \theta (1 + 2\mu_{LT} + \frac{E_L}{E_T} - \frac{E_L}{G_{LT}}) \right] \tag{4.17}
\end{aligned}$$

The elastic constants with respect to the directions x and y of Figure (4.7b) are related to the elements of compliance matrix as

$$\begin{aligned}
 E_x &= \frac{1}{C_{11}^{xy}}, & E_y &= \frac{1}{C_{22}^{xy}}, & G_{xy} &= \frac{1}{C_{66}^{xy}} \\
 \mu_{xy} &= \frac{C_{12}^{xy}}{C_{11}^{xy}}, & \mu_{yx} &= -\frac{C_{21}^{xy}}{C_{22}^{xy}}
 \end{aligned} \tag{4.18}$$

The next step is to evaluate elastic constants for a symmetrical arrangement of two unidirectional layers, the reference directions being the directions of symmetry. The system is shown diagrammatically in Figure (4.7c). The two layers are assumed to be perfectly bonded together, so that there is no shearing between them when normal stresses in the directions l or t are applied. Also it is assumed that equal number of fibers lie symmetrically at angles $+\theta$ and $-\theta$ with respect to the direction l . Such a system, then, requires only four constants for planar analysis, the compliance matrix being represented as,

$$[C^{lt}] = \begin{bmatrix} C_{11}^{lt} & C_{12}^{lt} & 0 \\ C_{12}^{lt} & C_{22}^{lt} & 0 \\ 0 & 0 & C_{66}^{lt} \end{bmatrix} \tag{4.19}$$

The compliance elements $[C^{lt}]$ of the symmetrical system are related to $[C^{xy}]$ of the previous non-symmetrical system as

$$\begin{aligned}
C_{11}^{lt} &= C_{11}^{xy} - \frac{(C_{16}^{xy})^2}{C_{66}^{xy}} \\
C_{22}^{lt} &= C_{22}^{xy} - \frac{(C_{26}^{xy})^2}{C_{66}^{xy}} \\
C_{12}^{lt} &= C_{12}^{xy} - \frac{C_{16}^{xy} C_{26}^{xy}}{C_{66}^{xy}} = C_{21}^{lt} \\
C_{66}^{lt} &= C_{66}^{xy} - \left[\frac{C_{11}^{xy} (C_{26}^{xy})^2 + C_{22}^{xy} (C_{16}^{xy})^2 - 2 C_{11}^{xy} C_{12}^{xy} C_{26}^{xy}}{C_{11}^{xy} C_{22}^{xy} - (C_{12}^{xy})^2} \right]
\end{aligned}
\tag{4.20}$$

The four elastic constants with respect to the directions of symmetry l and t are given as

$$\begin{aligned}
E_l &= \frac{1}{C_{11}^{lt}} & E_t &= \frac{1}{C_{22}^{lt}} \\
G_{lt} &= \frac{1}{C_{66}^{lt}} & \mu_{lt} &= -\frac{C_{12}^{lt}}{C_{11}^{lt}}
\end{aligned}
\tag{4.21}$$

Real systems neither have unidirectional nor symmetrical $(+\theta, -\theta)$ fiber orientation, but rather a fiber orientation distribution. Based on the concept of affine deformation of an initially random composite, a theoretical fiber orientation distribution function has been derived both

for planar (all fibers lying parallel to a plane) and spatial (three dimensional fiber orientation) cases (Sudlow (24), Charrier et. al. (25)).

For the planar case,

$$dV(\theta) = \frac{d\theta}{\pi \left(\frac{\cos^2 \theta}{C_\ell^2} + \sin^2 \theta C_\ell^2 \right)} \quad (4.22)$$

Here $dV(\theta)$ represents fraction of fibers that are oriented in the direction θ with respect to the reference direction ℓ and C_ℓ is the orientation parameter. $C_\ell = 1$ corresponds to random-in-plane orientation while $C_\ell > 1$ represents a preferential orientation in the ℓ direction.

For evaluating the overall elastic constants for a composite with fiber orientation distribution, one may assume the composite to be made up of several elements corresponding to different values of angle θ . As described in Section 4.1 for fiber length distribution, again several alternative approaches are possible: parallel arrangement gives, for ℓ direction,

$$\bar{E}_\ell = \int_0^{\pi/2} E_\ell(\theta) dV(\theta) \quad (4.23)$$

while series arrangement gives

$$\frac{1}{\bar{E}_\ell} = \int_0^{\pi/2} \frac{1}{E_\ell(\theta)} dV(\theta) \quad (4.24)$$

The real answer probably corresponds to an intermediate arrangement and the logarithmic summation seems more justified,

$$\ln \bar{E}_\ell = \int_0^{\pi/2} \ln E_\ell(\theta) dV(\theta) \quad (4.25)$$

A similar equation can be written for the modulus in the t direction.

An extension to spatial case has also been pursued (Sudlow (24)), however, this review is confined to the simpler two dimensional case.

4.3 Elastic Constants of Composite with Non-Uniform Fiber Orientation Distribution Across Thickness

The model reviewed in Section 4.2 assumes a uniform fiber orientation distribution, i.e., for a planar case, a single value of C_ℓ is assumed to be sufficient to describe the fiber orientation distribution throughout the composite.

However, particularly in case of injection molded samples, the orientation distribution is not found to be homogeneous (Darlington et al. (54), Folkes (57)). It has been suggested that the structure through the thickness can be divided into several layers. Usually, the high shear stresses and high viscosity near the walls of the mold cavity during mold-

ing lead to preferential fiber alignment in the flow direction below the surface of the molded samples. In the core, the decelerating flow may cause random or even transverse fiber orientation (Figure (4.8)). Consequently a single value of the orientation parameter C_ℓ may not be sufficient to describe the orientational structure of the system.

4.3.1 Model for Non-Uniform Fiber Orientation Distribution

A perfect simulation for a composite with non-uniform fiber orientation distribution would require a complete structural characterization through the thickness to get the knowledge about point by point variation of the orientation parameter C_ℓ . In the absence of such a knowledge, a simple model was developed where C_ℓ was assumed to vary from the center to the surface giving rise to a non-homogeneous orientation distribution. Such a case, though far from the actual situation, can illustrate the concepts of non-uniform structure and its influence on the composite properties in a simple manner.

In this model, the central plane is assumed to have a random-in-plane fiber orientation corresponding to $C_\ell = 1$. It is assumed, that C_ℓ varies linearly across the thickness, (Figure (4.9)) so that at any location from the central plane

$$C_\ell = 1 + \frac{h}{h_m} (C_{\ell M} - 1) \quad (4.26)$$

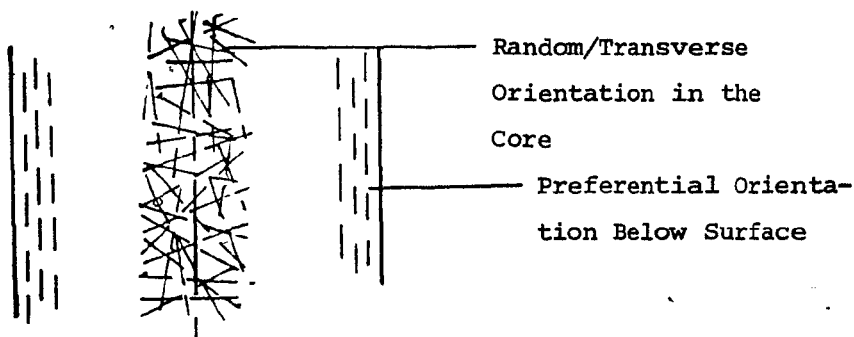


Figure (4.8). Non-homogeneous Structure in Molded Parts.

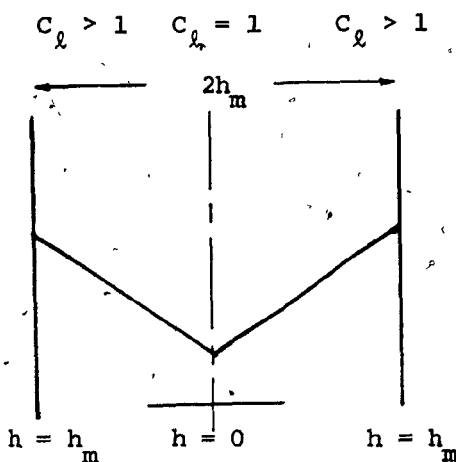


Figure (4.9). Variation of C_l across the Thickness for Model.

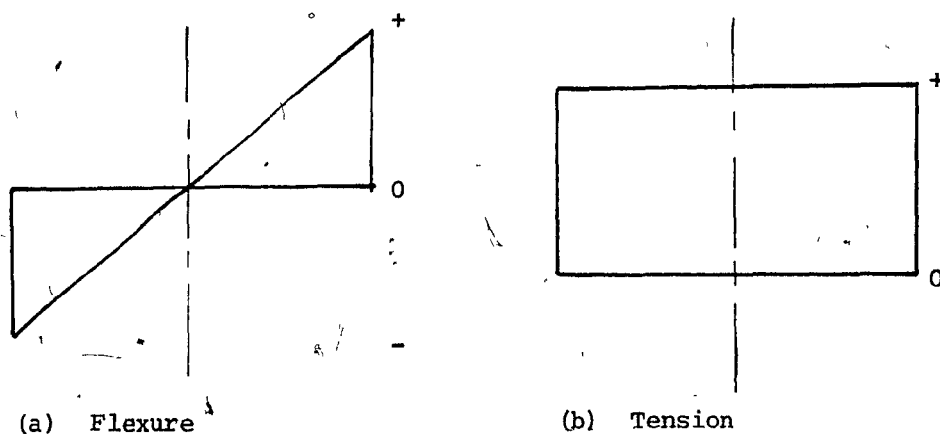


Figure (4.10). Strain Distribution across the Cross-section.

where $C_{\ell M}$ is the maximum value of C_{ℓ} at $h = h_m$ at the surface.

By assuming the central plane to be random, one is thus left with a single parameter $C_{\ell M}$, thus simplifying the situation.

The overall composite modulus can be determined using the laminate analogy of the parallel model, since here it is appropriate to assume various layers corresponding to different values of C_{ℓ} to share load in parallel with each other. The elastic constants for any layer corresponding to a given value of C_{ℓ} can be determined by the method described in Section 4.2. The overall composite modulus can then be obtained by carrying out a summation across the thickness.

Due to non-uniformity of the structure, material is no longer homogeneous even on gross scale. Because of the variation of the moduli, the stress-strain relationships across the thickness are not equivalent. Consequently, the elastic moduli in the directions of symmetry in tension and flexure are no longer equal, since flexure leads to highest tensile or compressive strains near the surface while the strain at the neutral axis (central plane) is zero as shown in Figure (4.10a). Tension, on the other hand, causes uniform strain throughout the cross-section (Figure (4.10b)).

The observed differences in the composite tensile and flexural moduli may thus be direct products of structural inhomogeneities and in fact, independent measurements in tension and flexure may be used

to throw light on the through thickness structural variations. In the following, the effect of the non-homogeneous structure is illustrated in terms of the ratio of the overall flexural to the tensile moduli of the composite.

The overall composite modulus can be evaluated as follows, Deflection δ for a layer corresponding to a particular value of C_l under a force dF in a three point bending test is given by

$$\delta = \frac{dFS^3}{48 E(h) dI} \quad (4.27)$$

where S represents the span length, dI is the elemental moment of inertia and $E(h)$ is the modulus, a function of C_l and hence of h .

The total load F acting on the composite section for a deflection δ , is

$$F = \int dF = \int_{-h_m}^{+h_m} \frac{48 \delta}{S^3} E(h) dI \quad (4.28)$$

However, if E^f represents the overall flexural modulus, then for bending of the entire section

$$F = \frac{48 E^f I \delta}{S^3} \quad (4.29)$$

where I is the moment of inertia of the entire section. Equating equations (4.28) and (4.29),

$$E^f = \frac{1}{I} \int_{-h_m}^{+h_m} E(h) dI \quad (4.30)$$

Since I and dI can be expressed in terms of cross-sectional dimensions of composite

$$E^f = \frac{3}{2} \int_{-1}^{+1} E(h) \left(\frac{h}{h_m} \right)^2 d\left(\frac{h}{h_m} \right) \quad (4.31)$$

This relationship is valid for both l and t directions.

Hence, overall longitudinal flexural modulus is given as

$$E_l^f = \frac{3}{2} \int_{-1}^{+1} \bar{E}_l(h) \left(\frac{h}{h_m} \right)^2 d\left(\frac{h}{h_m} \right) \quad (4.32)$$

and overall transverse flexural modulus is given as

$$E_t^f = \frac{3}{2} \int_{-1}^{+1} \bar{E}_t(h) \left(\frac{h}{h_m} \right)^2 d\left(\frac{h}{h_m} \right) \quad (4.33)$$

The overall longitudinal tensile modulus is simply given by

$$E_l^t = \frac{1}{2h_m} \int_{-h_m}^{+h_m} \bar{E}_l(h) dh \quad (4.34)$$

and the overall transverse tensile modulus is given by

$$E_t^t = \frac{1}{2h_m} \int_{-h_m}^{+h_m} E_t(h) dh \quad (4.35)$$

The ratios $\left(\frac{E^f}{E^t}\right)_\ell$ and $\left(\frac{E^f}{E^t}\right)_t$ can then be used to illustrate the effect of non-homogeneous fiber orientation distribution.

4.3.2— Results and Discussion

Table (4.3) shows the values of material parameters used for these calculations. These were chosen to represent a typical injection molded utility thermoplastic-glass fiber system. Table (4.4) shows the values of $C_{\ell M}$ at the surface chosen for computations. As indicated earlier, in all cases the central plane was assumed to have a random fiber orientation corresponding to $C_\ell = 1$.

Figure (4.11) shows the variations of E_ℓ and E_t across the thickness for variation of C_ℓ from 1 to $C_{\ell M} = 2$ and $V_f = 0.2$. Here, the elastic moduli have been reduced by the matrix modulus E_m for convenience. As expected, the modulus in the direction ℓ is quite high and that in the direction t is low near the surface which is subjected to the highest strain in flexure.

Figure (4.12) shows the variation of $(E^f / E^t)_\ell$ and $(E^f / E^t)_t$ with fiber volume fraction for the above case. Again, the

TABLE (4.3)

VALUES OF PARAMETERS USED IN COMPUTATIONS OF OVERALL MODULI
OF COMPOSITES WITH NON-HOMOGENEOUS ORIENTATION DISTRIBUTION

PARAMETER	VALUE OR RANGE OF VALUES
E_f	68.9 GPa (10^7 psi)
E_m	1.378 GPa (2×10^5 psi)
(\bar{z}/d) (monodisperse)	30
μ_m	0.3
μ_f	0.2
V_f	0 - 1

TABLE (4.4)

VALUES OF C_{LM} USED IN COMPUTATIONS OF SECTION 4.3

NO.	C_{LM} (SURFACE)
1	2
2	5
3	10
4	50
5	100

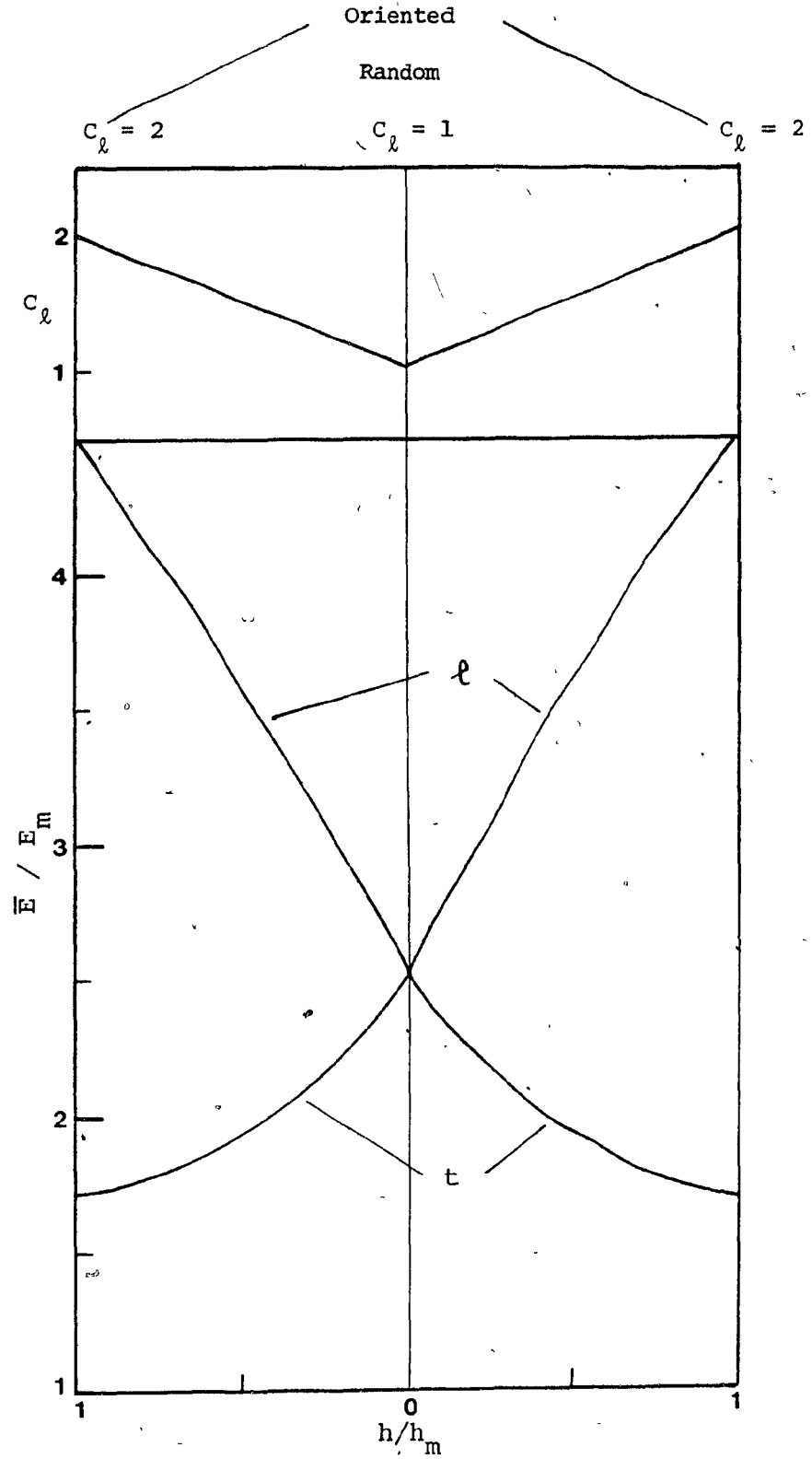


Figure (4.11). Variation of \bar{E}_ℓ and \bar{E}_t across the Thickness for Variation of $C_\ell = 1$ to $C_{\ell M} = 2$ ($E_f/E_m = 50$, $V_f = 0.2$, $(\bar{z}/d) = 30$).

results are presented for the entire range of V_f for the sake of completeness. It is seen that for the case of structural non-homogeneity discussed, the flexural modulus in the ℓ direction is significantly higher than the tensile modulus, while in the t direction, the tensile modulus is higher.

Table (4.5) shows the comparison of the moduli ratios for the various values of $C_{\ell M}$ considered when $V_f = 0.2$. It is seen that as the value of $C_{\ell M}$ is increased, the ratios E^f / E^t in both directions approach unity. This appears to be related to the fact that the moduli E_ℓ and E_t become relatively insensitive to value of C_ℓ when C_ℓ becomes larger.

There are a few points that should be emphasized here. The above analysis assumed a linear variation of C_ℓ across the thickness, but in an actual case, abrupt variations in the degree of fiber alignment from the center to the surface can occur and hence the effect of structural non-homogeneity can be even stronger (Pouliot (66)). Also, in the above analysis, the central plane was assumed to have random fiber orientation with $C_\ell = 1$. But a strong transverse fiber orientation ($C_\ell < 1$) has been found (Darlington et. al. (54)) in some injection molded parts. For such a case, the differences in measured flexural and tensile moduli can be even greater. Though the scope of the present theoretical work and time limitations did not allow further modifications in the model, it does illustrate an approach whereby experimentally determined moduli can be used to assess the structural inhomogeneity in the molded parts.

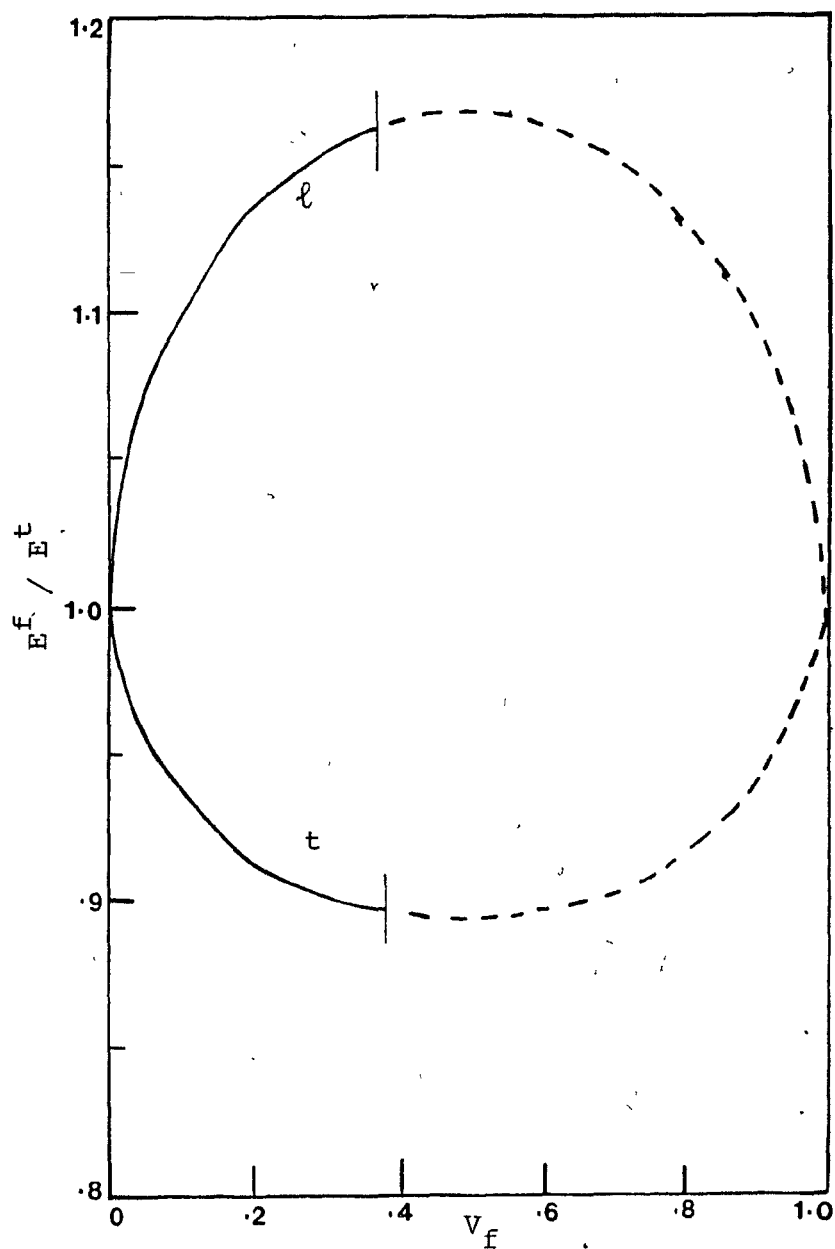


Figure (4.12). Variation of $(E^f/E^t)_l$ and $(E^f/E^t)_t$ with V_f for Variation of $C_\ell = 1$ to $C_{\ell M} = 2$ ($E_f/E_m = 50$, $(\bar{z}/d) = 30$).

TABLE (4.5)

COMPARISON OF RATIOS OF $(E^f/E^t)_\ell$ AND $(E^f/E^t)_t$ FOR VARIOUS VALUES OF $C_{\ell M}$ FOR $V_f = 0.2$

C_ℓ VARIATION	$(E^f/E^t)_\ell$	$(E^f/E^t)_t$
1 - 2	1.1386	0.913
1 - 5	1.156	0.92
1 - 10	1.106	0.95
1 - 50	1.02	0.98
1 - 100	1.015	0.987

CHAPTER V

EXPERIMENTAL PROGRAMME

The essential aim of the experimental programme was to mold plates with preferential fiber orientation of selected short glass fiber filled thermoplastic composite systems, measure selected mechanical properties in order to characterize their mechanical anisotropy and analyze this anisotropy in terms of structure.

The composite materials were supplied in the form of approximately 6 mm long cylindrical pellets with desired glass fiber contents. Molding was carried out using the shearing device referred to in Chapter III, but a modified procedure was used with some changes in the device itself in order to make the whole operation easier and less time consuming. The molded plates were then tested for selected mechanical properties.

The experimental programme can be summarized as:

- (1) Molding of composite materials available in pellet form into 100 mm x 100 mm (4 in. x 4 in.) square plates of two thicknesses, 1.6 mm (1/16 in.) and 3.2 mm (1/8 in.) with preferential fiber orientation.
- (2) Cutting of small test-pieces from the molded plates both in the direction of preferential fiber orientation (l) and the direction normal to it (t).

- (3) Testing of these test-pieces for selected mechanical properties in order to characterize the mechanical anisotropy of molded plates.

Section 5.1 below describes the molding devices and molding operation in detail. Section 5.2 presents information on the materials used for this study. This is followed by detailed description of testing procedures in Section 5.3.

5.1 Molding Operation

In order to make plates with preferential fiber orientation, a set of two devices have been built by previous researchers in the group. These are referred to as the "premolding device" and the "shearing device" (Pouliot (66)).

5.1.1 Review of the Procedure used by Previous Researchers

The premolding and shearing devices were used in sequence in order to make a plate with preferential fiber orientation.

5.1.1.1 Premolding Device

The basic components of the premolding device were two symmetrical halves and a piston. Figure (5.1) shows one half of the

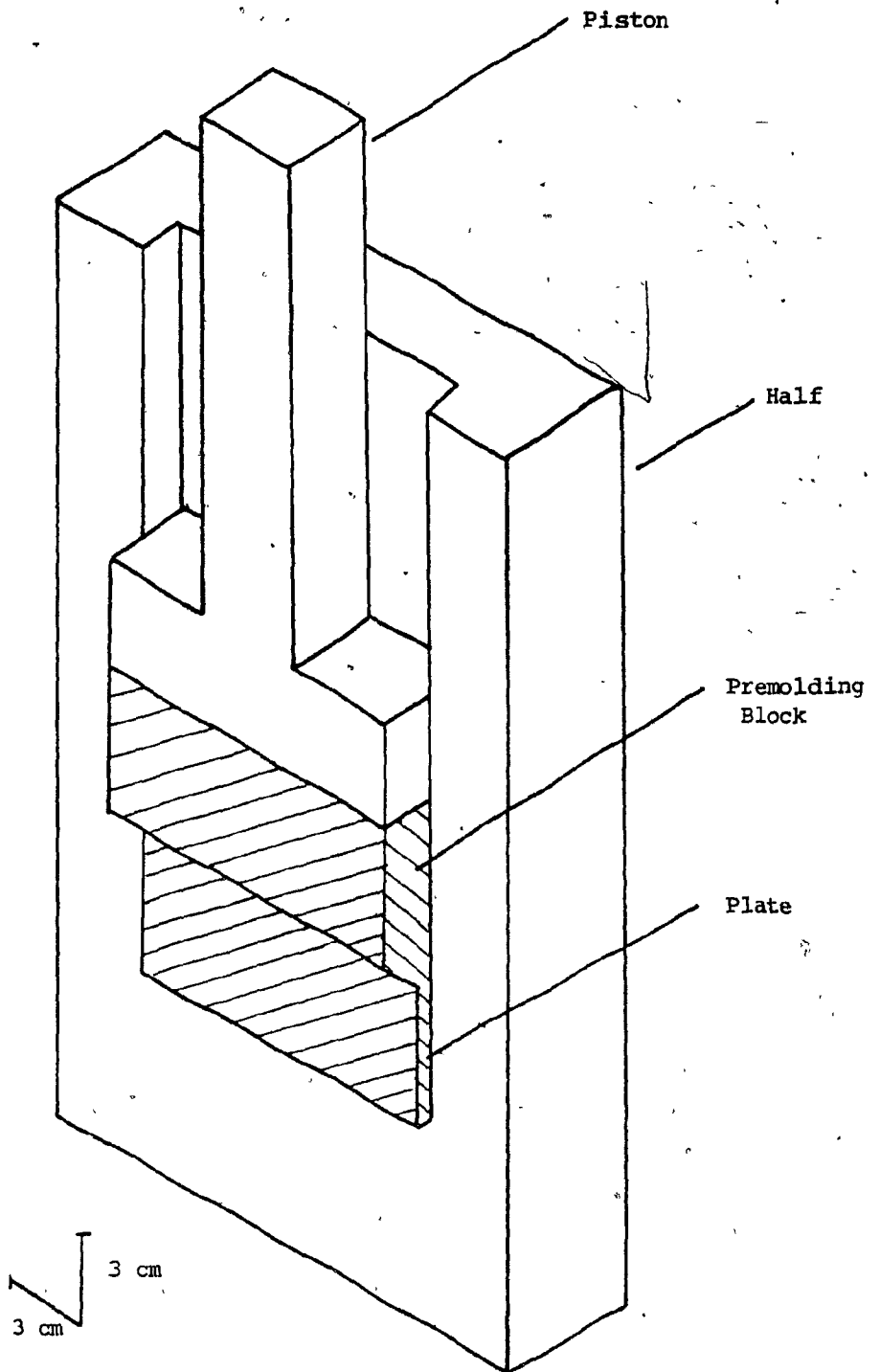


Figure (5.1). A Half of the Premolding Device with a Premolding.

device. When closed, the two halves formed a space consisting of a reservoir and a thin slit or gap. Each of the half was provided with four 12 mm (1/2 in.) diameter holes drilled through, so that four cartridge heaters (300W each) could be inserted into each half for heating. For cooling, the heaters were removed and cooling water tubes were inserted into the holes. Figure (5.2) shows a sketch of the device assembled for molding.

For making a "pre molding" in this device, the two halves were closed and pellets were placed in the gap. The device was heated in order to melt the pellets and then the piston was introduced into the reservoir and used to compress the pellets into a "pre molding" consisting of a block of composite with randomly oriented fibers (formed in the reservoir) and a thin plate (formed in the gap). During this compressing operation, the two halves were held together using a hydraulic cylinder as shown in Figure (5.2). The compressed block was cooled by running cooling water through the holes in each half while maintaining under pressure so as to reduce void formation and then the pre molding was removed after opening the device. Figure (5.3) shows a sketch of a pre molding made in this way.

5.1.1.2 Shearing Device

The shearing device was of a more complex design and operation than the pre molding device. Its basic components were two halves,

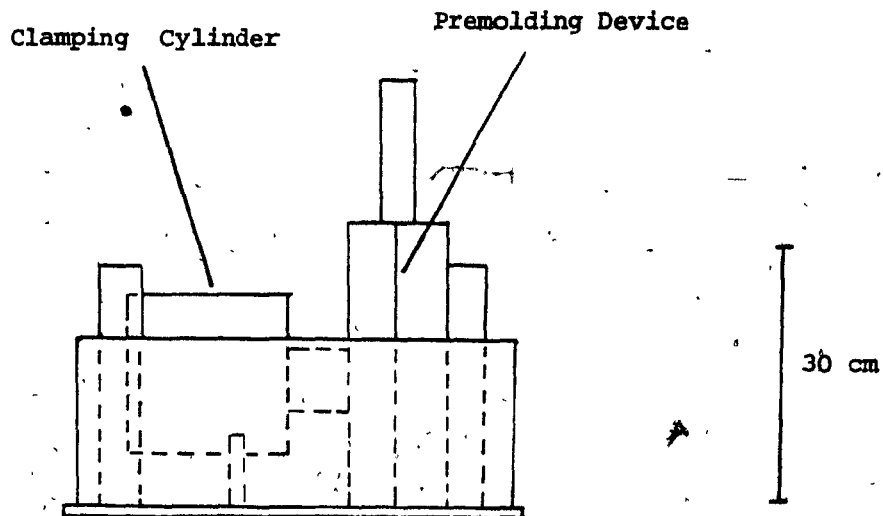


Figure (5.2). Assembled Premolding Device.

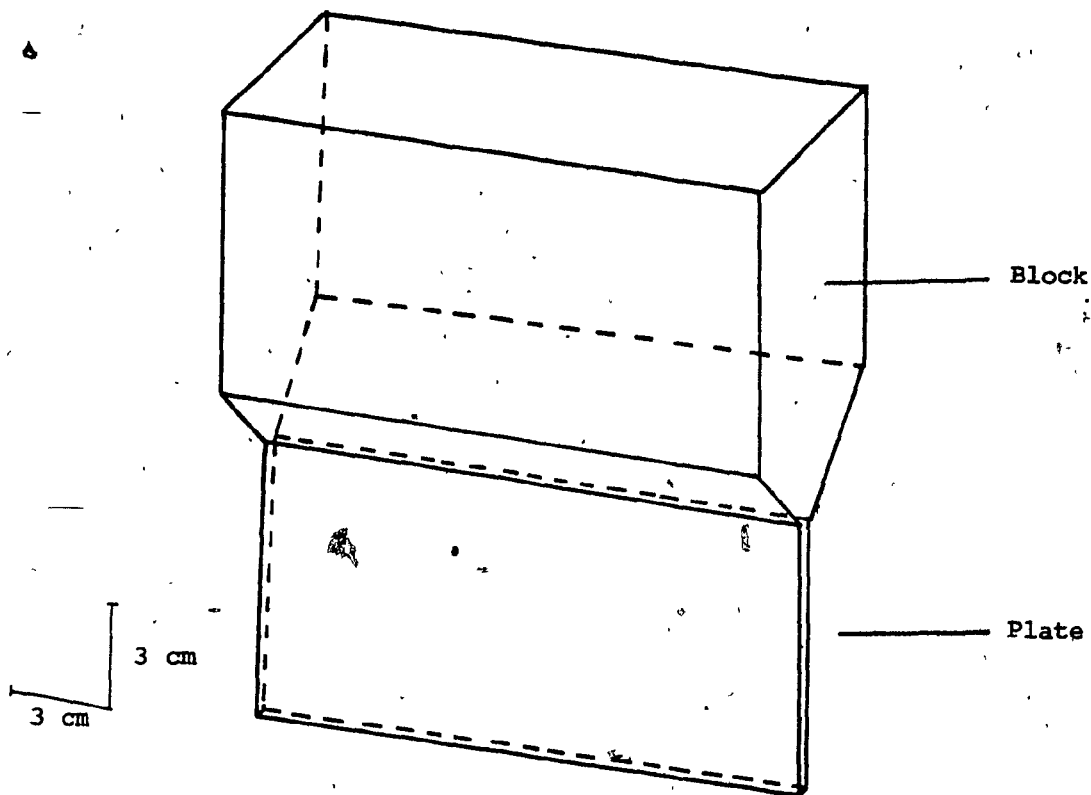


Figure (5.3). Premolding.

two pistons and two hydraulic cylinders - pumps assemblies. Figure (5.4) shows a half of the shearing device. When assembled, the two halves enclosed a space that consisted of three regions: an upper reservoir, a central thin gap or a slit and a lower reservoir. Each half was provided with a replaceable spacer so as to change the width of the central gap. As shown schematically in Figure (5.5), three different widths of 1.6 mm (1/16 in.), 3.2 mm (1/8 in.) and 6.4 mm (1/4 in.) could be obtained. Each half was also provided with four 12.7 mm (1/2 in.) diameter cylindrical holes for insertion of cartridge heaters. Also, right behind each spacer, a rectangular cooling cavity was provided through which cooling water could be circulated for efficient and fast cooling. Figure (5.6) shows the assembled shearing device.

The essential shearing operation consisted of placing two premolding blocks into the upper and lower reservoirs of the shearing device. The premoldings could then be melted by heating the device. By creating a pressure differential across the two pistons, the molten material from the upper reservoir could be transferred through the central gap into the lower reservoir. During the operation, the two halves were held together by means of a hydraulic cylinder as shown in Figure (5.6).

The flow of the molten material into a converging channel from the upper reservoir into the gap followed by shearing in the narrow

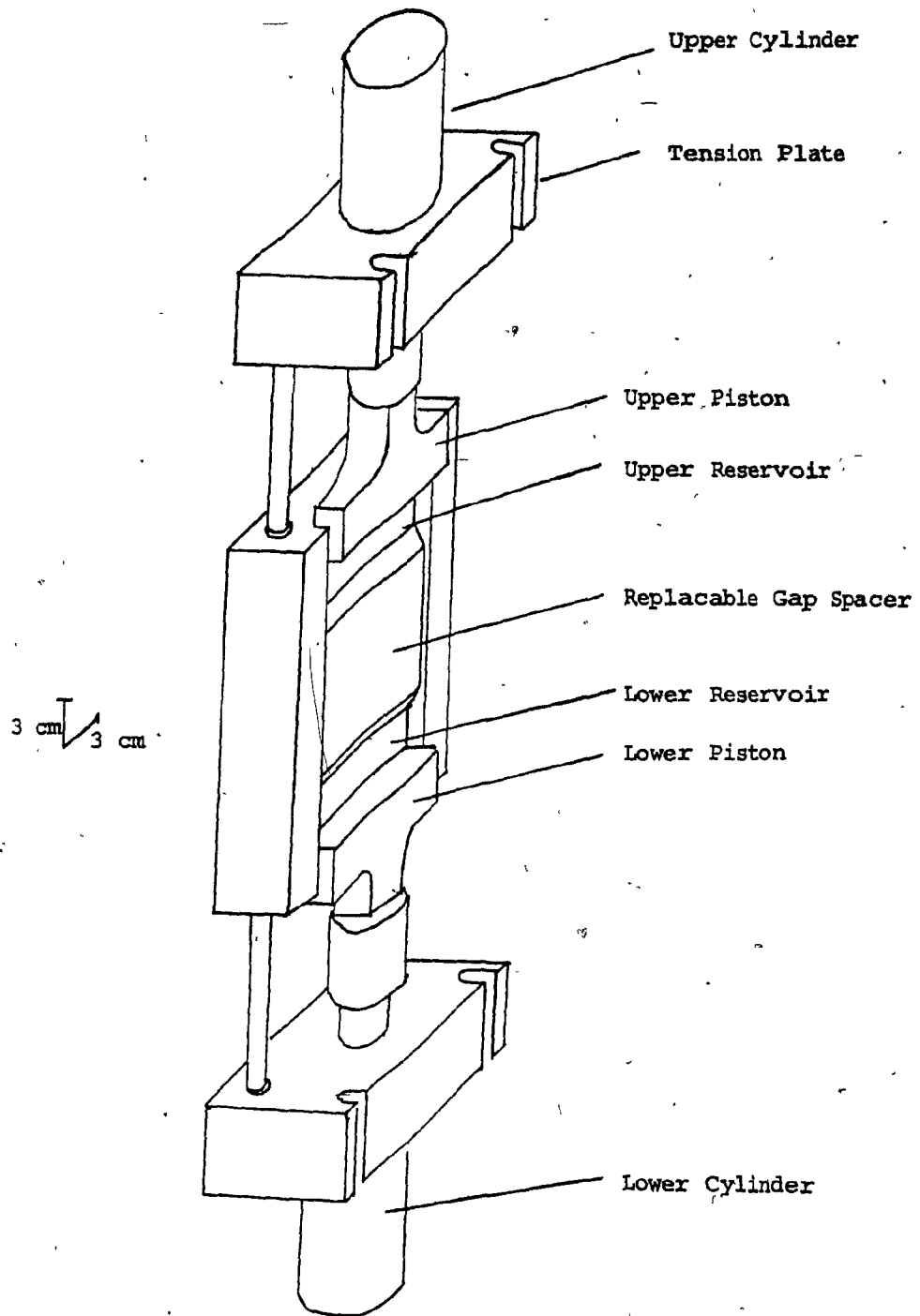


Figure (5.4). A Half of the Shearing Device.

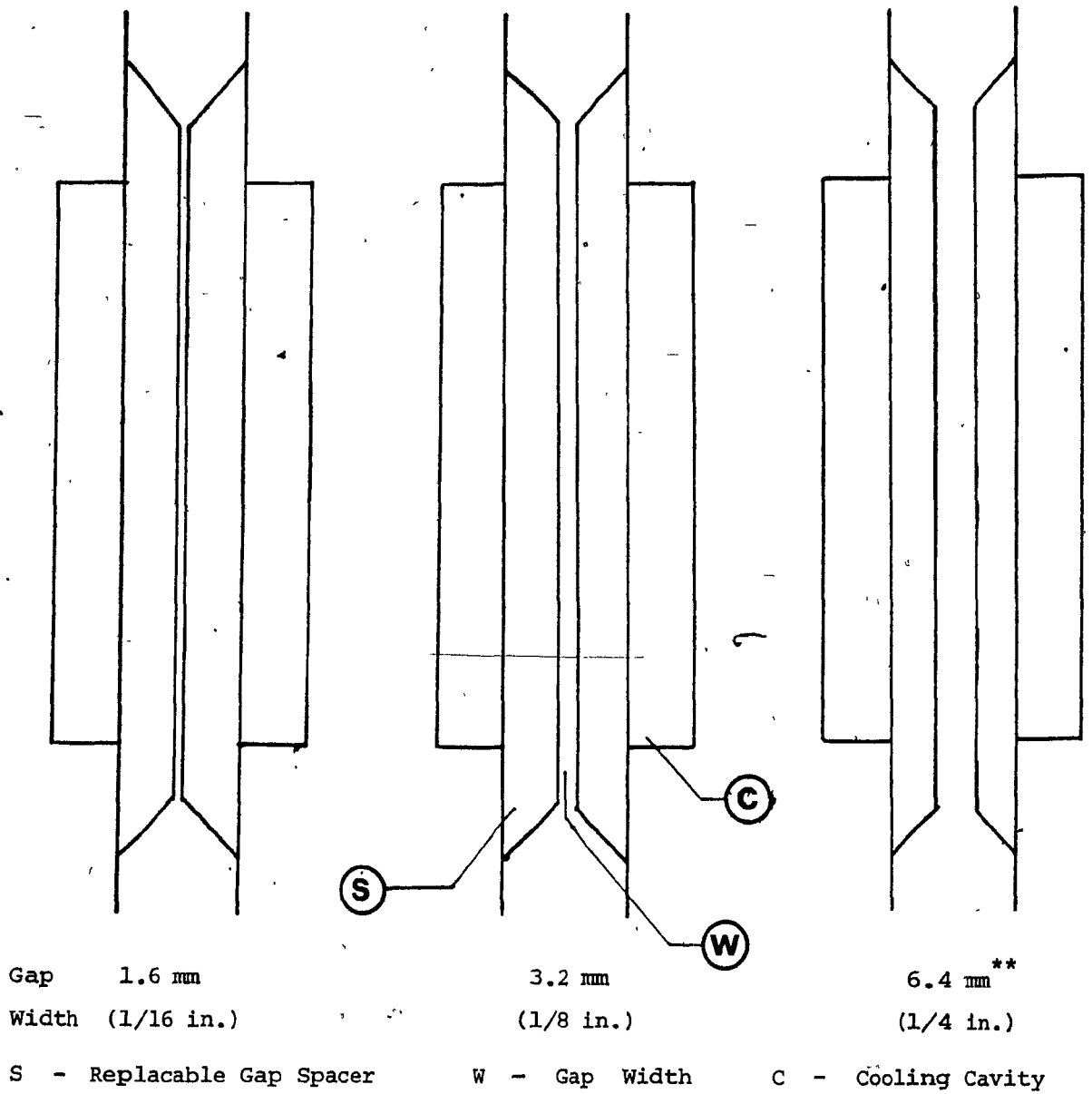


Figure (5.5). Arrangement for Changing Gap Width in the Shearing Device.

(** Not used in this study).

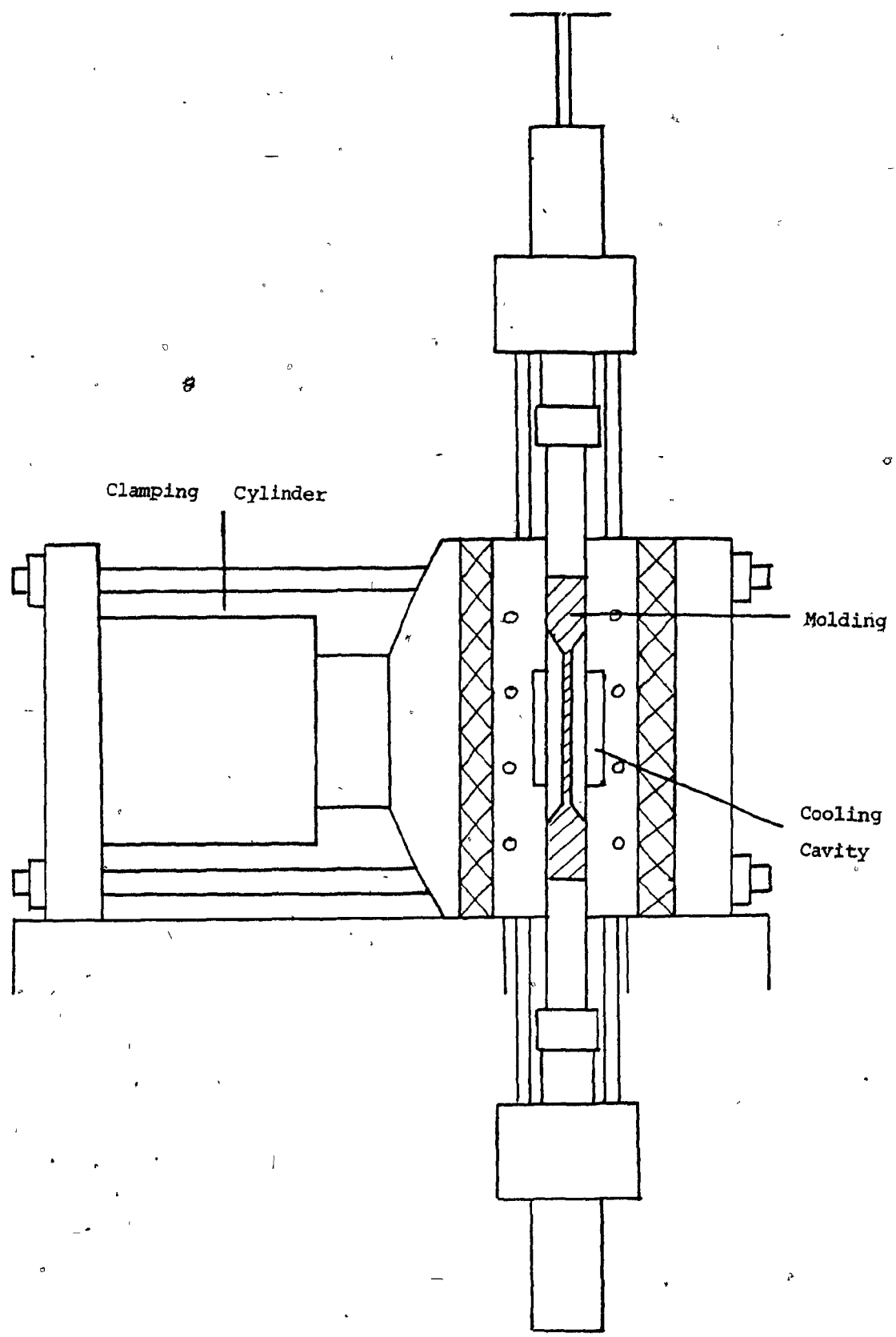


Figure (5.6). Assembled Shearing Device.

gap caused many of the glass fibers to get aligned preferentially in the direction of flow and hence the resulting "sheared plate" had preferential fiber orientation in the flow direction. The device was then water-cooled and opened to get the "sheared" molding. Figure (5.7) shows a sheared molding.

The different gap widths of the central section allowed different shear rates to be achieved during the transfer operation and hence different degree of fiber alignment and a study of other effects of part thickness. A thinner gap was expected to generate a more "in-plane" fiber lay-out compared to the thicker gap, thus allowing a "two-dimensional" or "three-dimensional" fiber orientation.

The shearing device was designed to permit the transfer operation in three possible ways:

The first method was to connect the upper transfer and compression cylinder to a hydraulic single speed - hand pump and to replace the lower transfer and compression cylinder by a spring and stopper system (see Figure (5.8a)). The spring acted to provide a counterforce during the transfer. The lower piston moved downwards during the transfer operation till it reached the stopper. Further application of force on the upper piston caused the pressure on the molten material to rise to a desired level and the material could then be cooled under pressure.

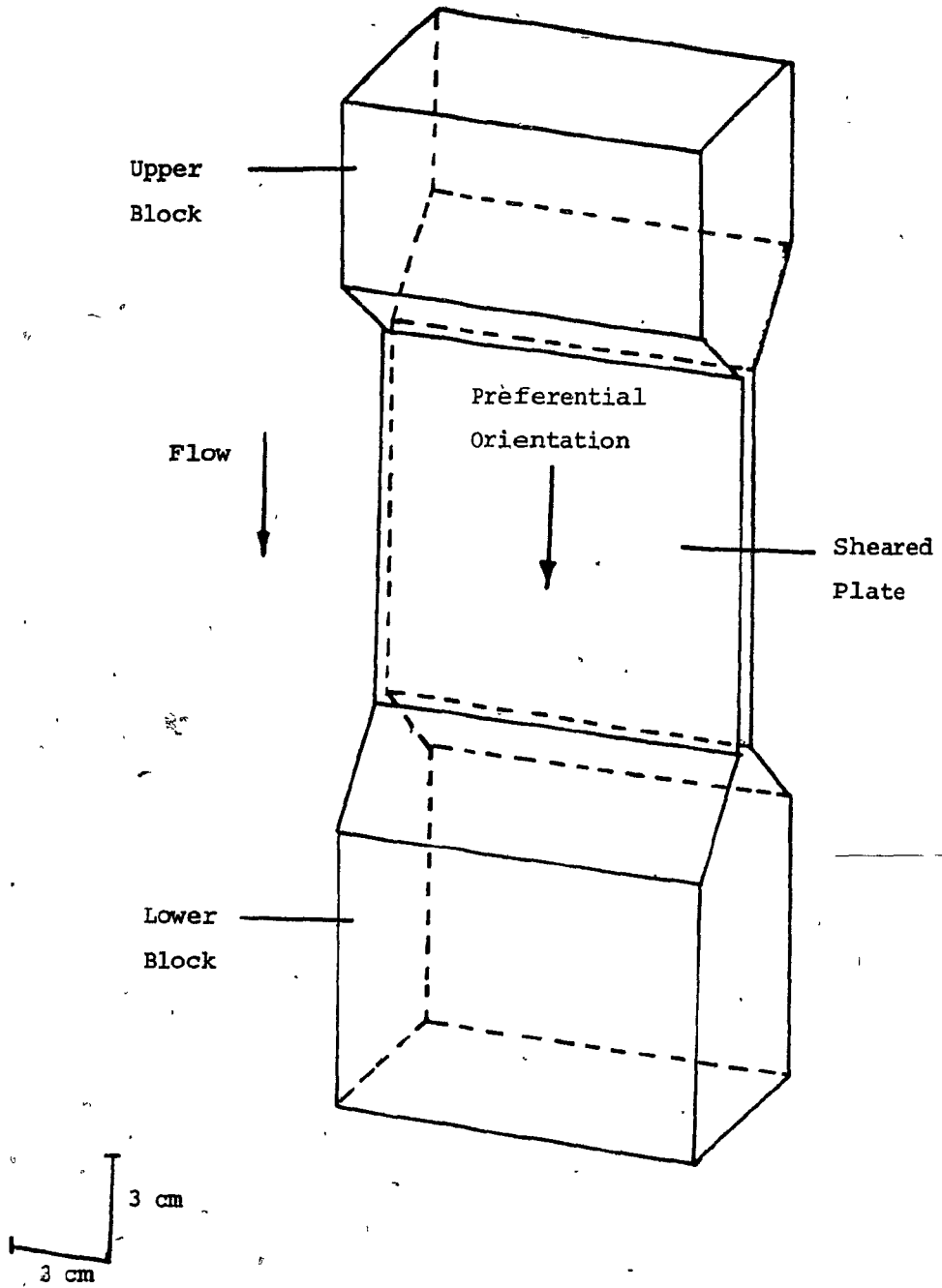


Figure (5.7). Sheared Molding.

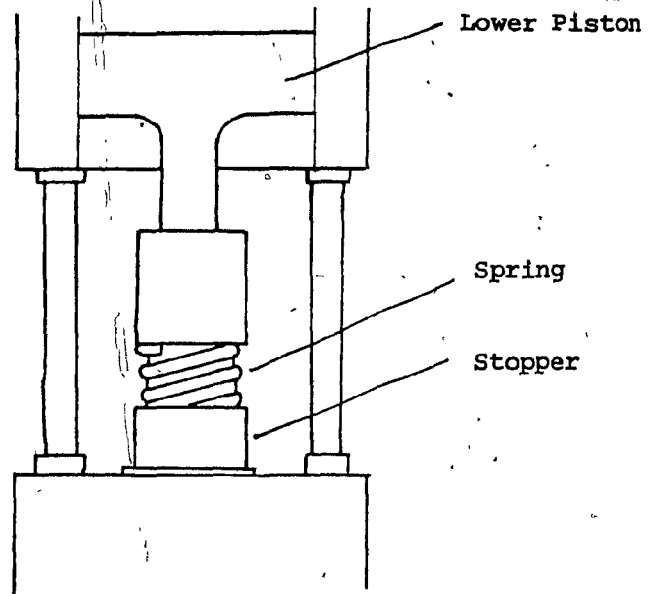


Figure (5.8a). Spring and Stopper Arrangement for Lower Piston.

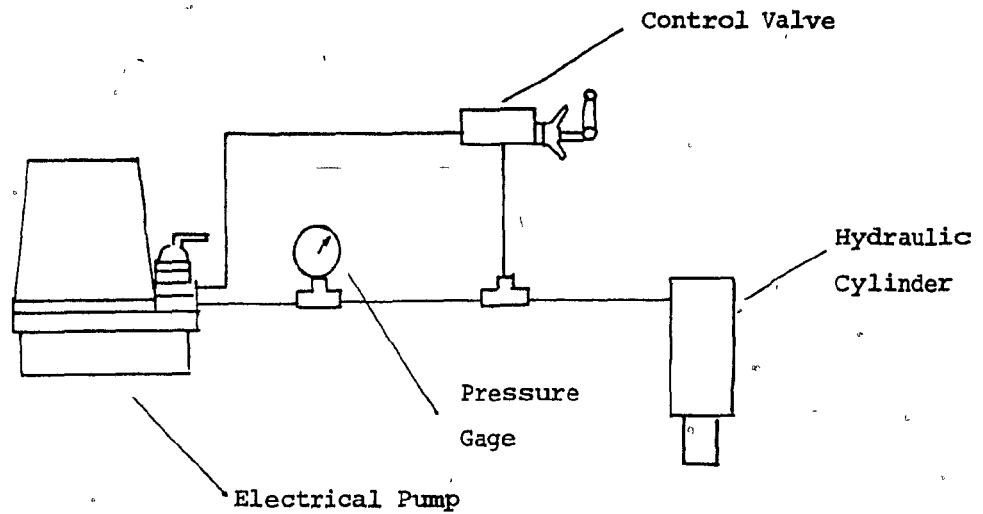


Figure (5.8b). Hydraulic Control System.

The second method was to adapt the shearing device to an Instron tester by coupling the upper piston to the Instron cross-head. The upper piston could then be driven mechanically at desired speed and hence the flow rate could be accurately controlled.

The third method was to make use of a hydraulic control system for each cylinder as shown in Figure (5.8b). Each piston system could be attached to electrically driven hydraulic pumps and an adjustable pressure relief or control valve. The pressure difference could then be adjusted to give a controlled flow through the gap.

The first method was the simplest one and was used by the previous researchers. This method did not allow precise flow rate control, but it was felt that such a precision was not essential due in particular to the existence of several other uncontrolled variables.

5.1.2 Modification of Shearing Device and Molding Procedure

5.1.2.1 Modification in Lower Piston Assembly

For the present work, it was decided that the shearing device be used in accordance with the first method described above, but with a modified spring and stopper system.

5.1.2.1.1 Reasons for Modification

The original spring and stopper assembly necessitated travel of the lower piston through a constant distance before the stopper was reached. Consequently, a large amount of material sometimes had to be transferred from the upper reservoir through the gap into the lower reservoir before the system pressure could be built up.

It was decided to modify this assembly so that the travel of the lower piston could be preset before the transfer operation. In this way, any desired amount of material could be transferred. Consequently, the blocks in the reservoirs could be re-used for making successive plates.

5.1.2.1.2 Operation of Modified Lower Piston Assembly

Figure (5.9) shows the new lower piston assembly. It essentially consisted of two concentric cylinders and a threaded piston-rod. The lower piston was attached to the piston-rod. A spring between the inner and outer cylinders provided the counterforce during the transfer operation. The position of the inner cylinder could be adjusted in relation to the lower piston and the outer cylinder by a hexagonal nut. During the transfer operation, the inner cylinder moved down with the lower piston into the outer cylinder till it reached the bottom. No further transfer could then occur and hence the system pressure would start increasing upon application of more force on the upper piston.

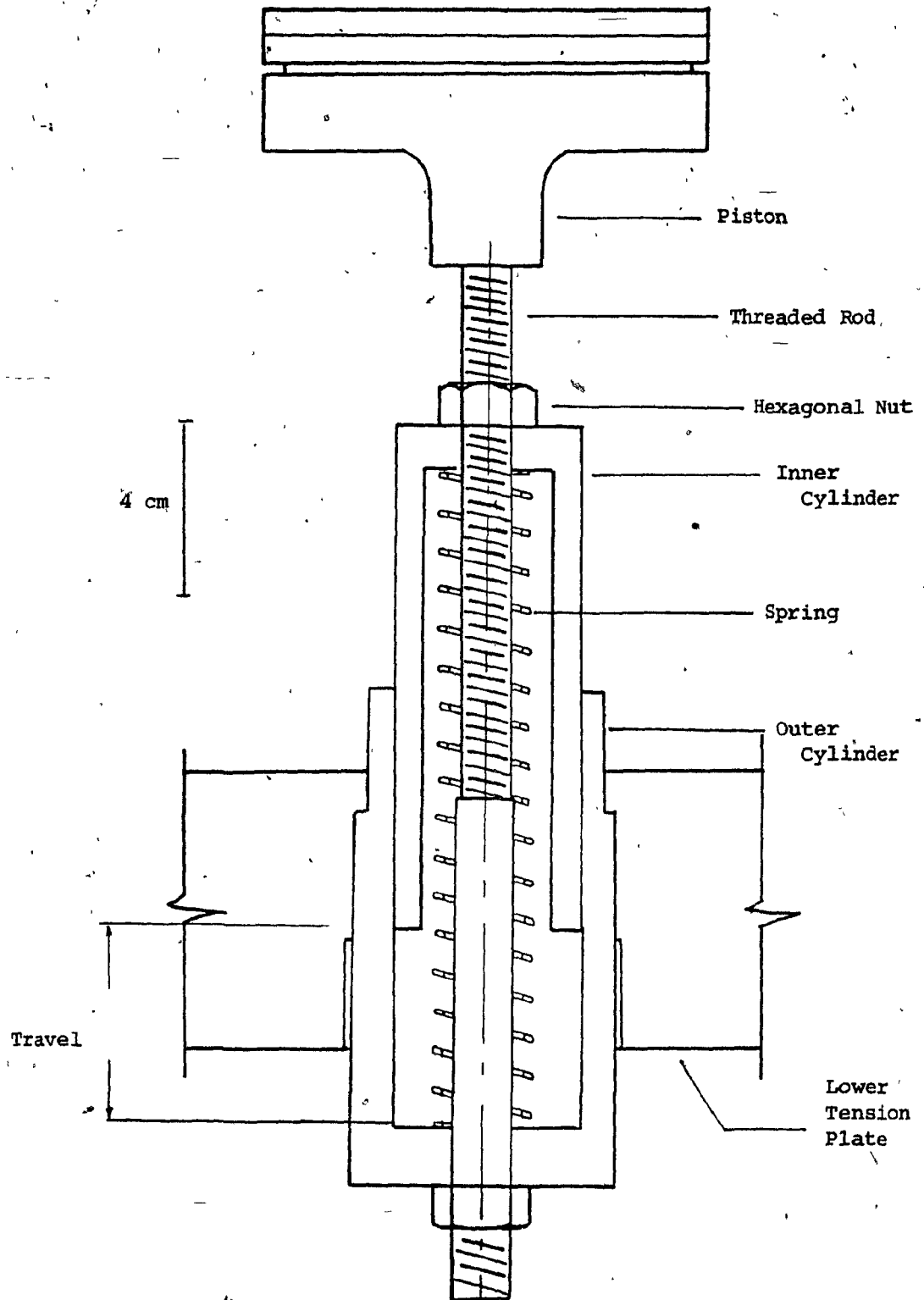


Figure (5.9). Modified Lower Piston Assembly.

Since the position of the inner cylinder with respect to the outer cylinder could be adjusted by the hexagonal nut, a precise amount of material could be transferred before the system pressure started rising. Thus the lower piston could each time be adjusted to transfer just enough material from the upper reservoir into the gap and then the transfer operation could be stopped.

5.1.2.2 Modification in Molding Procedure

5.1.2.2.1 Reasons for Modification

As discussed previously, the sheared plates were made in two stages: first a pair of premoldings with randomly oriented fibers was obtained which was then used in the shearing device. The basic objective behind using the compressed premolding blocks in the shearing device was to minimize the inclusion of air bubbles or voids in the sheared plates. However, some preliminary experiments showed that the premolding operation was relatively involved.

During heating of the premolding device, four cartridge heaters were installed in the holes of each half of the device, while during cooling cycle, the heaters had to be removed to be replaced by cooling tubes. This practice made the entire procedure highly laborious and time consuming. Also, the four drilled holes gave relatively ineffective cooling as against the shearing device where each half was provided with a large rectangular cooling cavity adjacent to the thin central gap.

It appeared that sheared plates of good quality could be made by directly using the pellets in the shearing device and avoiding the use of the premolding device completely, making the whole operation quite efficient. The pellets could be compressed in the shearing device to make an "equivalent premolding" and two such blocks could be used to make a sheared plate as described before. Time saving could be achieved both by efficient cooling in the shearing device and re-use of the reservoir blocks for making successive sheared plates.

5.1.2.2.2 Modified Procedure

(a) Basic Procedure in making a Premolding in the Shearing Device.

For this purpose, pellets of the material were introduced into the upper reservoir. The space between the two halves was closed at the bottom by the lower piston just to prevent any pellets that passed through the central gap into the region of the lower reservoir from falling out. Some pellets would thus collect in the lower reservoir, in the case of the wider gap, however, in almost all the cases, most of them filled the upper reservoir. Approximately 200 - 250 ml of pellets were used for making a block.

The device was heated by four 300W cartridge heaters installed in each half. Because of the large mass of metal involved, it took approximately 35 - 40 minutes for the entire device to heat up to the desired temperature of 190°C . The power supply to the heaters

was controlled manually via two autotransformers (Variacs) and this method proved adequate for controlling temperature within $\pm 2^{\circ}\text{C}$ during compression or transfer stage. The highly viscous molten mass was then compressed under reasonable pressure applied hydraulically to the upper piston, so as to pack the mass but not to cause excessive flow. Throughout the operation the two halves were held together by a horizontal force (of 50000 lb.) applied by the hydraulic cylinder.

After compression, heating was stopped and cooling water was turned on. It was possible to cool the device to below 50°C in about 35 minutes time. Device was then opened to remove the block of polymer. It may be noted that though the pressure during cooling was quite low (of the order of $2 - 4 \text{ N/mm}^2$ (300 - 500 psi)) (as against 20 N/mm^2 (3000 psi) used in premolding device), inclusion of air bubbles in the blocks was not very high.

The resulting block is shown in Figure (5.10). A partial flow into the gap was unavoidable, however, the resulting portion could be cut off and the remaining block could be used in the upper or lower reservoir.

(b) Basic Procedure in making Successive Plates from a given pair of Reservoir Blocks

Once two blocks of a material were made by the procedure described above, they were placed in the two reservoirs, the central gap

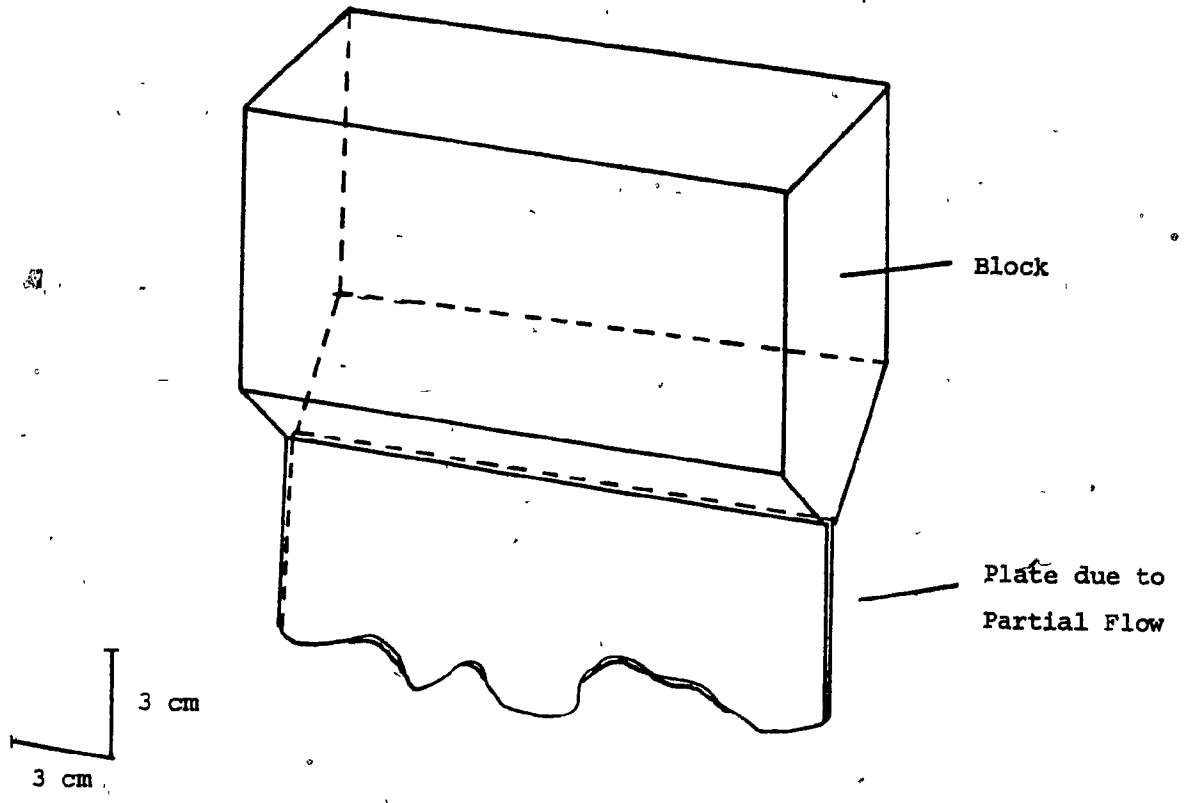


Figure (5.10). "Equivalent Premolding" Made in Shearing Device.

remaining empty. The device was heated to 190°C . The inner cylinder of the lower piston assembly was adjusted to proper level in order to allow transfer of a volume of the molten material slightly more than that necessary to fill the gap. The two halves were held together during the transfer operation by a horizontal force of about $5 \times 10^6 \text{ N}$ (120,000 lbs.). The air initially present in the gap must have been forced out through thin spaces between the two halves, but no significant leakage of plastic was ever noticed.

When transfer was complete, the pressure on the molten polymer was increased to approximately 2000 N/cm^2 (3000 psi). The heaters were turned off and the device was cooled to below 50°C by circulating water in the channel to get the sheared molding shown in Figure (5.7). The central sheared plate with preferential fiber orientation in the flow direction was cut off and retained. It may be noted that air inclusions or voids in the plates were insignificant for all the composite systems studied.

The upper and lower reservoir blocks were re-used for making more plates. Re-use of blocks meant reheating of the material and on successive usage, it might be expected to cause degradation of the polymer. However, probably due to relatively lower temperature involved, there was no visual sign of degradation in any of the three to four plates which could be made from one pair of blocks. Also, the mechanical properties tested later did not indicate any systematic reduction in properties

(cf. Chapter VI). Hence, this procedure was considered satisfactory for the purpose.

As more plates were made, the upper block reduced in size while the lower block increased in volume. This larger block was used in the upper reservoir for making more plates. It might be expected that the divergent flow from the central gap into the lower reservoir would cause some rotation of the fibers in the transverse direction resulting ultimately into a more or less random orientation distribution. Hence, the structure of the material in the upper and lower reservoirs can be considered almost identical, and not significantly affected by the shearing in the gap. The mechanical properties measured later also did not reveal any systematic difference for the plates made by re-use of the larger block from the lower reservoir in the upper reservoir.

In this manner, it was possible to make usually three sheared plates of 1.6 mm (1/16 in.) thickness and two plates of 3.2 mm (1/8 in.) thickness, using one pair of the reservoir blocks, that were practically identical as far as structure and mechanical properties were concerned.

There is an additional point to be noted. The fast rate of cooling in injection molding can have significant influence on the properties of the final product. In this study, the rate of cooling was rather slow as is evident from the time required for cooling and was not considered a parameter. Consequently, all the plates for both 1.6 mm

and 3.2 mm thicknesses were made under essentially identical conditions of heating and cooling.

The slow rate of cooling may allow molecular rearrangements within the material, resulting into randomization and possibly partial elimination of internal stresses. However, it cannot have any significant influence on the fiber structure which plays a dominant role in determining the composite properties.

Also, the rate of cooling for 3.2 mm thick plates was somewhat lower due to greater gap width as compared to that for 1.6 mm thick plates. This can have some influence on the matrix properties in the plates of these two thicknesses.

5.2 Materials Used

The composite systems used in this study were based on Polystyrene (PS) and high density Polyethylene (PE).

Polystyrene represents an example of a brittle matrix while polyethylene is one from the class of ductile materials. Effect of addition of brittle glass fibers to these materials on mechanical properties under different loading conditions (static versus impact, for example) and nature of failure could be very different. Also, matrix - fiber adhesion is generally found to be better in PS than in PE. All these factors motivated the choice of these two matrices.

The PS based systems were kindly supplied by Fiberglas Canada (Guelph, Ontario) and were specially compounded for the group's research. The PE based systems were of commercial grade and were kindly supplied by Wilson - Fiberfil International (Evansville, Indiana). Details on these polymers are provided in Table (5.1).

The fibers used for reinforcement in both cases were of a typical 'E' glass, approximately 10 μ m in diameter and initially in the form of 6 mm (1/4 in.) chopped strands. The fiber contents of various systems were as follows:

(1) PS - 0% , 20% and 40%

by weight

(2) PE - 0% , 20% and 30%

by weight

These are nominal compositions and exact compositions may differ slightly from these (Padmanabhan (64)).

It may be noted that for the PS based systems, the compounding process included extrusion and pelletization and PS (0%) was also processed in a similar manner in an attempt to achieve identical matrices in both the unfilled and filled systems. This was not done in the case of PE based systems, consequently, PE in the unfilled and filled systems did not have exactly identical history.

TABLE (5.1)DETAILS ON MATRIX MATERIALS

<u>PROPERTY</u>	<u>PE (REF. 68)</u>	<u>PS (REF. 64)</u>
Manufacturer	Amoco	Monsanto
Resin Identification	4140B	HF - 55
Density (g/cc)	0.95	1.05
Melt Index (9/10 min.)	20.0	-
Grade of SFRTPs	Commercial	Specially Compounded

5.3 Testing Procedures

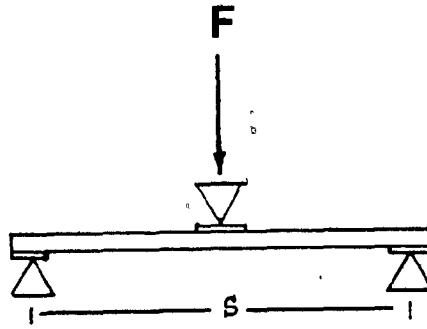
The sheared plates were tested in the direction of flow (longitudinal direction l) and the one normal to it (transverse direction t) for the following mechanical properties.

- (1) Flexural Modulus.
- (2) Tensile Modulus.
- (3) Tensile Strength.
- (4) Izod-type Impact Strength.
- (5) Tensile Impact Strength.

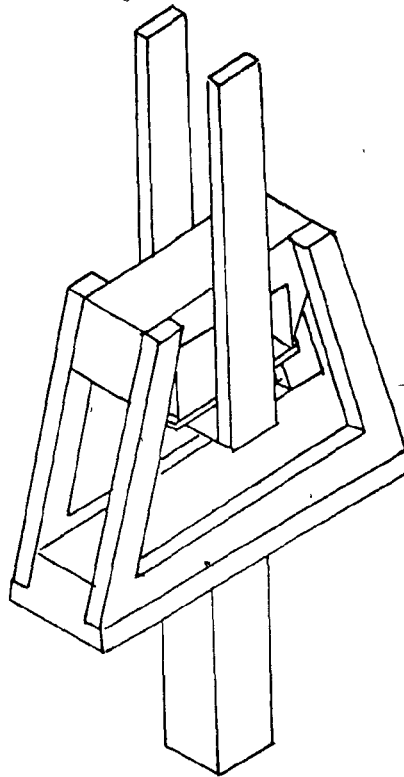
Because of the relatively involved procedure for making the sheared plates, a compromise was essential between maximizing the number of test-pieces cut from a single plate and having adequately large test-piece sizes. Attention was always given to reliable measurements and sufficient data points for each property. The methods adopted for various tests were quite similar to those recommended by ASTM (69), but in several cases actual procedures and test-piece dimensions had to be modified according to the necessities and convenience.

5.3.1 Flexural Modulus

Flexural modulus was determined by three-point bending tests of rectangular test-pieces cut from the sheared plates (ASTM D790



(a) Schematic Diagram.



(b) Three-Point Bending Device. (Not to Scale).

Figure (5.11). Three-Point Bending Test.

(69)). Figure (5.11a) schematically shows the three-point bending test, with the actual device in Figure (5.11b).

The pattern of cutting test-pieces from 1.6 mm (1/16 in.) thick plates is shown in Figure (5.12a). This method allowed six test-pieces to be cut in either direction from a single plate. The edges of test-pieces were machined on a Tensilkut router to exact dimensions using a die of corresponding shape and dimensions. The actual test-piece dimensions are shown in Figure (5.12b). For these thin test-pieces, a span of 25 mm (1 in.) for three-point bending test was adequate.

The pattern of cutting test-pieces from 3.2 mm (1/8 in.) thick plates is shown in Figure (5.13a) with actual test-piece dimensions in Figure (5.13b). Here, it was possible to obtain only four test-pieces in a given direction from one plate. For these thicker samples, a span of 50 mm (2 in.) was used for the three-point bending test.

Test was carried out by mounting the three-point bending device on an Instron testing machine (Model 1125). All the measurements were done at a low crosshead speed of 2 mm/min. Deflection of the test-pieces was kept as low as possible to avoid irreversible damage in the material, thus allowing the same test-pieces to be subsequently utilized for measuring other properties. A test of reversibility was done for each test-piece by turning it over and carrying out the bending test again.

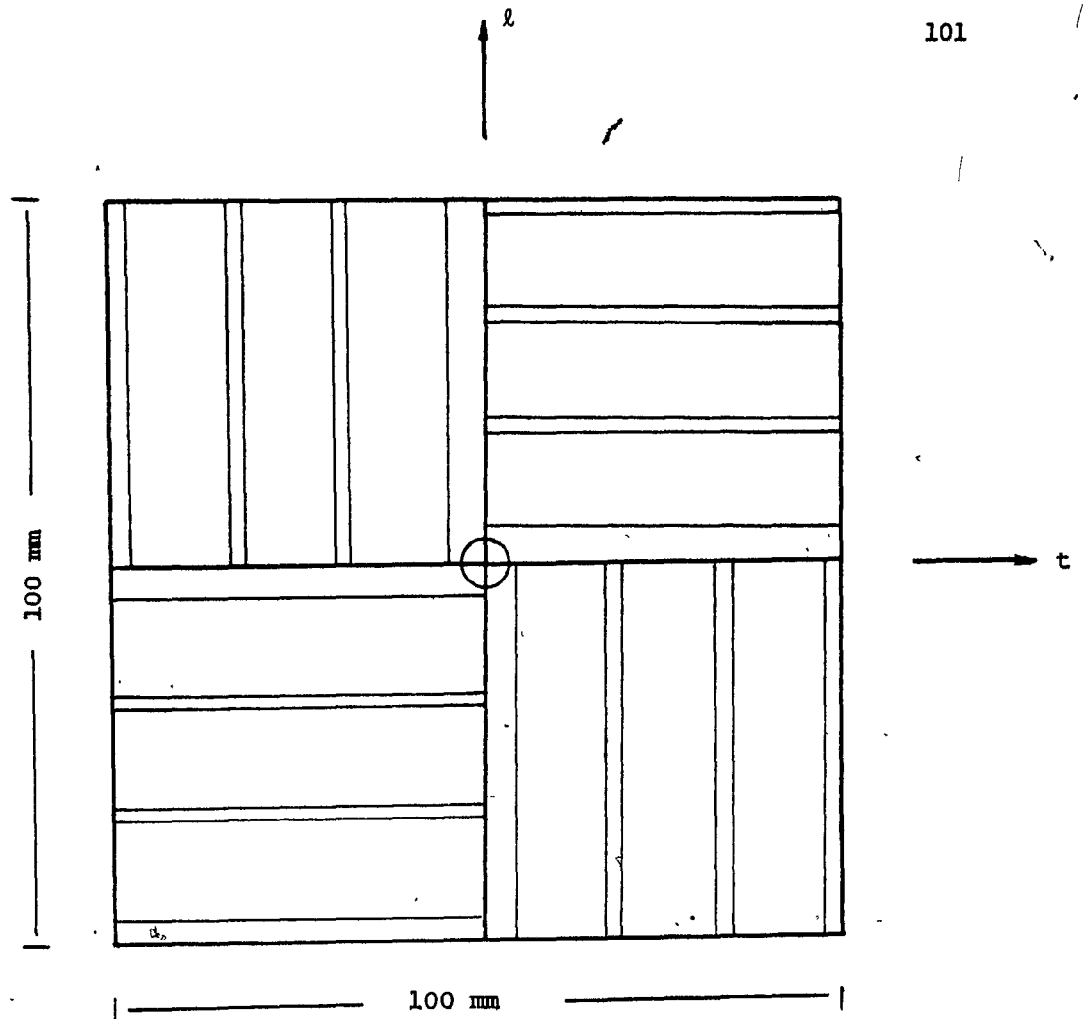


Figure (5.12a). Pattern for Cutting Flexural Test-pieces from 1.6 mm (1/16 in.) Thick Plates.



Figure (5.12b). Actual Dimensions of 1.6 mm (1/16 in.) Thick Flexural Test-pieces.

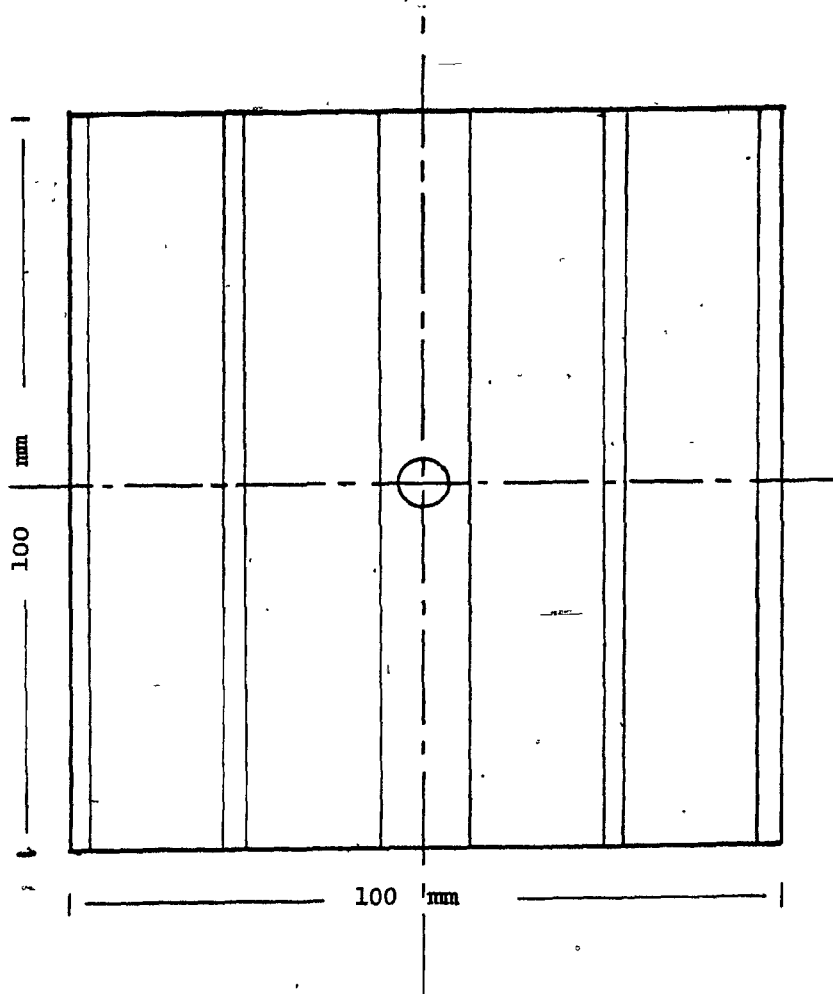


Figure (5.13a). Pattern for Cutting Flexural Test-pieces from 3.2 mm (1/8-in.) Thick Plates.

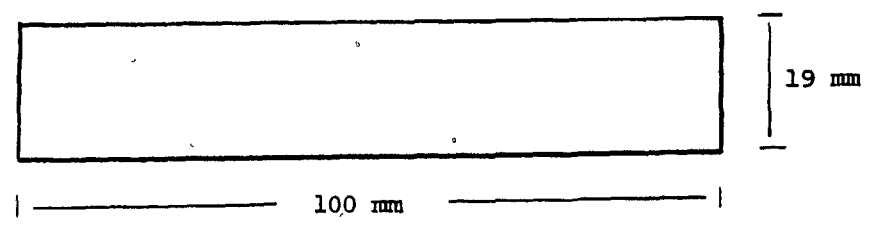


Figure (5.13b). Actual Dimensions of 3.2 mm (1/8 in.) Thick Flexural Test-pieces.

A load v/s deflection curve was obtained on the Instron chart recorder. The flexural modulus could be determined as

$$E^f = \frac{1}{4} \frac{S^3}{bd^3} \left(\frac{F}{\delta} \right) \quad (5.1)$$

where S is the span length,

b is the sample width,

d is the sample thickness

and (F/δ) is the initial slope of the load-deflection curve.

It should be noted that in the three-point bending test, the crosshead movement may not be only due to the test-piece deflection, but also due to the bending or twisting of the device and/or machine (Daniels et. al. (70), Wagner et. al. (71)). Deformation attributable to the device, in particular, was found to be appreciable in our case. Consequently, it was necessary to apply a correction before E^f could be determined.

A load-deflection curve corresponding to the 25 mm (1 in.) span three-point bending device was obtained using a steel bar of the same width as the test-pieces, but four times thicker (thickness of the bar = 6.4 mm). Since the deflection of the bar itself was negligible (cf. Appendix A), the measured deflection essentially represented the deflection due to the device. Five individual measurements were taken.

Table (5.2a) lists the values of the slopes of the load - deflection curves. The mean was used for correcting the slope of load - deflection curve of each test-piece as

$$\frac{1}{(F/\delta)_{\text{corr.}}} = \frac{1}{(F/\delta)_{\text{app.}}} - \frac{1}{K} \quad (5.2)$$

where $(F/\delta)_{\text{corr.}}$ represents corrected slope,

$(F/\delta)_{\text{app.}}$ represents measured slope

and K represents the mean slope for the device load - deflection curve.

The correction factor for the 50 mm (2 in.) span three-point bending device was also determined using a steel bar of 19 mm width (same as that of test-pieces) and 6.4 mm thickness. Table (5.2b) shows the five individual measurements and the mean value was used in equation (5.2) for correcting the slopes for bending tests of 3.2 mm thick test-pieces.

The corrected slopes for both 1.6 mm and 3.2 mm thick test-pieces could then be used in equation (5.1) for determining the flexural moduli. Further details on this correcting procedure may be found in Appendix A .

TABLE (5.2)

SLOPES OF LOAD VERSUS DEFLECTION CURVES
FOR DEFLECTION OF THREE-POINT BENDING DEVICES

(a) 25 mm Span		(b) 50 mm Span	
NO.	SLOPE (N/m) $\times 10^{-4}$	NO.	SLOPE (N/m) $\times 10^{-4}$
1	10.26	1	3.038
2	13.72	2	3.266
3	10.85	3	3.811
4	11.11	4	3.322
5	10.88	5	3.385
MEAN	11.364	MEAN	3.364

5.3.2 Tensile Modulus

Tensile modulus was determined by low speed tensile testing on the Instron testing machine (ASTM D638 (69)). The tensile testing arrangement is schematically shown in Figure (5.14).

Dumbbell.- shaped test-pieces similar to ASTM type IV were used for this purpose, though the length was slightly smaller. Actual dimensions of the test-pieces are shown in Figure (5.15). These test-pieces were prepared by cutting rectangular pieces from the sheared plates and machining them to the dumbbell - shape using a die on a router as illustrated in Figure (5.16).

An Instron extensometer (Model 2630-004, Gage length 25 mm, Range 0 - 1% for this study), was attached to the reduced section of the test-pieces for measuring extension accurately. During the test, the Instron recorder chart is made to move in proportion to the test-piece extension by a signal from the extensometer, while the recording pen moves in proportion to the load. Thus load versus strain can be accurately recorded.

Initial slope of the load-strain curve was determined and the tensile modulus was calculated as

$$E^t = \frac{\text{stress}}{\text{strain}} = \frac{F/A}{\epsilon} = \frac{1}{A} \left(\frac{F}{\epsilon} \right) \quad (5.3)$$

where A is the area of cross-section of the reduced part of the test-piece

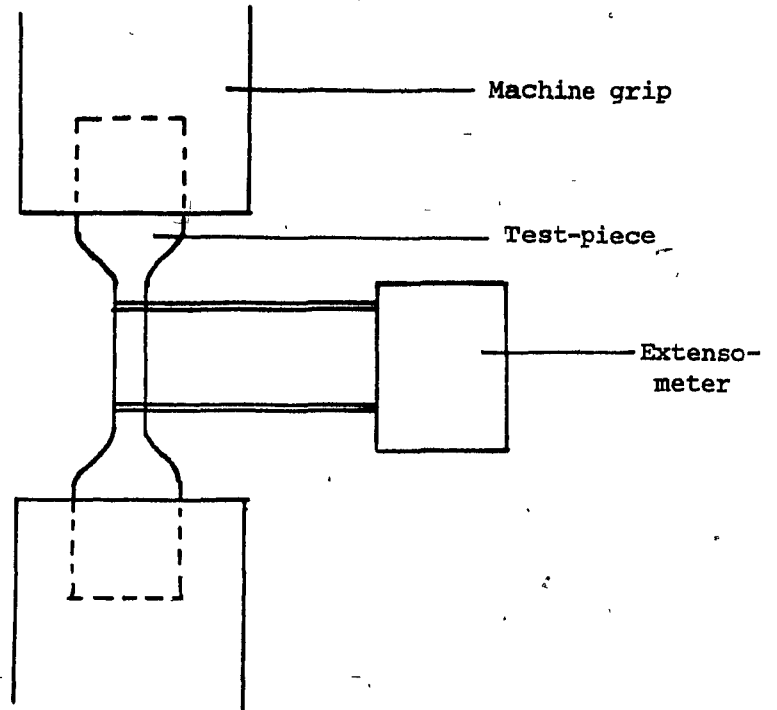
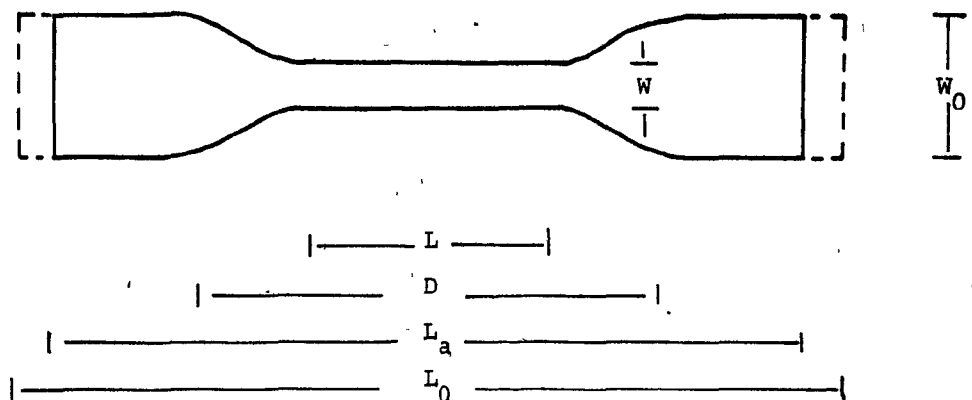


Figure (5.14). Schematic Diagram of Tensile Modulus Measurement.



- L Length of narrow section (33 mm).
- D Distance between grips (64 mm).
- L_a Actual overall test-piece length (100 mm).
- L₀ Overall length for ASTM type IV (115 mm).
- W Width of narrow section (6 mm).
- W₀ Overall width (19 mm).

Figure (5.15). Actual Dimensions of Tensile Modulus Test-pieces.

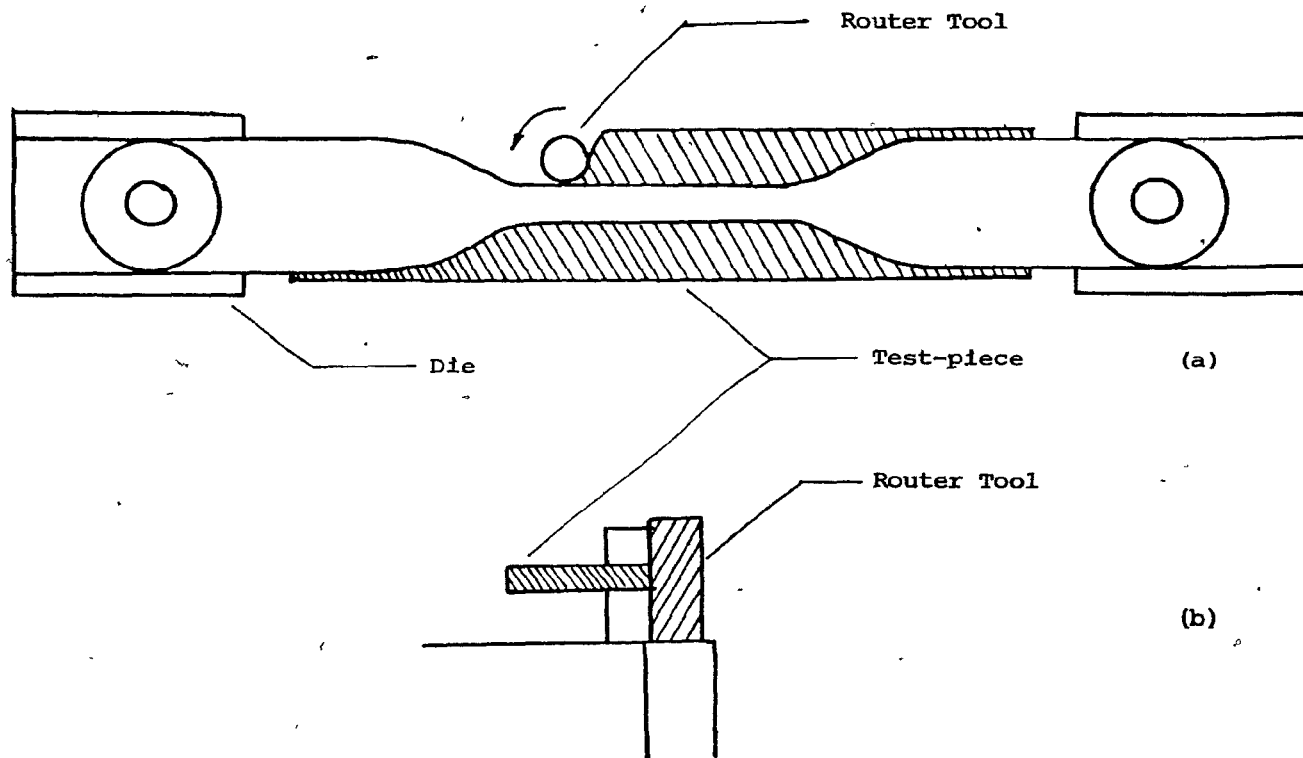


Figure (5.16). Schematic Diagram Showing Machining of Dumbbell Shaped Test-pieces.
(a) Top View. (b) Side View.

and (F/ϵ) is the initial slope of the load-strain curve.

The main advantages of using an extensometer versus using crosshead displacement as equivalent to test-piece extension were:

- (1) it allowed accurate recording of deformation,
- (2) it eliminated the use of an arbitrarily defined gage length l_0 in the calculation of strain $(\epsilon = \Delta l / l_0)$.

5.3.3 Tensile Strength

Tensile strength measurements were similar to tensile modulus measurements (ASTM D638 (69)) except that test-pieces were taken to yield or break point.

For 1.6 mm (1/16 in.) plates, the test-pieces were prepared by machining those first used for flexural test to dumbbell shape. The actual dimensions of these test-pieces are shown in Figure (5.17a). For 3.2 mm (1/8 in.) plates, again test-pieces similar to ASTM type IV, shown in Figure (5.15), were used.

The test-pieces were held in the grips of the machine with almost identical tightening pressure every time. Figure (5.17b) shows a

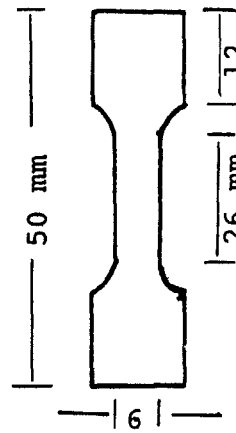


Figure (5.17a). Actual Dimensions of 1.6 mm (1/16 in.) Thick Tensile Strength Test-pieces.

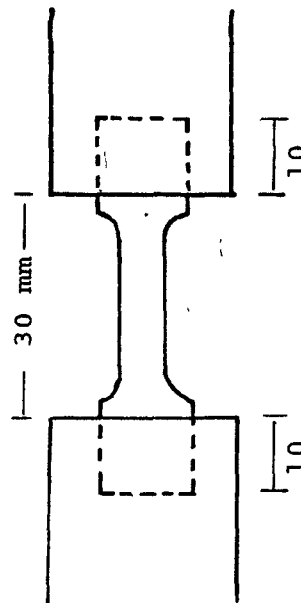


Figure (5.17b). 1.6 mm (1/16 in.) Thick Tensile Strength Test-piece Held in Grips.

1.6 mm (1/16 in.) thick test-piece held between two grips. Admittedly, the test-piece dimensions were non-standard and end tab areas available for gripping were relatively small, however, as would be seen later (cf. Chapter VI), results obtained were quite reproducible and comparable to those obtained for the standard sized 3.2 mm (1/8 in.) thick test-pieces.

For brittle PS systems and filled PE systems, break occurred before yield and hence maximum force at break was used for calculating tensile strength. For highly ductile unfilled PE, excessively high elongation was necessary before the test-piece could break. Consequently, maximum force at yield point was used to calculate strength at yield. Figure (5.18) illustrates this point.

The tensile strength was calculated as

$$\sigma^t = \frac{F_m}{A} \quad (5.4)$$

where F_m is the maximum force at yield or break

and A is the cross-sectional area for the reduced part of the test-piece.

5.3.4 Izod Impact Strength

Izod-type impact strengths were determined using Testing

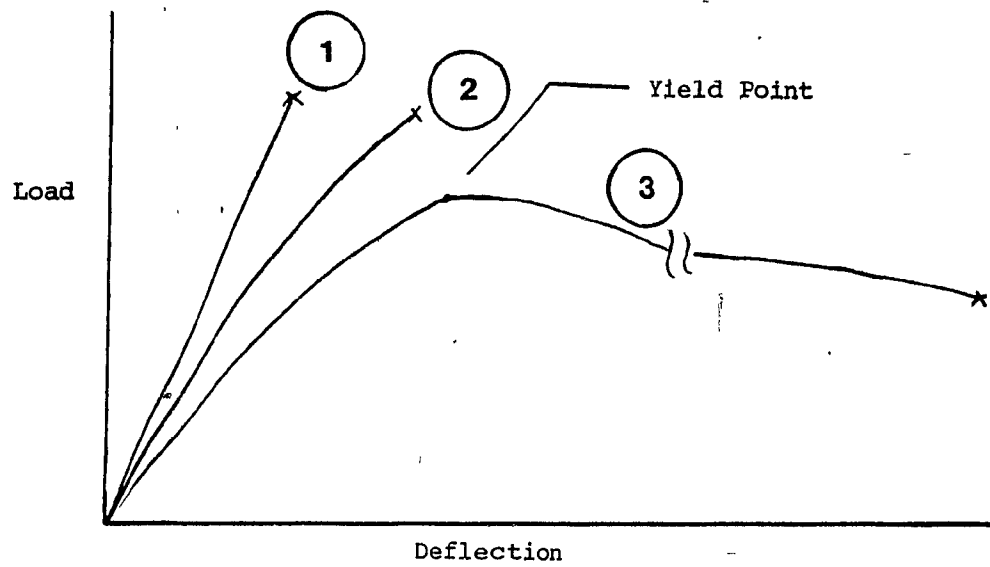


Figure (5.18). Typical Load-Deflection Curves.

- (1) PS Systems.
- (2) Filled PE Systems.
- (3) Unfilled PE .

Machine International (TMI) pendulum impact tester. The standard ASTM D256 (69) procedure had to be modified to suit the test-piece size and shape. Consequently the results obtained should be considered only for comparisons among themselves.

A 2.72J (2 ft/lb) hammer was used that struck the specimen at a speed of 3.44 m/s (11 ft/s). The test is shown schematically in Figure (5.19).

The test-pieces for both 1.6 mm and 3.2 mm plates were cut as shown in Figure (5.20a). Actual dimensions of the test-pieces are shown in Figure (5.20b).

According to ASTM D256 (69) procedure, an Izod test-piece should be struck by the hammer on the narrow side of the cross-section (see Figures (5.21a)). However, in our case, it was not possible to hold the thin test-pieces according to the specified procedure. Consequently, the test-pieces were held such that the hammer struck the wider side of the cross-section. (See Figure 5.21b).

The amount of energy W_a^I required to break the test-piece was measured directly on a dial on the machine. However, it was necessary to make a correction for frictional and windage losses. For this purpose, the hammer was allowed to swing without any test-piece, and the energy W_c^I so measured on the dial corresponded to machine frictional and windage losses (ASTM D256).

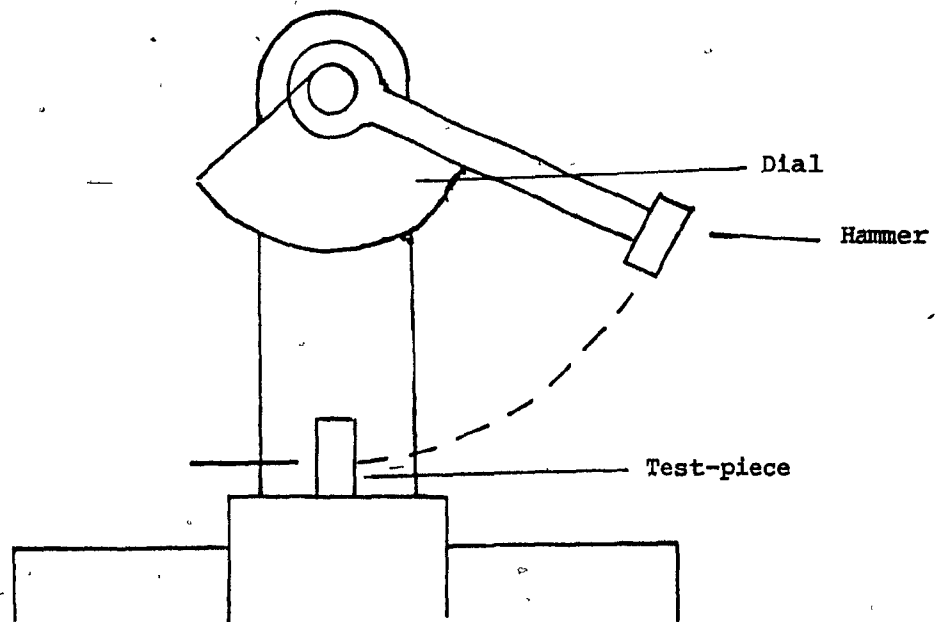


Figure (5.19). Schematic Diagram of Izod Impact Testing.

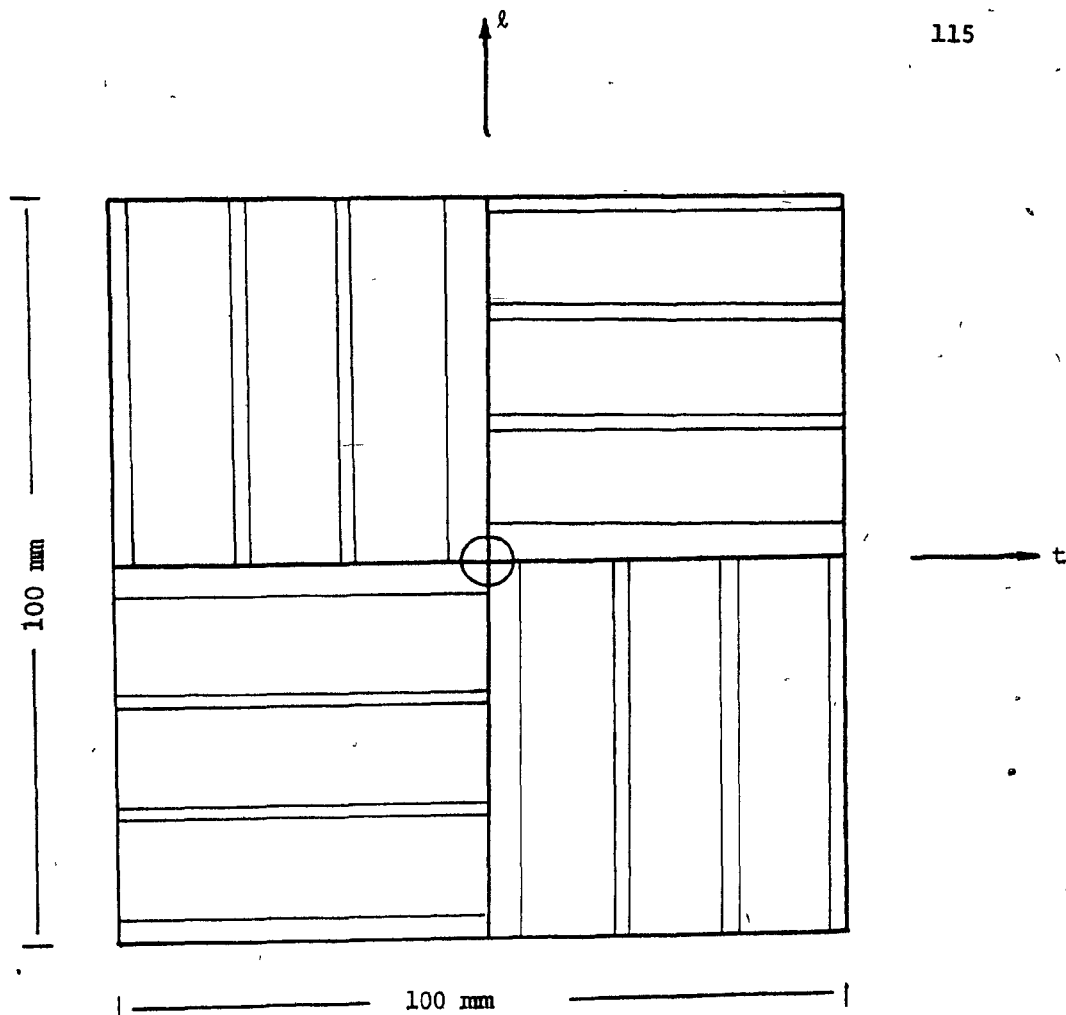


Figure (5.20a). Pattern of Cutting Test-pieces for Izod-type Testing.

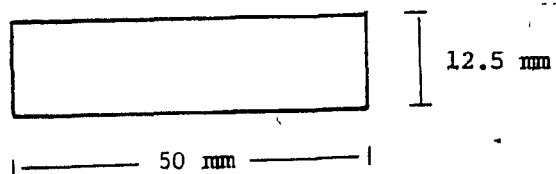


Figure (5.20b). Actual Dimensions of Izod-type Impact Test-pieces.

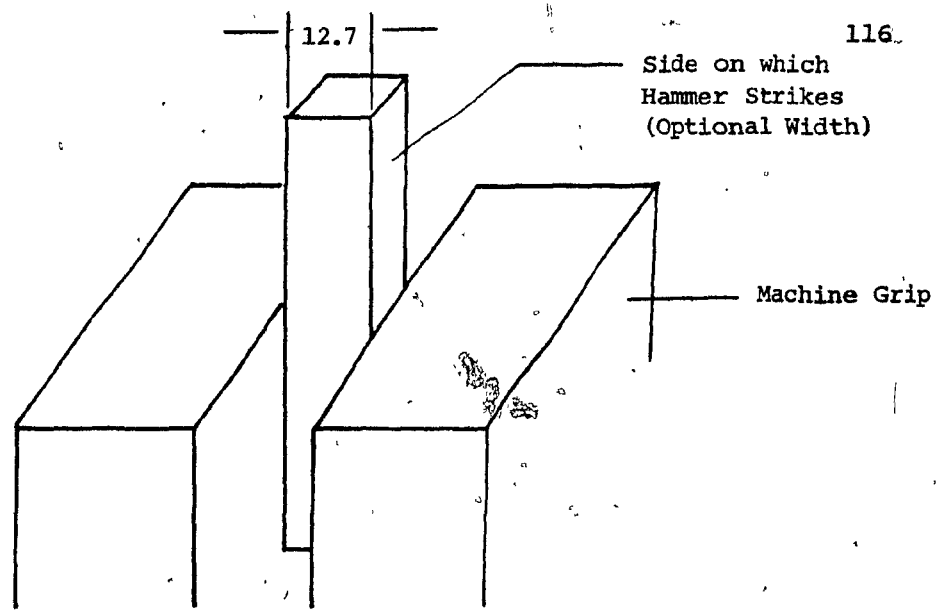


Figure (5.21a). Holding the Test-piece in Standard Izod Impact Test.

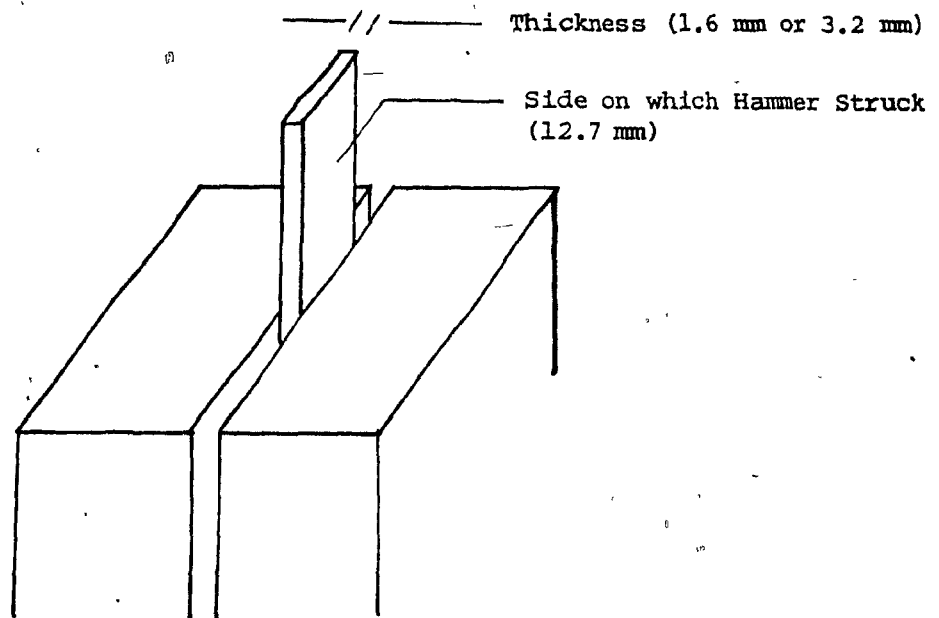


Figure (5.21b). Schematic Diagram of Izod-type Test Carried out in this Study.

The Izod impact energy W^I to break the sample was calculated as

$$W^I = W_a^I - W_c^I \quad (5.5)$$

5.3.5 Tensile Impact Strength

Tensile impact strength determinations were carried out using the same Testing Machines International (TMI) pendulum Impact tester. The testing procedure was similar to that recommended by ASTM D 1822 (69), but test-piece geometry was modified for reasons discussed below.

A 2.72 J (2 ft/lb) hammer was used for all the tests. The test-pieces for both the 1.6 mm and 3.2 mm thick plates were prepared by cutting rectangular pieces as in Figure (5.20a) and machining them to a shape similar to that specified by ASTM D 1822 (see Figure (5.22a)).

The test is schematically shown in Figure (5.23). The test-piece is held between two grips, one attached to a pendulum head and the other in a crosshead. During the swing of the pendulum, the crosshead strikes an anvil at the bottom of the swing bringing one end of the test-piece suddenly to rest while the other end keeps moving with the

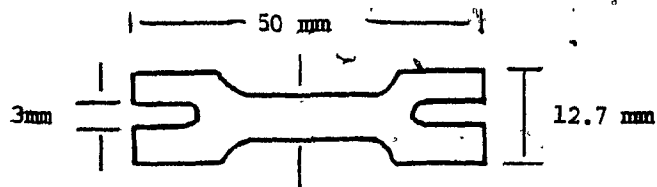


Figure (5.22a). Actual Dimensions of Tensile Impact Test-piece.

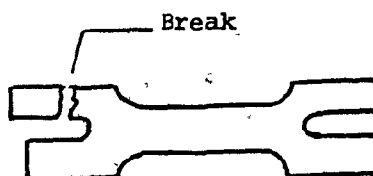


Figure (5.22b). Break Under Tensile Impact at the End.

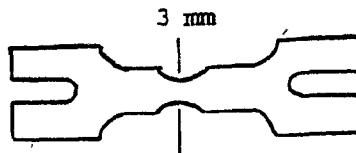
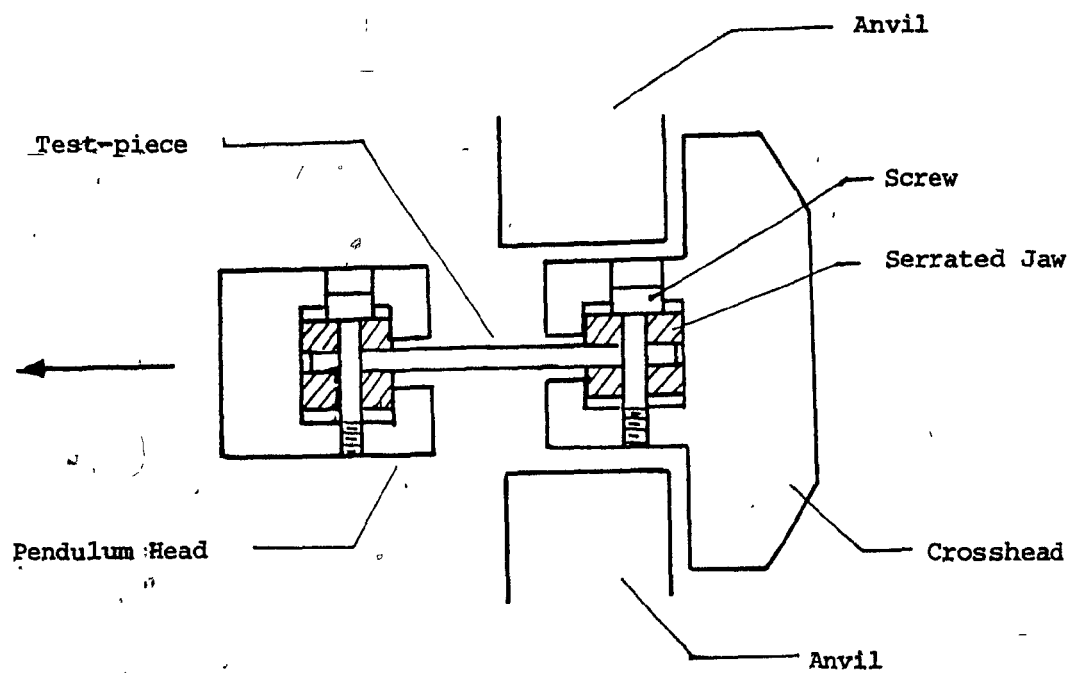


Figure (5.22c). Modified Tensile Impact Test-piece.



(a) View along Pendulum Arm.



(b) Holding the Test-piece.

Figure (5.23). Schematic Diagrams of Tensile Impact Testing.

pendulum, causing ultimately a failure under tensile impact. The loss in energy of the pendulum can be measured on a dial.

As shown in Figure (5.22a), the wide end tabs of the dumbbell shaped test-pieces have to be reduced by cutting slots for the screws holding two jaws of the grips to pass through (Figure (5.23b)). Hence, the area at the ends becomes comparable to that of the central reduced section. Some preliminary testing showed that, due to this, many times the failure occurred near the end rather than in the central section (Figure (5.22b)). Development of some extraneous stresses around the slots due to slight test-piece misalignment might also have contributed towards making the end tab areas vulnerable to failure.

To circumvent this problem, the central reduced section of each test-piece was reduced further as shown in Figure (5.22c). It was then possible to confine the break to the narrowest central section. This, however, obviously reduced the amount of energy required to break the test-piece and hence the overall accuracy of the measurements.

During testing, the crosshead upon striking the anvil, bounces backwards with a certain velocity and hence contributes to the energy required for breaking the test-piece. The energy measured on the dial, however, represents only that lost by the pendulum. Consequently it is necessary to incorporate a crosshead bounce correction factor for determining the true energy for test-piece failure. It is also necessary to make a correction for the windage and frictional losses.

The corrected tensile impact energy, W_c^t , could be calculated as:

$$W_c^t = W_a^t - W_f^t + W_b^t \quad (5.6)$$

where W_a^t is the energy measured on the dial,

W_f^t is the correction for windage and frictional losses,

and W_b^t is the crosshead bounce correction factor.

W_f^t was determined, as recommended by ASTM D 1822, by allowing the pendulum to swing without any test-piece and noting the corresponding energy loss. W_b^t was also determined by the method specified in ASTM D 1822. Details on this correction procedure are provided in Appendix B.

CHAPTER VIEXPERIMENTAL RESULTS

Before discussing the results of mechanical testing, it would be appropriate to make additional notes about the conditions under which the plates were made.

Plates for both the PS and PE based systems were made by carrying out the transfer operation in the shearing device at a temperature of $190 \pm 2^{\circ}\text{C}$ and at a volumetric flow rate of approximately 0.5 cc/sec and 1.2 cc/sec for 1.6 mm and 3.2 mm thicknesses respectively. These correspond to the apparent wall shear rates ($\dot{\gamma}_w$) of 12 sec^{-1} and 7 sec^{-1} respectively, calculated according to the equation:

$$\dot{\gamma}_w = \frac{6Q}{t w} \quad (6.1)$$

where Q is the volumetric flow rate, t is the thickness and w is the plate width.

6.1 Results of Mechanical Testing

The results of various mechanical tests carried out for the determination of the properties of the molded plates are presented below and discussed in terms of the expected structure.

6.1.1 Flexural Modulus

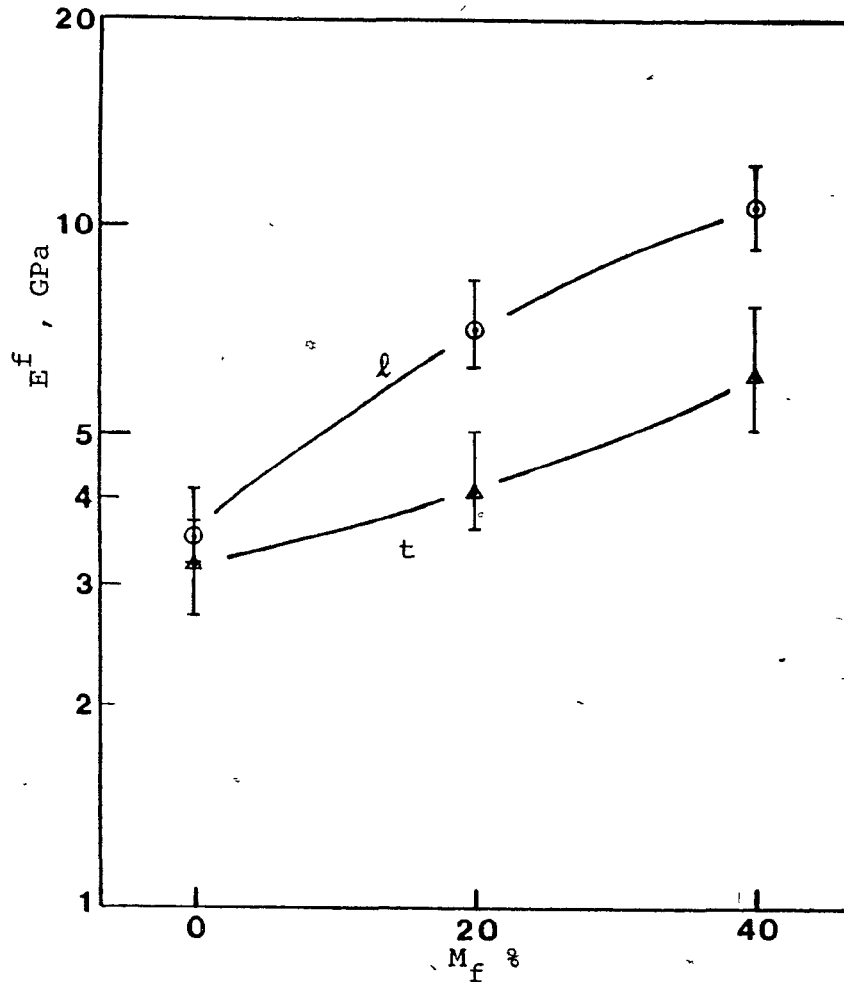
In the case of the 1.6 mm thick plates, eight to ten test-pieces were tested for each composite system and each direction in order to confirm the reproducibility of the plates obtained by the modified procedure of molding.

Figure (6.1a) shows the variation of the flexural moduli with the fiber content for the 1.6 mm thick plates of the PS composites with the bars indicating the maximum and minimum measured values. Though the apparent reproducibility of the measurements is quite good, it was desirable to check it, particularly in two respects:

- (1) Reproducibility with respect to the test-piece location in the plate.
- (2) Reproducibility with respect to the plates made by successive melting of the reservoir blocks and shearing.

In order to illustrate the reproducibility with respect to the test-piece position, individual flexural moduli are listed in Table (6.1) for the test-piece locations identified in Figure (6.2). It is seen that the variations are of a random nature and do not reflect any specific trend.

(a) 1.6 mm (1/16 in.) Thickness.



(b) 3.2 mm (1/8 in.) Thickness.

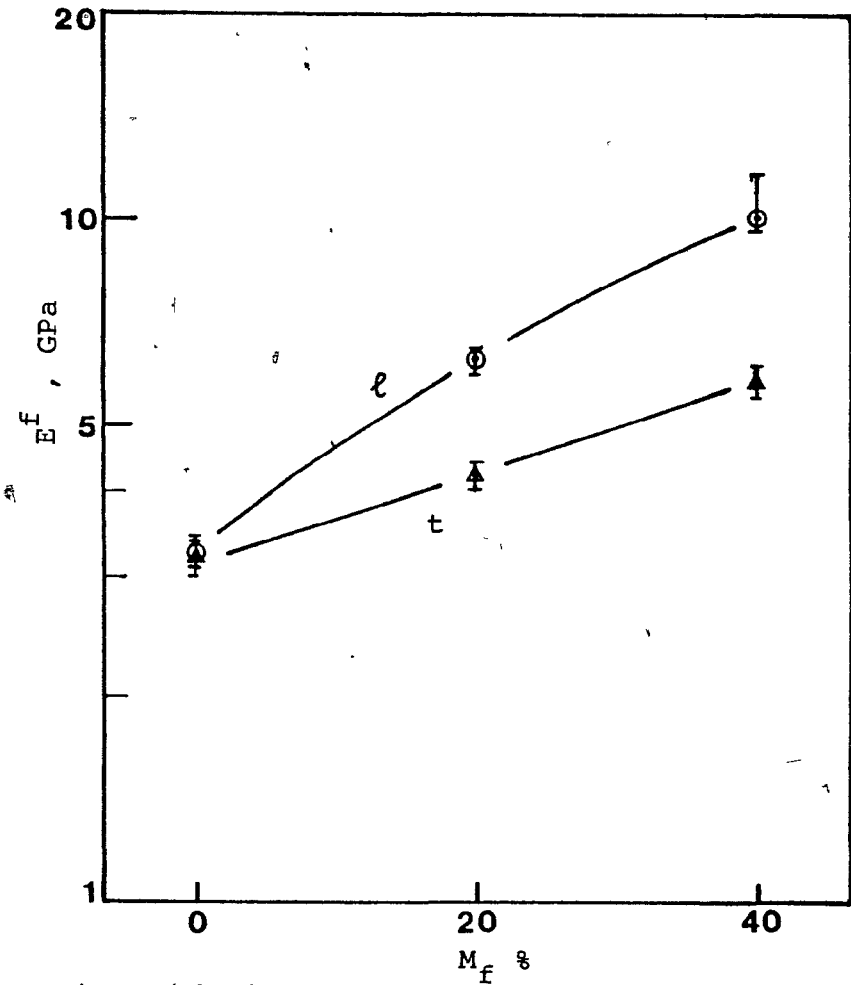


Figure (6.1).. Variation of Flexural Moduli of PS Composites with Fiber Content.

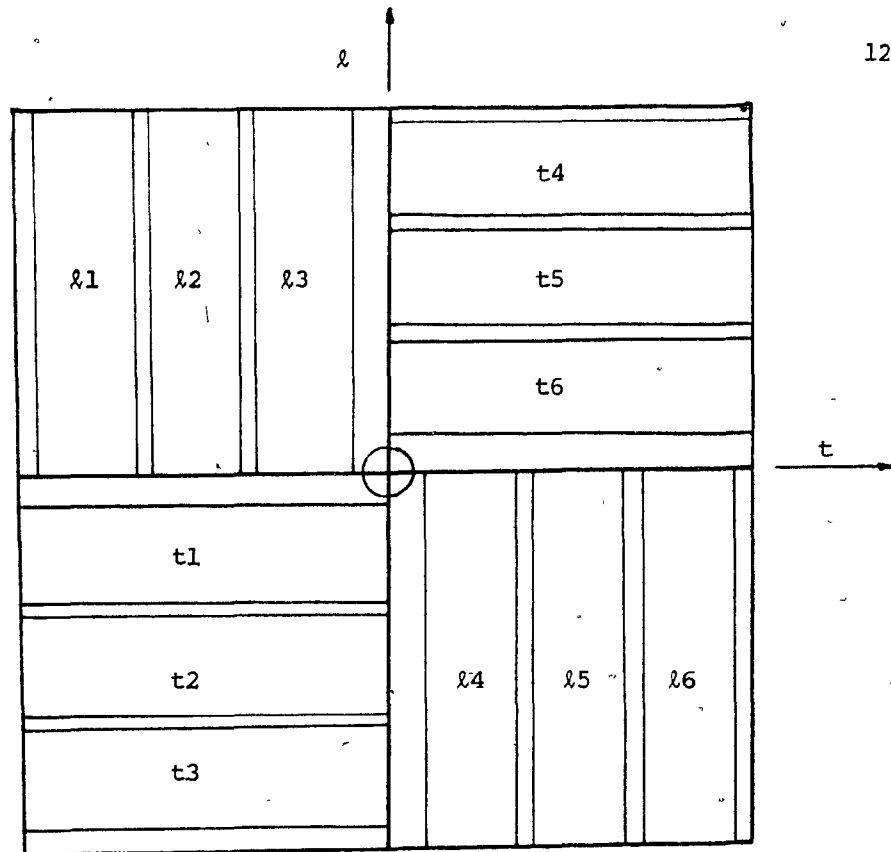


Figure (6.2). Identification of Specimen Location for Table (6.2).

TABLE (6.1) .

FLEXURAL MODULI FOR TEST-PIECES

CUT FROM A GIVEN 1.6 mm THICK PS PLATE

(a) Longitudinal		(b) Transverse	
Test-piece Location (L)	Flexural Modulus (GPa)	Test-piece Location (T)	Flexural Modulus (GPa)
l1	3.54	t1	3.26
l2	3.32	t2	3.18
l3	3.27	t3	3.44
l4	3.62	t4	2.87
l5	3.48	t5	3.40
l6	3.33	t6	3.19

Table (6.2) shows individual flexural moduli for test-pieces cut from three plates made by successive heating and shearing of a given pair of reservoir-blocks. Again, the variations are of a random nature indicating that there was no significant degradation of the material during reheating and that the structures of the resulting plates were similar.

Once the reproducibility with respect to the test-piece position and the molded plates was confirmed, only five test-pieces were used for each composite system and each direction for the 3.2 mm thick plates. Figure (6.1b) shows the variations of the flexural moduli in both the l and t directions with the fiber content for 3.2 mm thick plates of the PS based composite systems. Again, the reproducibility is quite good.

For an easier comparison of the results for the two thicknesses, the mean values of the corresponding composite systems are presented side by side in Table (6.3). In the case of 3.2 mm thick plates of unfilled PS, the flexural moduli in both the l and t directions are essentially identical and these values are again comparable to the flexural modulus for 1.6 mm thick plates in the t direction. The flexural modulus in the l direction for 1.6 mm plates, however, is slightly higher. This may arise due to a somewhat greater degree of molecular orientation in the thinner plates of unfilled PS resulting from a relatively higher shear rate which may subsequently remain frozen due to comparatively shorter time for cooling the thinner plates.

TABLE (6.2).

FLEXURAL MODULI FOR TEST-PIECES CUT FROM THE THREE PS + 20 PLATES
MADE SUCCESSIVELY FROM A GIVEN PAIR OF RESERVOIR BLOCKS

(a) Longitudinal Direction

PLATE NO.	TEST-PIECE LOCATION	FLEXURAL MODULUS (GPa)
1	l3	7.04
	l5	7.033
2	l1	7.37
	l5	7.25
3	l3	6.17
	l6	7.15

(b) Transverse Direction

PLATE NO.	TEST-PIECE LOCATION	FLEXURAL MODULUS (GPa)
1	t2	4.04
	t3	4.03
2	t1	4.66
	t4	4.36
3	t2	3.56
	t5	4.20

TABLE (6.3).

MEAN FLEXURAL MODULI OF PS COMPOSITES

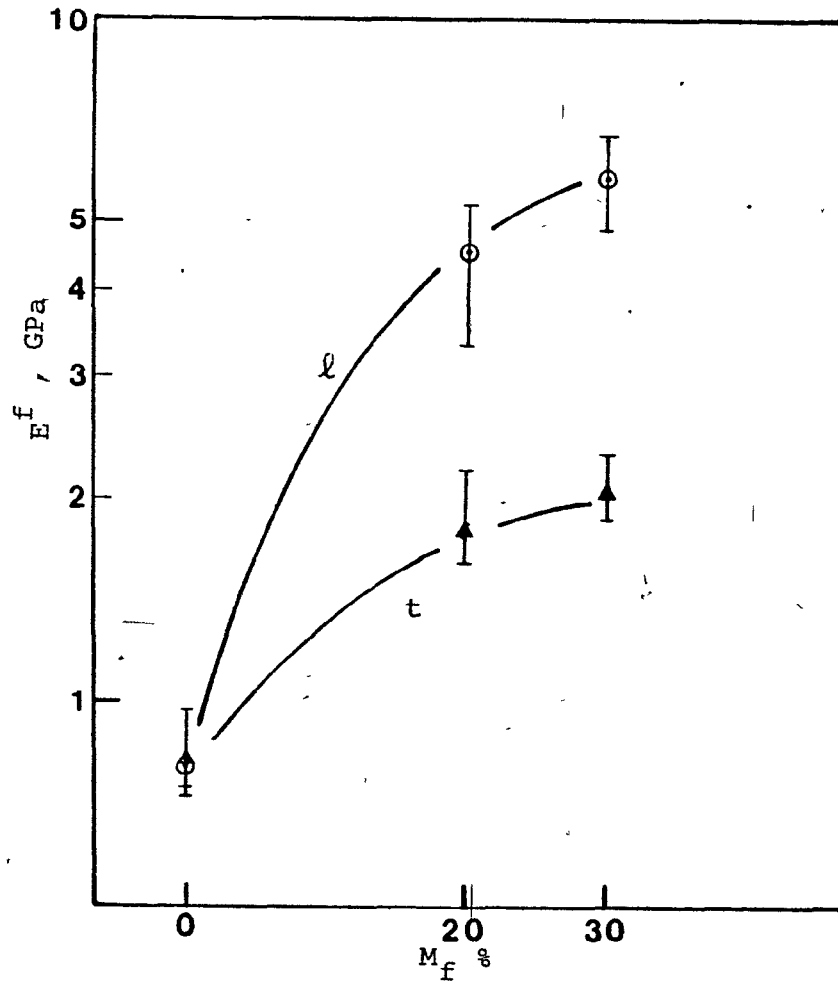
COMPOSITE	FLEXURAL	MODULUS	(GPa)
MATERIAL	1.6 mm	3.2 mm	
PS - l	3.52	3.22	
PS - t	3.19	3.23	
PS + 20 - l	6.91	6.23	
PS + 20 - t	4.11	4.19	
PS + 40 - l	10.76	10.25	
PS + 40 - t	6.14	5.87	

For the filled PS systems, the flexural moduli for thinner plates in the l direction are higher than those for the thicker plates. This may be due to more "in-plane" and greater orientation of the fibers in the flow direction in the thinner plates due to thinner gap and a higher shear rate. However, it should be remembered that the higher shear rate and smaller gap width might also lead to greater fiber breakage. Hence the fiber aspect ratio for the 1.6 mm plates may be smaller than that for the 3.2 mm plates. While a greater degree of fiber alignment leads to the enhancement of the mechanical properties, the smaller aspect ratio leads to their reduction. Consequently, the overall result of these two opposing factors may be reflected in the measured flexural moduli, though for low shear rates like that encountered in the shearing device the fiber attrition is expected to be minimal.

If the fiber orientation in the flow direction (l) is better in the thinner 1.6 mm plates, then 3.2 mm thick plates should be expected to be stiffer in the transverse direction (t). However, for PS + 40% wt. fibers composite, this is not found to be the case. This may be due to the fact that fibers in the thinner plate might be more "in-plane" than those in the thicker plates. Partially aligned out-of-plane fibers would not be as effective for reinforcement as the in-plane fibers.

Figures (6.3a and b) show the corresponding results for PE composites, the mean values being presented in Table (6.4).

(a) 1.6 mm (1/16 in.) Thickness.



(b) - 3.2 mm (1/8 in.) Thickness.

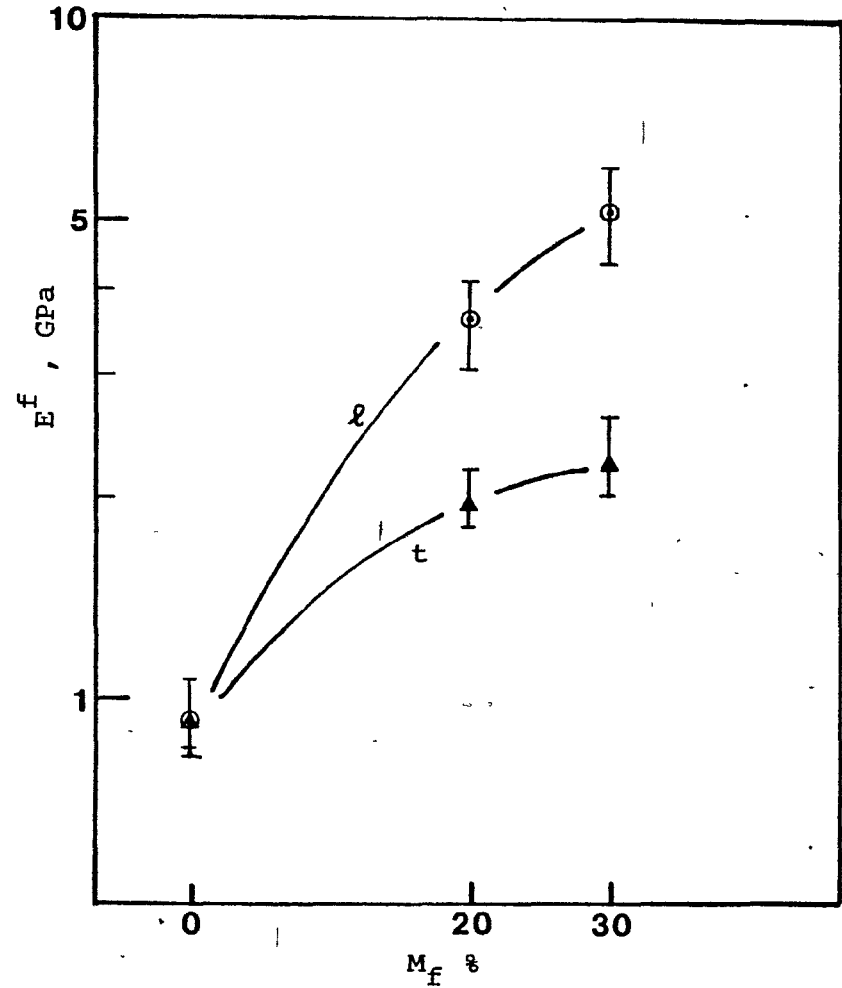


Figure (6.3). Variation of Flexural Moduli of PE Composites with Fiber Content.

TABLE (6.4).

MEAN FLEXURAL MODULI OF PE COMPOSITES

COMPOSITE	FLEXURAL	MODULUS (GPa)
MATERIAL	1.6 mm	3.2 mm
PE - l	0.80	0.95
PE - t	0.82	0.95
PE + 20 - l	4.54	3.6
PE + 20 - t	1.82	1.92
PE + 30 - l	5.86	5.14
PE + 30 - t	2.05	2.21

For unfilled PE, the thicker plates are comparatively stiffer. An apparent reason for this would be the higher degree of crystallivity in the thicker plates, due to relatively longer time for cooling. Also, it was observed that the warpage due to cooling shrinkage was quite pronounced in the case of the thinner 1.6 mm plates, while for 3.2 mm plates there was essentially no warpage. The in-built stresses in the unwarped material may make it apparently stiffer.

The flexural moduli for the filled PE composites followed the expected trend suggesting again that there was a greater degree of fiber alignment in the thinner plates than the thicker plates.

It should be noted that the flexural modulus determination involved several steps each of which can contribute to human and/or instrumental errors. Some of these are:

- (1) measurements of the test-piece dimensions, particularly the average thickness which appears as the third power in equation (5.1),
- (2) measurement of the load,
- (3) determination of the initial slope of the load versus deflection curve,
- (4) determination of the correction factor for accounting for the device deflection.

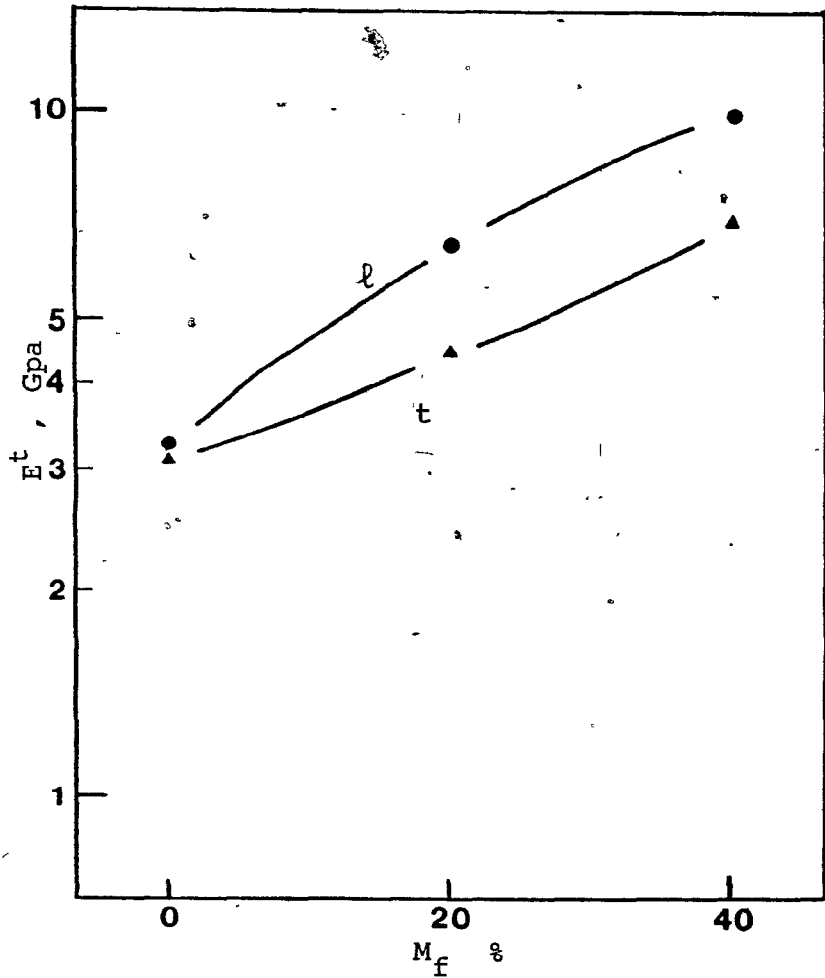
A complete error analysis was not attempted because the multitude of the sources of errors would not make it very meaningful. Nevertheless, the good reproducibility of the results did allow a ready comparison and meaningful conclusions.

6.1.2 Tensile Modulus

It was difficult to measure an accurate elongation during tensile modulus measurements by noting the distance moved by the Instron crosshead, because the measured distance also involved slip at the grips. Hence, as discussed in Section 5.3.2, an extensometer was used for accurately measuring the strain in the reduced section of the dumbbell shaped test-pieces.

The measurements were carried out for only 3.2 mm thick test-pieces and one test-piece was used for each composite system. In this way, a necessary number of test-pieces could always be saved for the tensile strength measurements without any possible pretesting structural damage, and at the same time measured tensile moduli allowed a comparison with the previously determined flexural moduli. It may be noted that necessity of using relatively large size specimens and some malfunctioning of the extensometer with associated time consumption, also did not allow tensile moduli measurements to be carried out as extensively as the flexural moduli determinations.

(a) 3.2 mm (1/8 in.) PS Composites.



(b) 3.2 mm (1/8 in.) PE Composites.

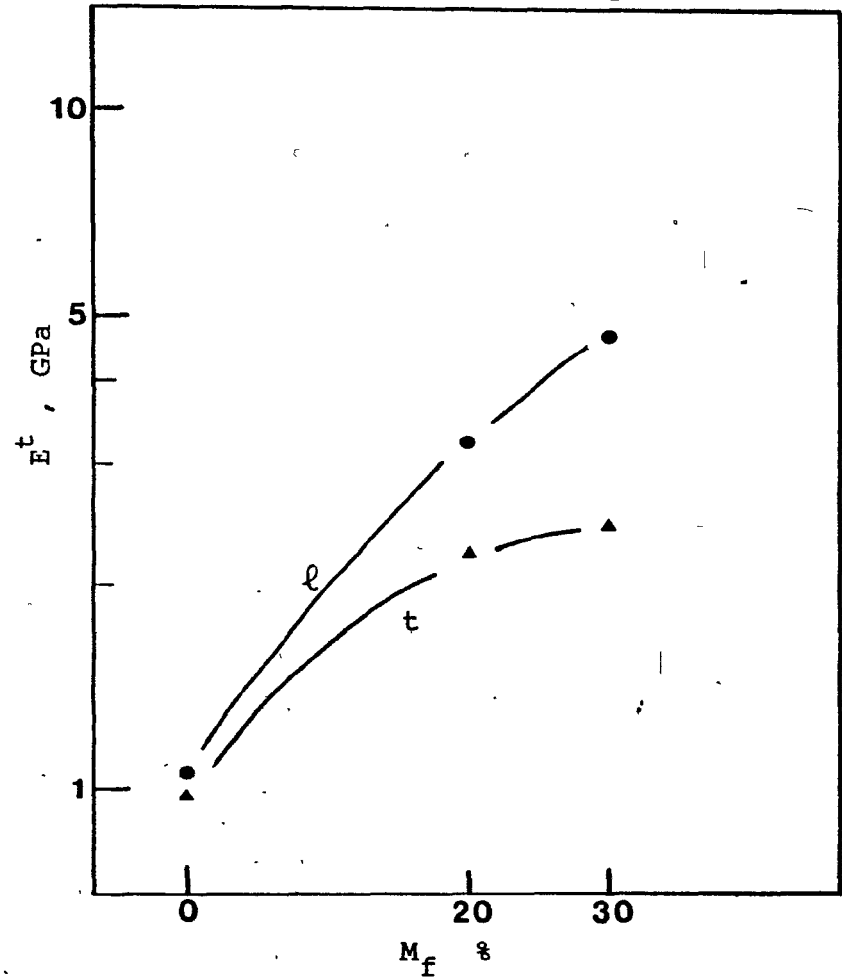


Figure (6.4). Variation of Tensile Moduli with Fiber Content.

TABLE (6.5).TENSILE MODULI OF PS COMPOSITES(3.2 mm THICKNESS)

<u>COMPOSITE MATERIAL</u>	<u>TENSILE MODULUS (GPa)</u>
PS - l	3.27
PS - t	3.14
PS + 20 - l	6.33
PS + 20 - t	4.51
PS + 40 - l	9.92
PS + 40 - t	6.91

TABLE (6.6).TENSILE MODULI OF PE COMPOSITES(3.2 mm THICKNESS)

<u>COMPOSITE MATERIAL</u>	<u>TENSILE MODULUS (GPa)</u>
PE - l	1.06
PE - t	0.99
PE + 20 - l	3.25
PE + 20 - t	2.24
PE + 30 - l	4.59
PE + 30 - t	2.44

The variations of the tensile moduli for both the PS and PE based systems with the fiber content are shown in Figures (6.4a and b). The individual values are also reported in Tables (6.5) and (6.6) for their ready comparison with the values for the flexural moduli. The measured tensile and flexural moduli are quite comparable for almost all the systems, and hence give credence to both measurements although it appears difficult to envisage a precise comparison.

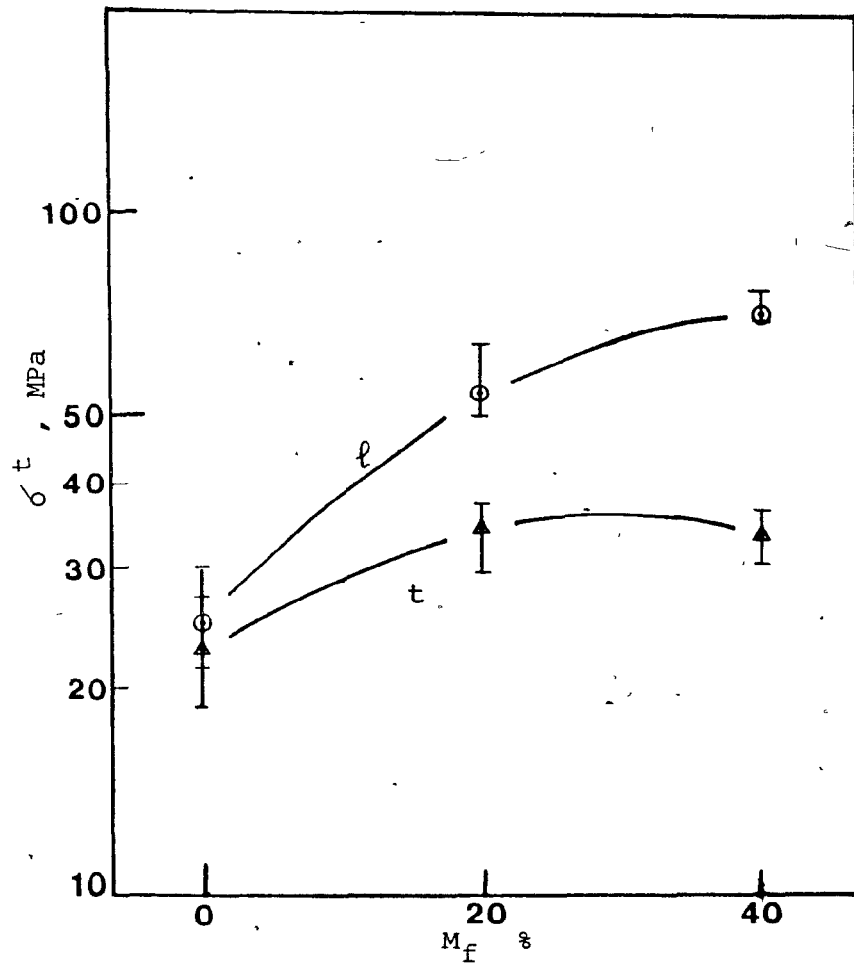
6.1.3 Tensile Strength

For the 1.6 mm thick plates, six to eight test-pieces were tested for tensile strength determination for each of the composite systems and each direction. For the 3.2 mm thick plates, five test-pieces were used for each case.

Figures (6.5a and b) show the variations of the tensile strengths with the fiber content in both l and t directions for the PS based systems for 1.6 mm and 3.2 mm thick plates respectively. The mean tensile strengths for these materials are tabulated in Table (6.7).

As mentioned in Section 5.3.3, it was anticipated that the non-standard smaller test-piece dimensions for the 1.6 mm thick plates might give erroneous estimates in strength determination. However, as

(a) 1.6 mm (1/16 in.) Thickness.



(b) 3.2 mm (1/8 in.) Thickness.

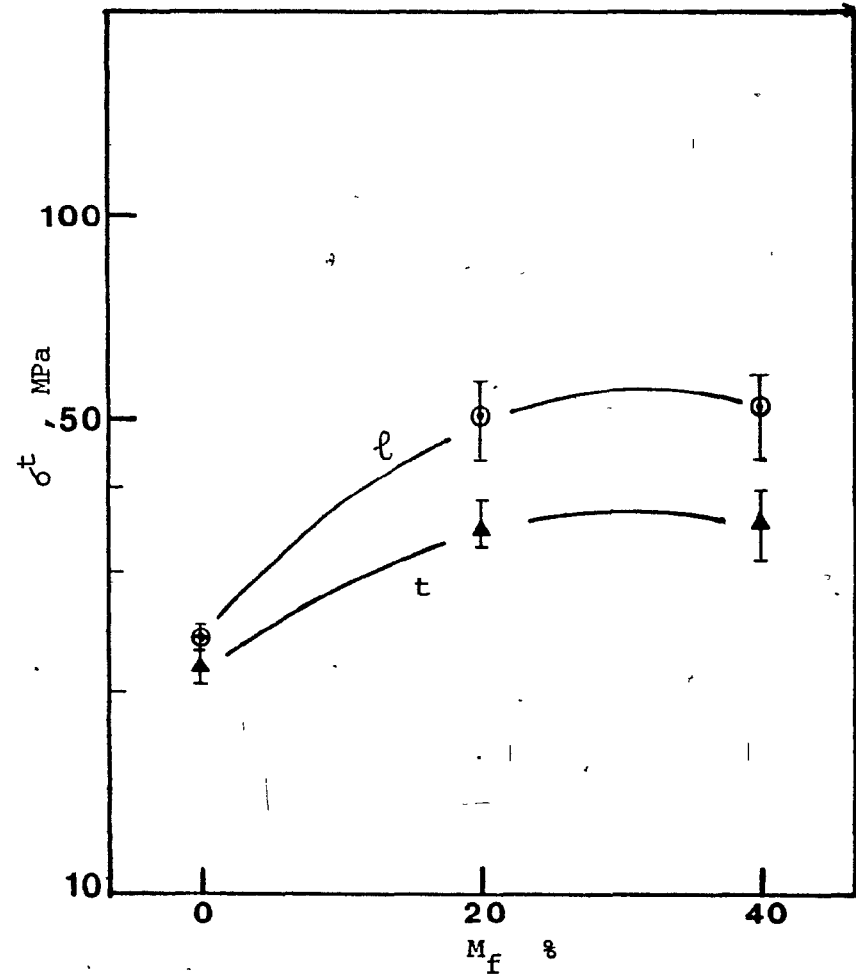


Figure (6.5). Variation of Tensile Strengths of PS Composites with Fiber Content.

TABLE (6.7).MEAN TENSILE STRENGTHS OF PS COMPOSITES

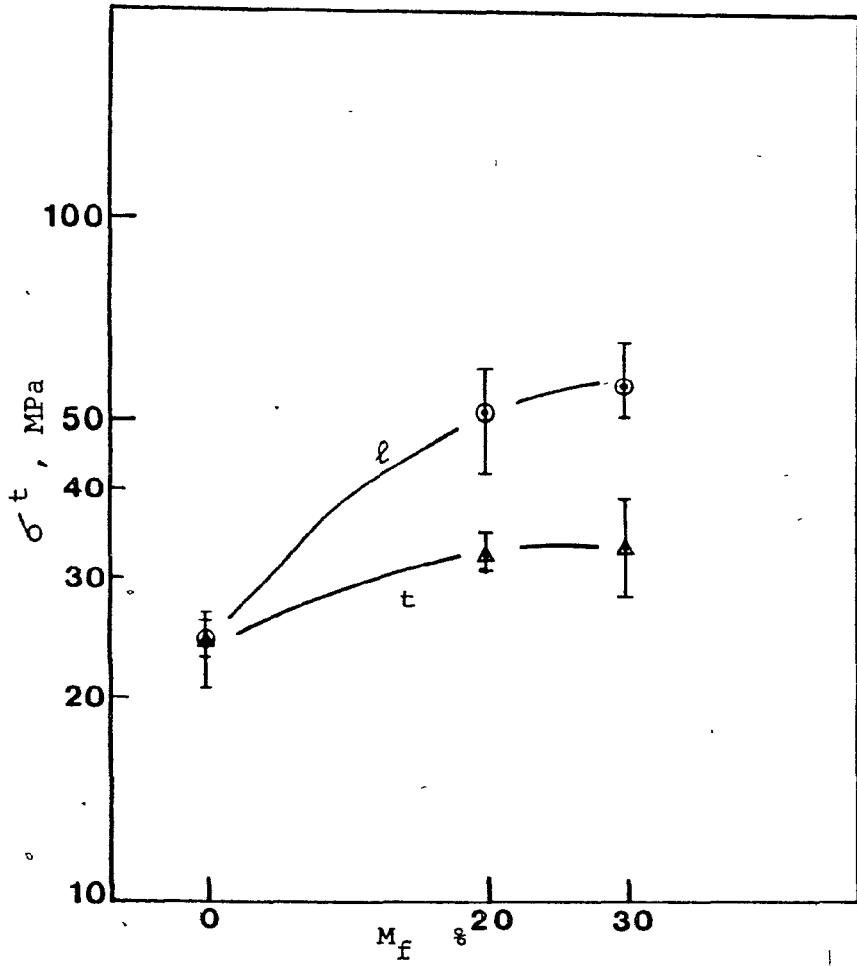
COMPOSITE MATERIAL	TENSILE STRENGTH (MPa)	
	1.6 mm	3.2 mm
PS - l	25.16	23.92
PS - t	22.78	22.06
PS + 20 - l	54.46	50.92
PS + 20 - t	34.57	37.33
PS + 40 - l	71.75	51.06
PS + 40 - t	33.80	35.05

seen from the values in Table (6.7), the results for both the 1.6 mm and 3.2 mm thick plates are quite comparable in most of the cases. As seen from Figures (6.5a and b) the reproducibility is reasonably good for all the cases.

For the unfilled PS, for both the 1.6 mm and 3.2 mm thick plates, the ℓ direction is slightly stronger with the value for the 1.6 mm thick plate being higher. This may again be due to the relatively higher molecular orientation frozen in the case of the thinner plates. For the filled materials, the 1.6 mm thick plates have higher strength in the ℓ direction and slightly lower strength in the t direction than the corresponding values for the 3.2 mm thick plates. This further justifies the expectation that a higher degree of fiber alignment might have occurred due to higher shear stresses. It must, however, be remembered that both the fiber length and fiber-matrix adhesion are of considerable importance in the determination of overall strength.

Figures (6.6a and b) show the variations of the tensile strengths with the fiber content for 1.6 mm and 3.2 mm thick plates of PE based materials. For unfilled PE, the strength corresponds to the yield point whereas for filled PE the values represent actual strengths at break. The corresponding mean values are summarized in Table (6.8).

(a) 1.6 mm (1/16 in.) Thickness.



(b) 3.2 mm (1/8 in.) Thickness.

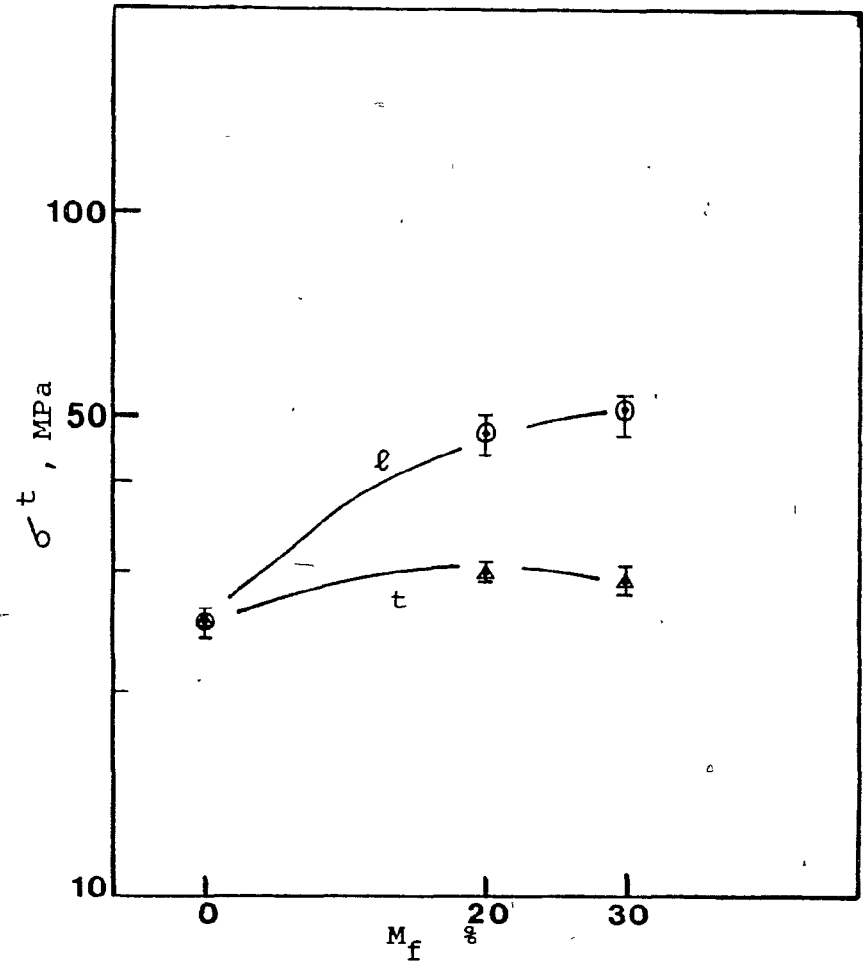


Figure (6.6). Variation of Tensile Strengths of PE Composites with Fiber Content.

TABLE (6.8).MEAN TENSILE STRENGTHS OF PE COMPOSITES

COMPOSITE MATERIAL	TENSILE STRENGTH (MPa)	
	1.6 mm	3.2 mm
PE - l	23.77	25.37
PE - t	23.85	25.42
PE + 20 - l	50.10	47.99
PE + 20 - t	32.05	30.07
PE + 30 - l	56.21	50.42
PE + 30 - t	32.50	28.55

For the unfilled PE, the 3.2 mm thick plates are stronger in both the directions than the 1.6 mm plates. This may again be explained in terms of the relatively higher degree of crystallinity in the thicker plates. Also the relatively slow cooling and crystallization would allow randomization of the molecular chains suppressing any molecular orientation and hence the strengths in the l and t directions can be expected to be very close.

For the filled PE systems, the strength in the l direction for the 1.6 mm thick plates is higher than that for the 3.2 mm thick plates for both the fiber contents. Reasons similar to those given for the PS systems may be invoked for such a trend.

One important observation is that for all the filled systems, the strength in the t direction remains almost constant or occasionally shows a slight decrease with an increase in the fiber content. The mechanism of failure of the SF RTP is a very complex issue. In the l direction, the stress transfer from the continuous phase to the inclusions has been explained in terms of the shear along the interface, but for the t direction, the exact mode of stress transfer is not very clear. However, in highly simplistic terms it may be visualized that if the load is acting on an element containing an embedded fiber at 90° to the fiber axis, the fiber-matrix interface would be under direct normal stresses and would represent a weak location for the failure initiation by debonding under tensile stresses. In fact, for a unidirectional fiber composite, the fibers may not contribute at all to the

strength in the t direction and may represent potential sources of crack initiation. For such a case, an increase in the fiber content would be expected to lead to a decrease in strength. It has, in fact, been suggested that for the SF RTP, the strength in the direction normal to that of the major fiber orientation be taken as the matrix strength for a conservative estimate (Hashin (33), Loughlin et. al. (28)).

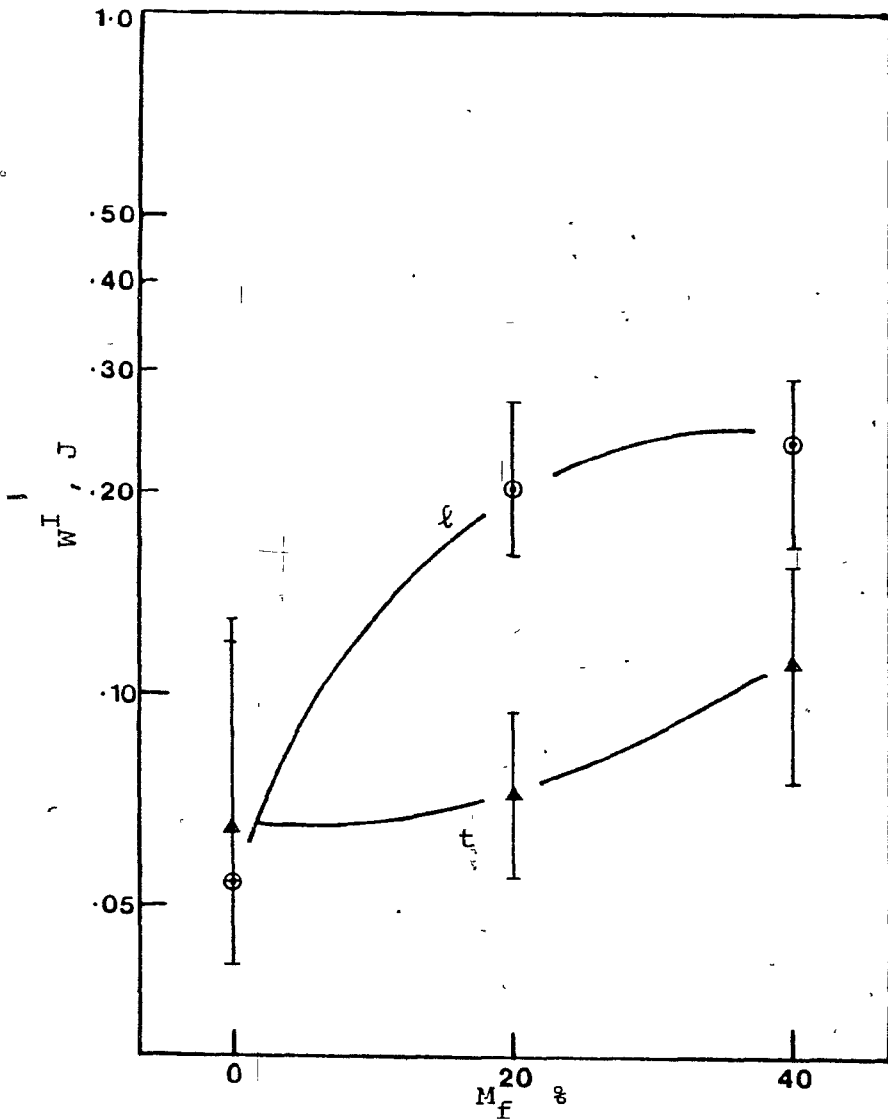
For a partially oriented fiber composite, some reinforcement would always be achieved, and this explains why the strength in the t direction is higher than the matrix strength for a low fiber loading.

6.1.4 Izod Impact Strength

As discussed in Section 5.3.4, an Izod-type impact strength was determined by a somewhat modified procedure with the hammer striking on the wider side of the specimen. The results reported here represent the energy required to break the test-pieces when tested under impact according to this specified procedure and are not directly comparable to standard Izod results.

Figures (6.7a and b) show the variations of the Izod-type impact strengths for the 1.6 mm and the 3.2 mm thick plates of PS composites respectively. Not surprisingly for an impact test of a two phase material, the reproducibility was not very good. Consequently,

(a) 1.6 mm (1/16 in.) Thickness.



(b) 3.2 mm (1/8 in.) Thickness.

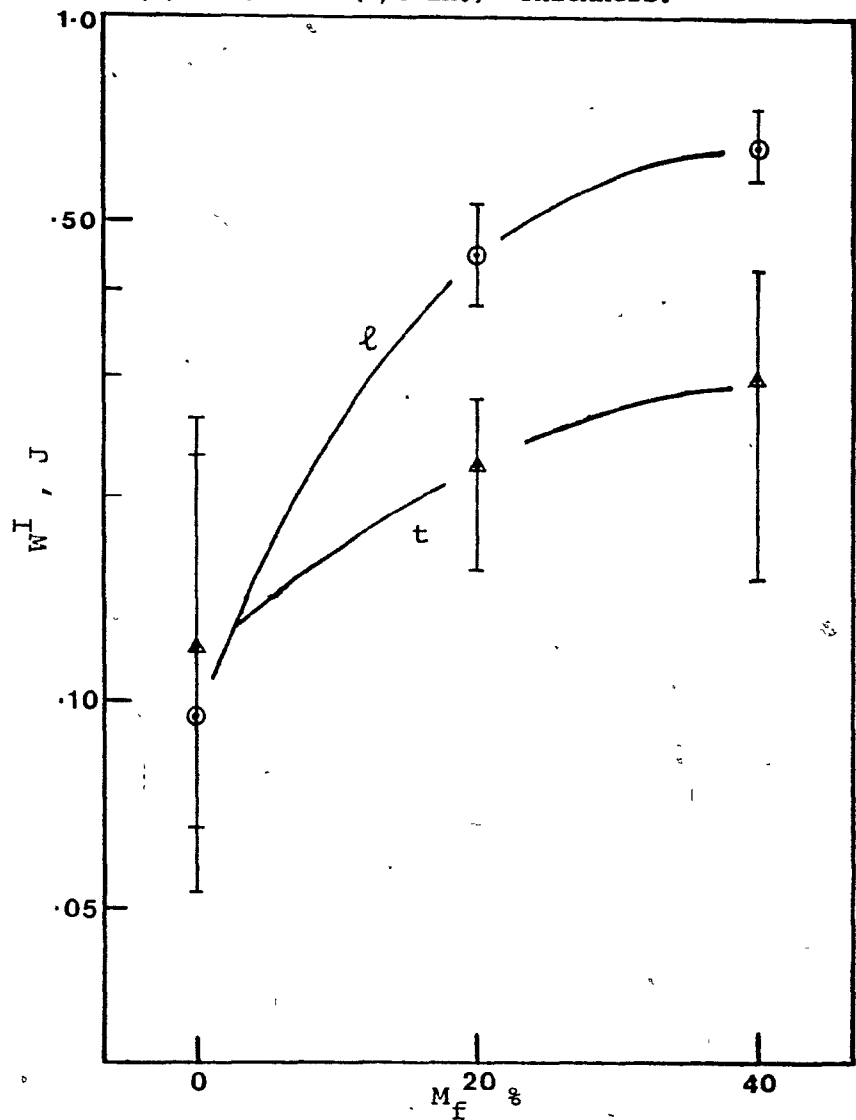


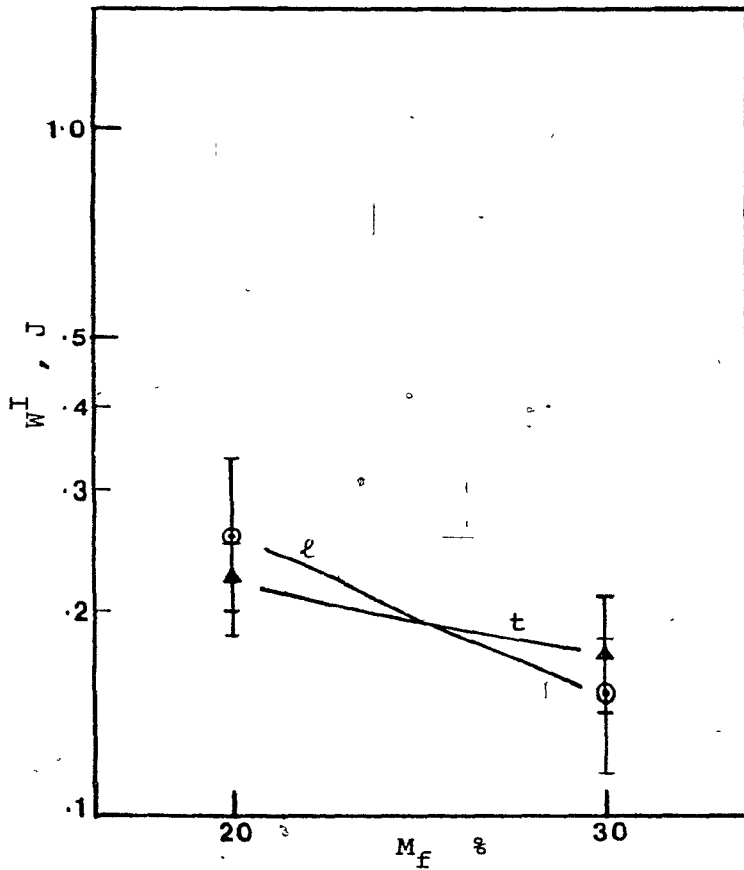
Figure (6.7). Variation of Izod-type Impact energies of PS Composites with Fiber Content.

ten to twelve test-pieces were used for each of the composite systems and each direction.

For the brittle matrix like PS , the incorporation of fibers led to a relatively tougher material with a better improvement in the direction of fiber orientation. For systems with stiff and strong fibers where the bond between fibers and matrix is not exceptionally strong, the failure occurs by fiber pull out rather than by fiber breakage (37). The extra energy required for pulling the fibers along the matrix-fiber interface can account for the observed enhancement in toughness. Also, it is suspected that presence of some fiber bunches might also have contributed to the improvement in the fracture energy.

For the highly ductile and tough unfilled PE no break could occur. However, the inclusion of glass fibers caused considerable embrittlement of the matrix. Figures (6.8a and b) show the variations of Izod-type impact energies for the 1.6 mm and 3.2 mm plates of filled PE systems respectively. In both the cases, there is seen to be a considerable overlap of the results obtained for the l and the t directions. This implies that for the Izod-type impact strength of ductile matrix - brittle fiber systems, the fiber orientation is probably not of primary importance. The embrittlement of the matrix is the dominating factor and this is why the increase in fiber content leads to a decrease in fracture energy.

(a) 1.6 mm (1/16 in.) Thickness.



(b) 3.2 mm (1/8 in.) Thickness.

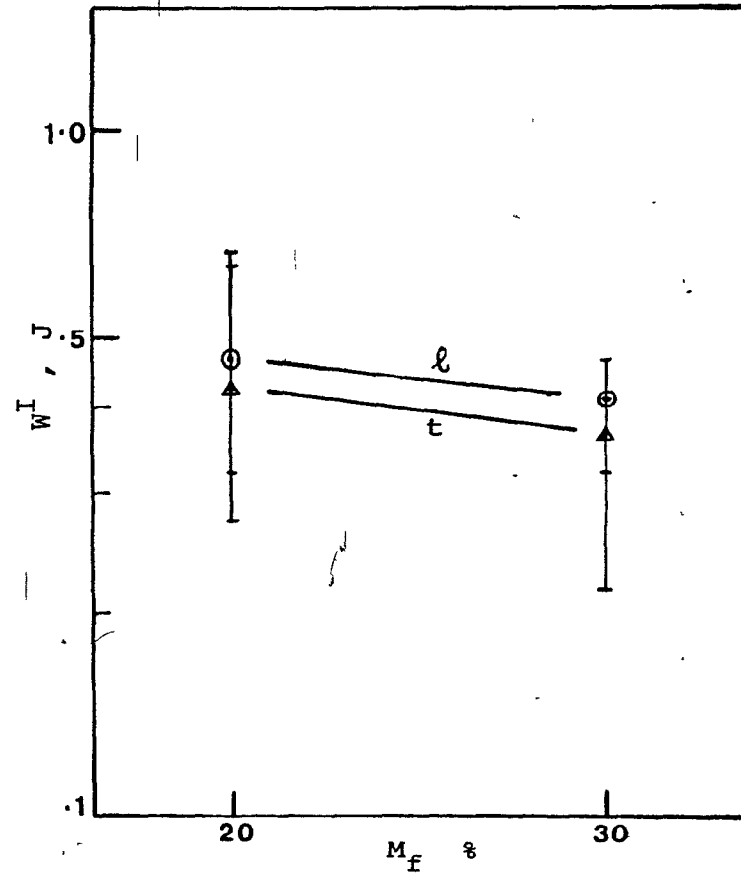


Figure (6.8). Variation of Izod-type Impact energies of PE Composites with Fiber Content.

TABLE (6.9).

MEAN IZOD-TYPE IMPACT ENERGIES OF PS COMPOSITES

COMPOSITE MATERIAL	IZOD IMPACT ENERGY (J)		RATIO 3.2 mm/1.6 mm
	1.6 mm	3.2 mm	
PS - l	0.054	0.095	1.75
PS - t	0.065	0.122	1.87
PS + 20 - l	0.204	0.446	2.18
PS + 20 - t	0.072	0.226	3.14
PS + 40 - l	0.230	0.638	2.72
PS + 40 - t	0.112	0.300	2.67

TABLE (6.10).

MEAN IZOD-TYPE IMPACT ENERGIES OF PE COMPOSITES

COMPOSITE MATERIAL	IZOD IMPACT ENERGY (J)		RATIO 3.2 mm/1.6 mm
	1.6 mm	3.2 mm	
PE - l			
PE - t	No Break	No Break	-
PE + 20 - l	0.26	0.473	1.8
PE + 20 - t	0.222	0.423	1.9
PE + 30 - l	0.153	0.408	2.67
PE + 20 - t	0.17	0.362	2.18

Tables (6.9) and (6.10) list the mean values of the Izod-type impact energies for the composite materials studied. The ratios of the fracture energies of the 3.2 mm thick specimens to those of the 1.6 mm thick specimens are also included in the last column of each table. It is seen that these ratios are around 2 to 3 indicating that for the range of thicknesses considered, the measured energy for fracture under the Izod-type impact was approximately proportional to the thickness.

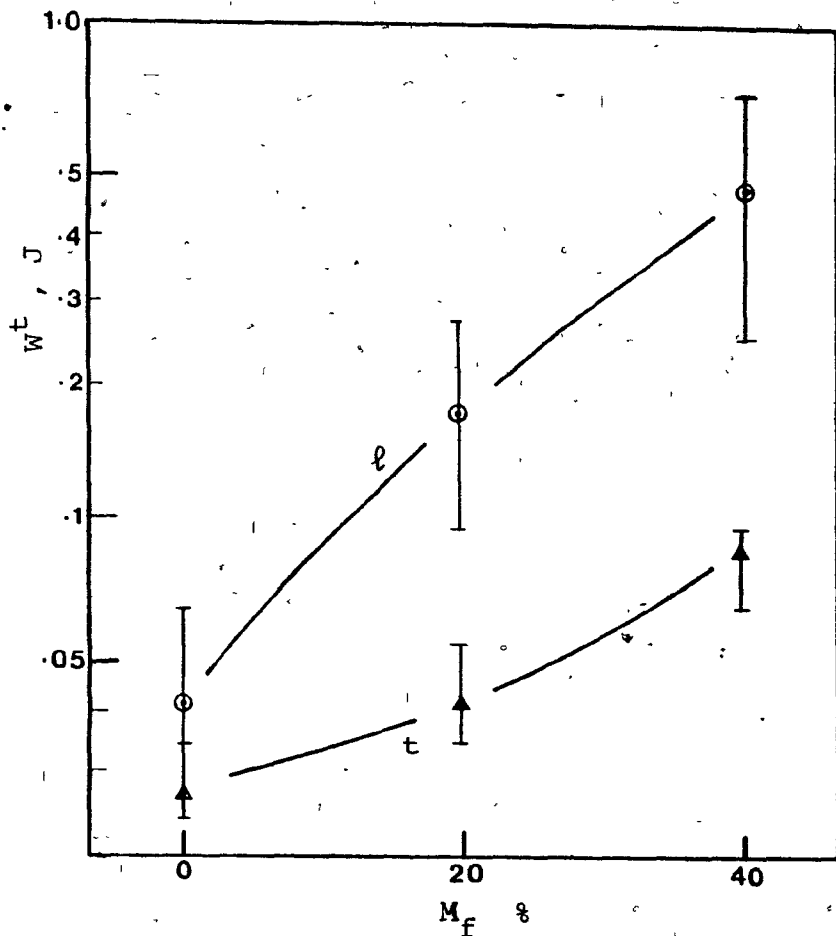
6.1.5 Tensile Impact Strength

The results for the tensile impact testing are presented as the energy required for the failure of the individual test-pieces of the geometry specified in Section 5.3.5 under tensile impact loading.

The test was carried out for ten to twelve test-pieces for each composite system and each direction. As discussed in Section 5.3.5 and Appendix B, a crosshead bounce correction factor and a friction correction factor were incorporated in the calculations of tensile impact energy.

The results for the PS based composites are shown in Figures (6.9a and b) for the 1.6 mm and 3.2 mm thick specimens respectively. Again, the reproducibility is not very good, however, there seems to be a definite improvement due to the incorporation of

(a) 1.6 mm (1/16 in.) Thickness.



(b) 3.2 mm (1/8 in.) Thickness.

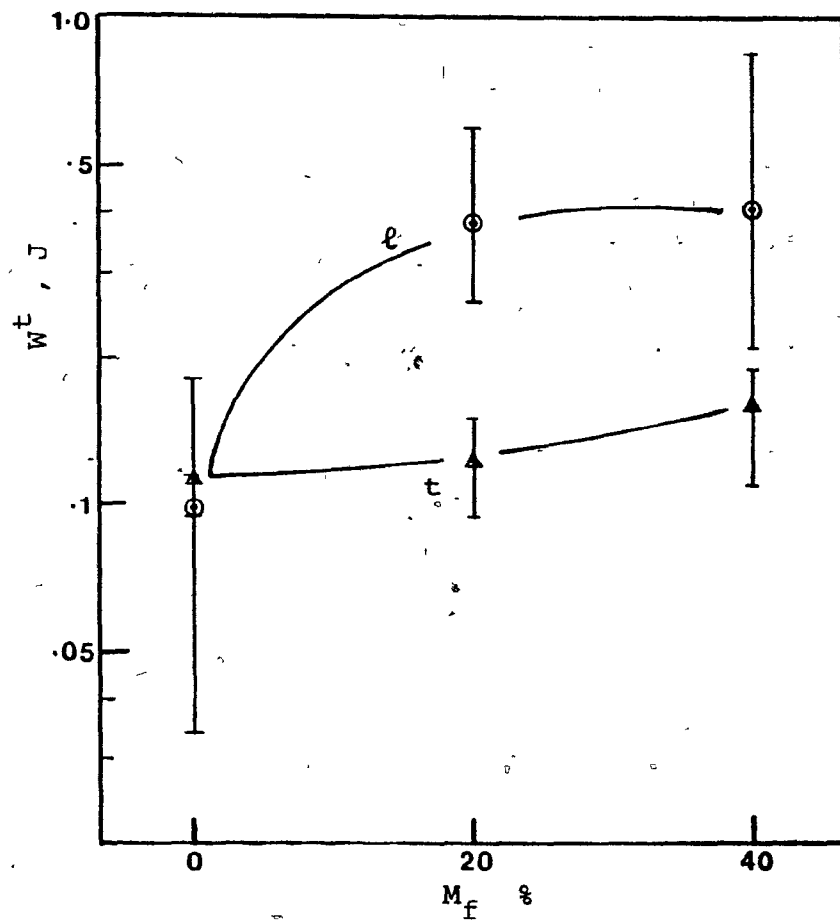


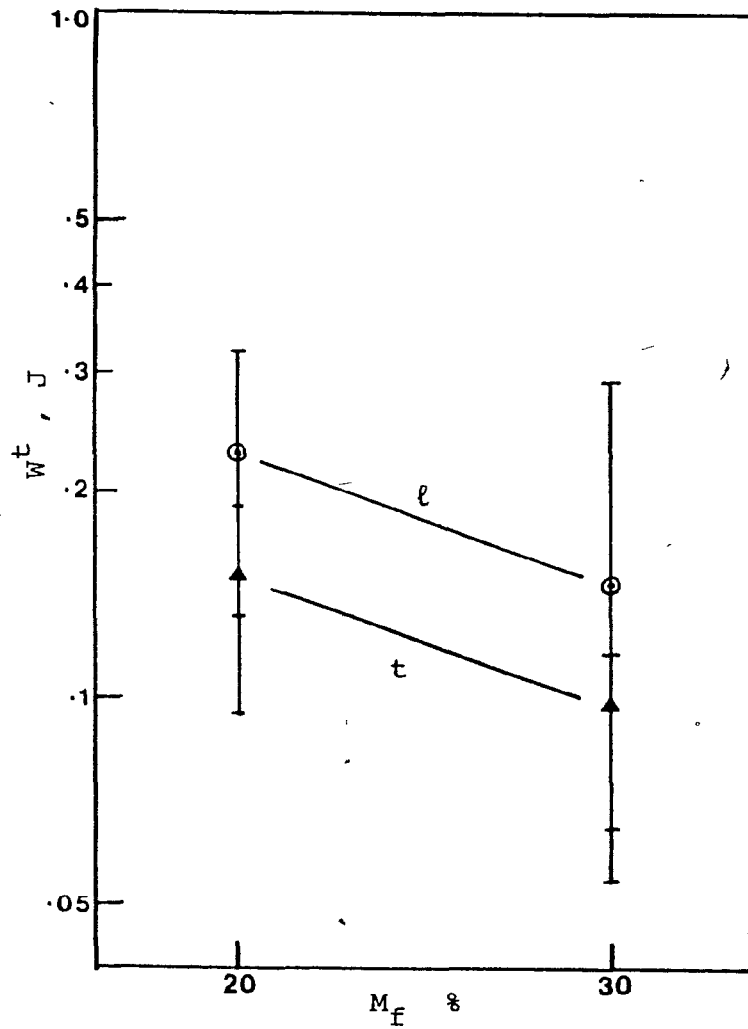
Figure (6.9). Variation of Tensile Impact Energies of PS Composites with Fiber Content.

fibers. The increase in the tensile impact energy is much better in the direction of fiber orientation than in the direction normal to it. Again, the presence of some fiber bunches might also be partially responsible for the observed improvement in this fracture energy.

For the unfilled PE, it was not possible to measure the tensile impact energy due to its high ductility. But incorporation of fibers caused high embrittlement of the matrix. Figures (6.10a and b) show the variations of the tensile impact energy for the filled PE systems. As seen from these figures, there is again a considerable overlap in the measured values. However, unlike the Izod impact energy results, the tensile impact energy appears to be higher in the l direction than the t direction for a given material. But this improvement due to fiber orientation is highly overmasked by the embrittlement caused by inclusions, and hence the tensile impact energy decreases with an increase in the fiber content.

Tables (6.11) and (6.12) list the mean values of the tensile impact energies for the systems studied along with the ratios for the values for 3.2 mm to those for 1.6 mm thick specimens. These ratios indicate a scatter around 2. Though measured energy would vary with the actual specimen geometry and dimensions, it seems reasonable to expect the fracture energy to vary linearly with the area of cross-section under impact.

(a) 1.6 mm (1/16 in.) Thickness.



(b) 3.2 mm (1/8 in.) Thickness.

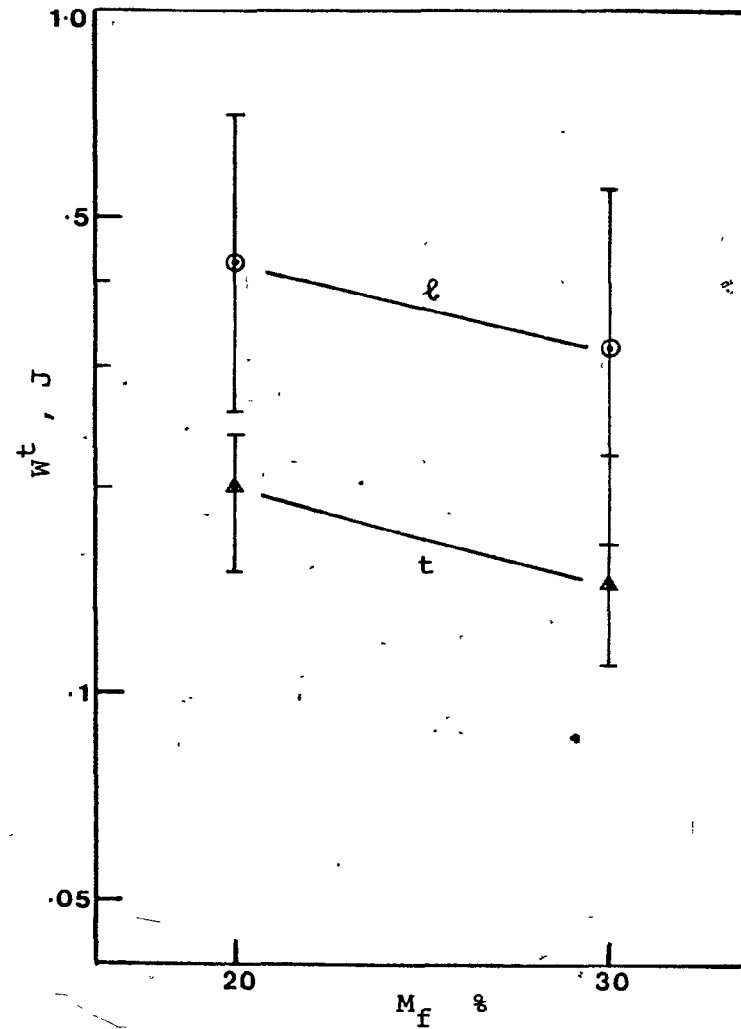


Figure (6.10). Variation of Tensile Impact Energies of PE Composites with Fiber Content.

TABLE (6.11).

MEAN TENSILE IMPACT ENERGIES OF PS COMPOSITES

COMPOSITE MATERIAL	TENSILE IMPACT ENERGY (J)		RATIO 3.2 mm/1.6 mm
	1.6 mm	3.2 mm	
PS - l	0.041	0.097	2.35
PS - t	0.0271	0.111	4.11
PS + 20 - l	0.163	0.377	2.3
PS + 20 - t	0.042	0.121	3.33
PS + 40 - l	0.471	0.404	0.86
PS + 40 - t	0.084	0.156	2.07

TABLE (6.12)

MEAN TENSILE IMPACT ENERGIES OF PE COMPOSITES

COMPOSITE MATERIAL	TENSILE IMPACT ENERGY (J)		RATIO 1.6 mm/3.2 mm
	1.6 mm	3.2 mm	
PE - l			-
	No Break	No Break	
PE - t			-
PE + 20 - l	0.229	0.430	1.88
PE + 20 - t	0.149	0.200	1.35
PE + 30 - l	0.146	0.325	2.22
PE + 30 - t	0.097	0.145	1.5

It should be remembered that the modes of failure under the two types of impact tests considered are different. However, for both cases, the behavior of the PS based composites seems to be similar. On the other hand, for the PE based composites, for the failure under flexure, the fiber orientation appears to be almost an unimportant factor. While for the failure under tension, the oriented fibers appear to contribute towards the fracture energy in the direction of their alignment, though the embrittlement overshadows this contribution.

6.2 Analysis of the Experimental Results in Terms of the Theoretical Predictions

The experimental results on the flexural moduli can be analyzed with the help of the predictions made by the theoretical model for the elastic properties discussed in Chapter IV so as to yield some information on the structure of the molded plates.

In the analysis presented here, the following assumptions have been made:

- (1) The fiber aspect ratio distribution can be represented by a mean value.
- (2) The fiber orientation is two dimensional or planar.

- (3) The fiber orientation distribution is uniform throughout the body of the composite plate and can be described by equation (4.22), using a single value for the orientation parameter C_ℓ .

The effect of considering a mean fiber aspect ratio instead of a distribution should be insignificant for a stiffer matrix like PS, though it may not be so in the case of a softer matrix like PE (cf. Chapter IV). However, the assumption of a uniform fiber aspect ratio represented by a mean value greatly simplifies the calculation procedure and such an assumption may be viewed to be more appropriate than others in the absence of actual data.

The second assumption is more or less justified for thin plates like those molded in this project. It is expected that most of the fibers would lie in the plane of the plate during the transfer through the narrow gap.

The third assumption should also prove satisfactory for the kind of molding procedure adopted in this study. The isothermal uniform flow at relatively low volumetric flow rates in a simple geometry is not expected to give the kind of structural variations encountered in injection molded specimens.

Finally, it must be stressed that this analysis is carried out to get only qualitative information regarding the degree of orientation achieved in various composite systems studied and should not be viewed as a rigorous comparison of the experimental data with the theoretical predictions.

With the above assumptions, the model discussed in the section 4.2 becomes directly applicable. Table (6.13) gives the values of the input parameters used for the theoretical predictions for the composite systems studied. The matrix moduli were chosen to be close to the experimental values for the unfilled polymers, but may represent an appreciable source of error.

Besides the values specified in Table (6.13) one needs the values for the orientation parameter C_ℓ and mean aspect ratio (\bar{z}/d) in order to predict the properties of a given SFRTF system or conversely, knowing two experimentally determined moduli for a given system, namely the moduli in the direction of preferential fiber orientation and in the direction normal to it, one should, in principle, be able to determine the representative values of C_ℓ and (\bar{z}/d) . However, it should be realized that the inherent errors in the experimental results and/or the theory itself may make such determinations impossible in the absence of additional experimental data.

TABLE (6.13).

VALUES OF VARIOUS PARAMETERS USED
IN THE THEORETICAL ANALYSIS OF THE EXPERIMENTAL RESULTS

(a) PS Composites

PARAMETER	VALUE
E_f	68.9 GPa
E_m	3.445 GPa
μ_f	0.3
μ_m	0.2
M_f, V_f	40, 20 (%)
M_f, V_f	20, 9.5 (%)

(b) PE Composites

PARAMETER	VALUE
E_f	68.9 GPa
E_m	0.827 GPa
μ_f	0.3
μ_m	0.2
M_f, V_f	30, 13.5 (%)
M_f, V_f	20, 8.5 (%)

In order to apply the above method for determining C_ℓ and (\bar{z}/d) , several curves were prepared showing the variation of the elastic modulus in both l and t directions with C_ℓ using (\bar{z}/d) as a parameter for each of the composite systems. Figures (6.11a and b) show these plots for the PS based systems with 20% and 40% fibers by weight respectively. Here the composite moduli are reduced by the matrix modulus used in the computations.

As seen from Figure (6.11a), for a reasonable degree of fiber orientation (higher value of C_ℓ), the effect of fiber aspect ratio on the modulus in the transverse direction is insignificant. Thus the experimentally determined modulus in the transverse direction can allow a direct determination of C_ℓ by comparison with the theoretical prediction, irrespective of the value of (\bar{z}/d) . Using the experimentally determined modulus in the l direction, one can then determine a representative value of (\bar{z}/d) for the previously determined value of C_ℓ again by comparison with the theoretical predictions.

In Figures (6.11a and b), the experimentally determined flexural moduli are represented by horizontal lines for both the 1.6 mm and 3.2 mm thicknesses. Intersection of these lines for the moduli in the t and l directions with the theoretical curves give values of C_ℓ and (\bar{z}/d) according to the above described procedure. These values are summarized in Table (6.14).

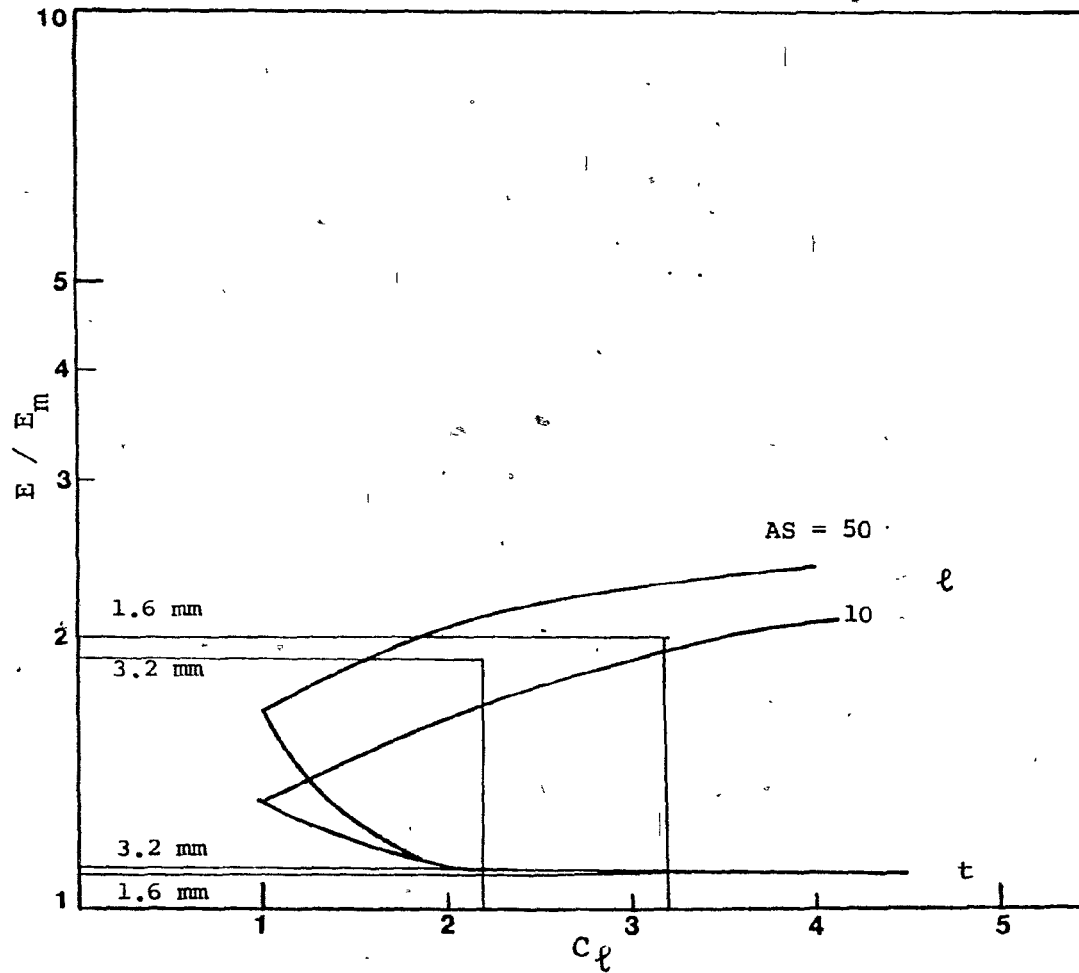


Figure (6.11a). Comparison of Experimental Results with Theoretical Predictions (PS + 20%) .

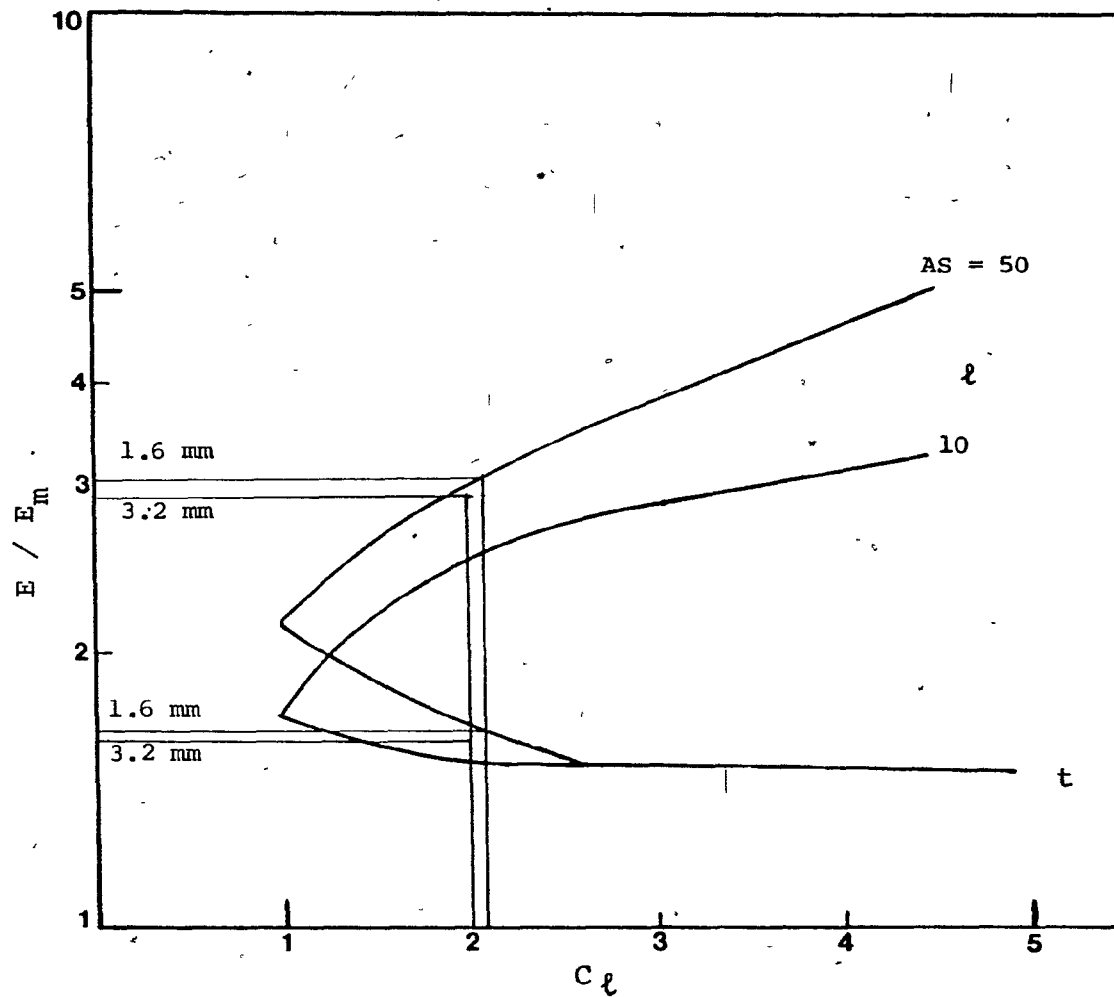


Figure (6.11b). Comparison of Experimental Results with Theoretical Predictions
(PS + 40%) .

TABLE (6.14).

VALUES OF C_{ℓ} AND (\bar{z}/d) FOR PS COMPOSITES

MATERIAL	THICKNESS (mm)	C_{ℓ}	(\bar{z}/d)
PS + 20%	1.6	3.2	15
	3.2	2.2	35
PS + 40%	1.6	2.05	50
	3.2	2.0	45

It is seen that for PS + 20% fibers by weight plates, the value of C_l for the 1.6 mm plates is higher than that for the 3.2 mm plates, indicating a higher degree of fiber orientation in the thinner plates. The representative mean aspect ratio, on the other hand, is smaller in case of the thinner plates. This can be explained by the fact that higher shearing stresses in the thinner gap during molding caused a greater fiber alignment, but also a greater fiber attrition, leading to a lower mean fiber aspect ratio.

For the PS + 40% fibers composite, both the C_l and (\bar{z}/d) for both the thicknesses are about the same. Comparison of these values with the corresponding values for the PS + 20% fibers plates shows that the degree of fiber alignment is lower for higher fiber loading. This could be attributed to the greater fiber-fiber interaction in the system with higher fiber concentration which could hinder the fiber movement and hence the orientation. The mean aspect ratios for both the thicknesses for the PS + 40% fibers composite are higher than the corresponding values for the PS + 20% fibers material. This may be due to the increased fiber bundling observed in the first material. The fibers present in a bundle would obviously not be broken easily, but would also be difficult to orient.

The theoretical curves for the PE based systems and the horizontal lines corresponding to the experimental values are shown in Figures (6.12a and b). Here, it was not possible to apply the above

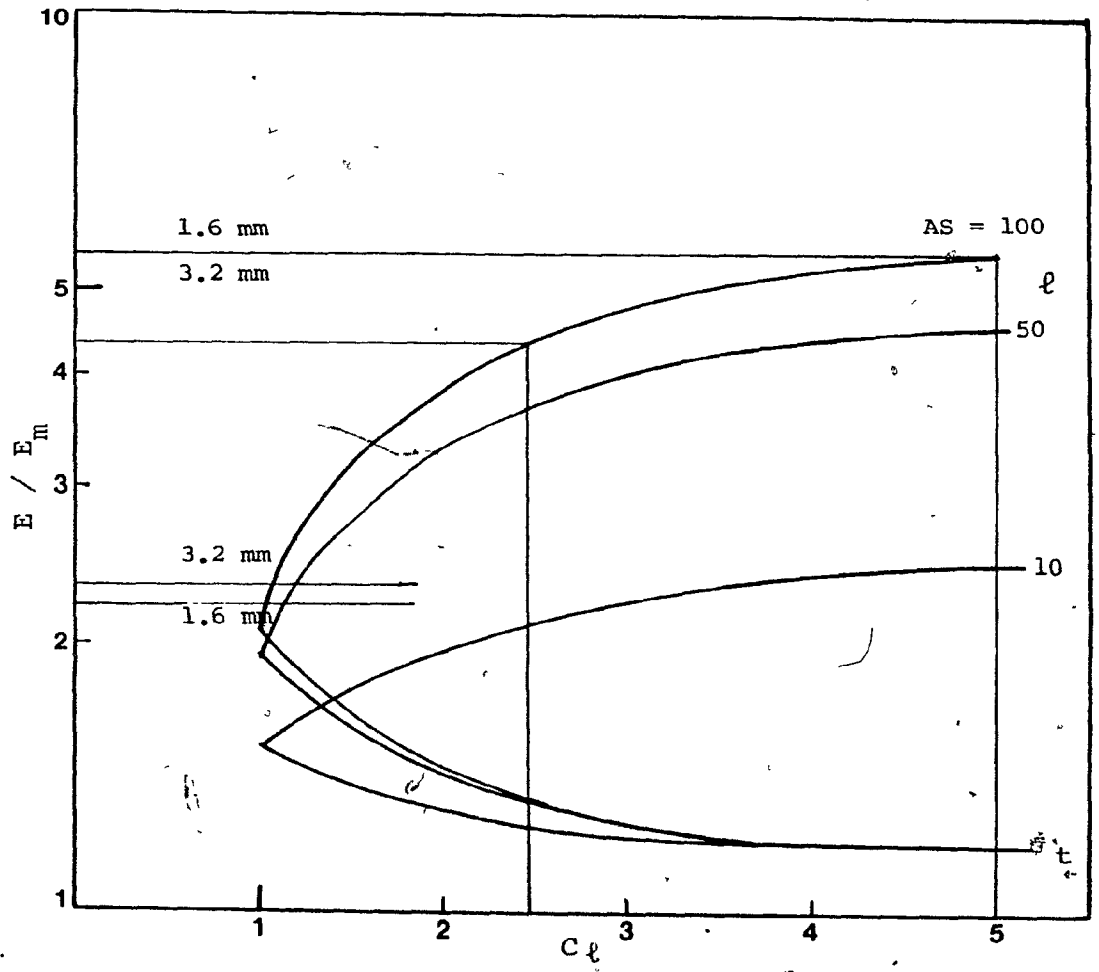


Figure (6.12a). Comparison of Experimental Results with Theoretical Predictions
(PE + 20%) .

(E+3)

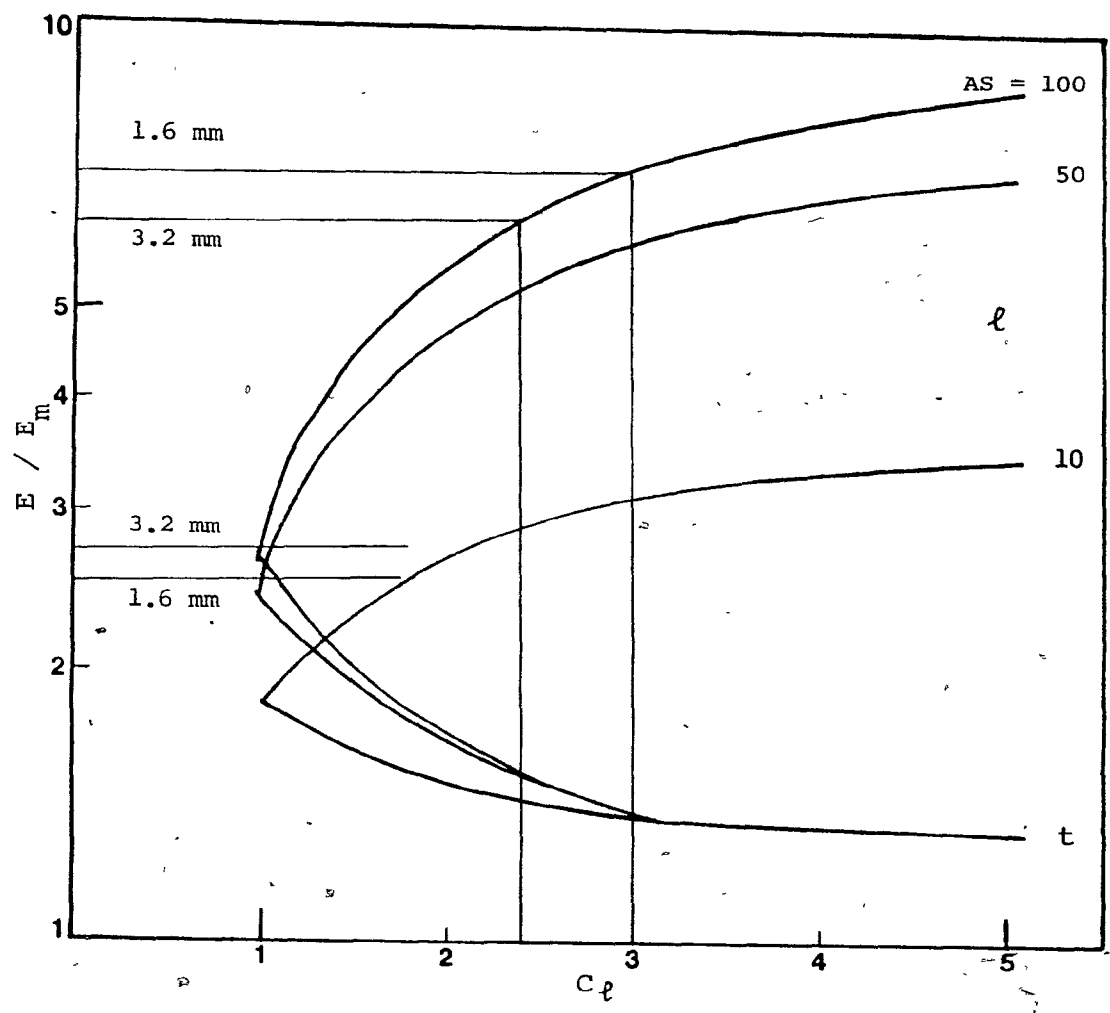


Figure (6.12b). Comparison of Experimental Results with Theoretical Predictions (PE + 30%).

described procedure for simultaneously determining C_ℓ and (\bar{z}/d) . This was because for both the filled systems, the measured moduli in the t direction were higher than those predicted by the theory for any aspect ratio, even for a random fiber orientation ($C_\ell = 1$). No straight forward explanation was evident for this observation.

Since the simultaneous determination of both the C_ℓ and (\bar{z}/d) was not possible, it was decided to assume a representative value for (\bar{z}/d) equal to 100. The experimentally determined moduli in the ℓ direction were close to the theoretical predictions for this value and hence the actual values of (\bar{z}/d) should be in the vicinity of the assumed value.

The values for C_ℓ for each thickness and composite material were determined for $(\bar{z}/d) = 100$ using the experimental moduli in the ℓ direction. These values are listed in Table (6.15).

Again it is seen that for both the fiber concentrations, the degree of fiber orientation in the thinner plate is higher. Also, comparing the results for the PE + 20% and PE + 30% fibers materials, it is seen that an increase in fiber loading leads to a decrease in the degree of fiber orientation.

An important conclusion can be drawn from the comparison of the results for the PS and PE based composites. Comparing the

TABLE (6.15).

VALUES OF C_{ℓ} AND (\bar{z}/d) FOR PE COMPOSITES

MATERIAL	THICKNESS (mm)	C_{ℓ}	(\bar{z}/d)
PE + 20%	1.6	5.0	100
	3.2	2.5	100
PE + 30%	1.6	3.0	100
	3.2	2.4	100

values of C_l for PS and PE with 20% by weight fibers, it appears that the degree of fiber alignment in the flow direction is significantly higher for the PE based system than for the PS based material. A qualitative explanation for this observation may be given in terms of the rheological behavior of these polymers, though actual rheological measurements were beyond the scope of this study. The PS matrix is likely to be much more viscous in the molten state than the PE matrix. Consequently in a Poiseuille flow in a slit like that encountered in the shearing device, the velocity profile for PS would be rather flat compared to that for PE (see Figure (6.13)). Lower viscosity of PE would result in higher shear rate and hence favor the alignment of the suspended fiber in the flow direction. A similar observation has also been reported by Goettler (52).

The above explanation appears to be valid even at higher fiber loading, though, the fiber contents in PS + 40% fibers and PE + 30% fibers are not equivalent. However, the differences in the degree of fiber alignment (differences in values of C_l) seem to decrease with increase in fiber content for the two systems. The fiber length seems to be the possible factor for this result as explained below.

It may be noted that if the assumed values for (\bar{z}/d) for PE based composites are appropriate, then the mean fiber aspect ratio for PE + 20% is much higher than that for PS + 20% , but this is not so for PE + 30% against PS + 40% . Since the differences in the

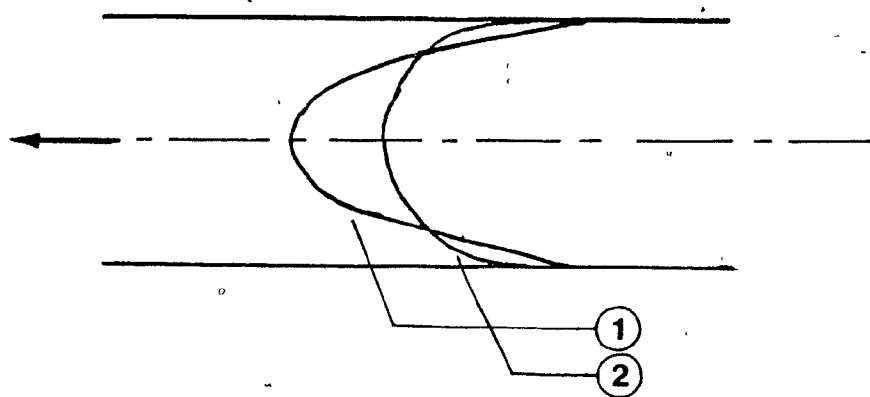


Figure (6.13). Velocity Profiles for Poiseuille Flow in a Slit (Schematic).

(1) For Less Viscous Material (PE).

(2) For More Viscous Material (PS).

degrees of orientation are higher for the lower fiber loading than for the higher fiber loading, the above observations seem to suggest that it might be easier to align longer fibers in the flow direction compared to shorter fibers.

To summarize, it may be concluded from the above analysis that:

- (1) higher shear rate can lead to higher fiber orientation in the flow direction in a simple flow geometry like that encountered in the molding procedure used in this project,
- (2) higher shear rate may lead to greater fiber attrition,
- (3) increasing fiber loading can hinder the fiber orientation,
- (4) greater fiber orientation may be achieved in a less viscous matrix for a given flow rate,
- (5) it appears to be easier to orient the longer fibers in the flow direction than the shorter fibers.

CHAPTER VIICONCLUSION

This project has contributed towards better understanding of the structure-property relationships of the SF RTP materials in addition to generating experimental data on their mechanical properties.

In particular, the following statements can be made:

- (i) A theoretical study was carried out to examine the influence of one of the structural parameters, namely fiber aspect ratio distribution on the composite elastic properties. The effect was found to be significant in the direction of fiber orientation, but not so in the normal direction. Also, the theoretical model developed by the group was extended further so as to simulate the non-homogeneous structure of molded parts, and study the effect on overall composite properties.
- (ii) Existing molding devices were used with a modified procedure so as to make the whole operation simpler and less time consuming. It was also proved that the plates made by the modified procedure were reproducible in terms of their mechanical properties.

- (iii) Moldings of SFRTTP systems based on two distinct matrix materials were made and tested for mechanical properties like stiffness and strength in order to characterize their anisotropy induced by fiber orientation and generate experimental data.
- (iv) The molded plates were also tested for their impact behavior. It was found that while fibers improved the toughness of brittle matrices, they reduced the impact strength of tough and ductile materials.
- (v) The experimental results were analyzed in terms of the previously developed model so as to yield useful information on the flow induced structure of the molded plates. This allowed some conclusions to be drawn regarding the mechanism of fiber orientation during flow and the influence of other structural and material parameters on the process. Such an analysis thus allowed a qualitative correlation of flow-structure-property aspects of the SFRTTP materials.

7.1 Suggestions for Future Work

On the basis of this study, the following suggestions may be made for further research:

- (i) It would be useful, although very time consuming, to fully quantitatively characterize the structure of the plates molded by the procedure adopted in this study and determine the input parameters for the proposed theoretical model accurately so as to test the validity of the model in the case of the moldings with relatively homogeneous structure.
- (ii) The simulation carried out in this study for the structure of non-homogeneous molded parts represented a somewhat idealized case. It would be of help to quantitatively examine the structure of injection molded parts and accordingly modify the simulation procedure so as to represent the structure more closely and then study its influence on the overall composite properties.
- (iii) On the basis of the observations made in this study, it would be useful to study the influence of individual parameters like matrix rheological characteristics, fiber content, fiber length and shear rate on the fiber orientation process during flow in greater depth.

- (iv) In the long run, it would be very helpful to theoretically study and model the flow behavior of non-Newtonian polymeric fluids with fiber suspensions so as to understand the orientation process. The results obtained from such a study could help represent the fiber orientation distribution in a molded part and allow a more accurate prediction of composite properties. Such an analysis can ultimately lead to optimization of material composition, processing techniques and part properties.
- (v) One of the aims of the group has been to work towards developing a globally applicable theory for predicting the properties of the SFRTF materials.

APPENDIX AMETHOD OF INCORPORATING CORRECTIONFOR DEVICE DEFLECTION IN THREE-POINT BENDING TEST

During the three-point bending test for flexural modulus determination, at any instance, the recorded total deflection δ under a force F is the sum of the test-piece deflection δ_1 and device deflection δ_2 .

$$\left(\frac{F}{\delta} \right)_{\text{measured}} = \left(\frac{F}{\delta_1 + \delta_2} \right) \quad (\text{A.1})$$

Therefore

$$\frac{\delta}{F} = \frac{\delta_1}{F} + \frac{\delta_2}{F} \quad (\text{A.2})$$

Hence

$$\frac{1}{(F/\delta_1)} = \frac{1}{(F/\delta)} - \frac{1}{(F/\delta_2)} \quad (\text{A.3})$$

The denominator of the left hand side represents the corrected slope, while that of the first term on the right hand side represents the measured slope. The last term is the correction term for device deflection, determined using an equivalent steel bar.

A.2 Deflection of Steel Bar used for Determining
Correction Factor

The deflection of the steel bar under a representative load of 500N using 25 mm span device can be calculated as

$$\delta_s = \frac{1}{4} \frac{FS^3}{Ebd^3} \quad (\text{A.4})$$

For force $F = 500 \text{ N}$,
 span $S = 25 \text{ mm}$,
 modulus $E = 1.72 \times 10^5 \text{ N/mm}^2$,
 width $b = 12.5 \text{ mm}$,
 and thickness $d = 6.4 \text{ mm}$.

$$\delta_s = 3 \times 10^{-3} \text{ mm} \quad (\text{A.5})$$

Similarly for the 50 mm span device and a steel bar with a width of 19 mm and a thickness of 6.4 mm ,

$$\delta_s = 1.82 \times 10^{-2} \text{ mm} \quad (\text{A.6})$$

Thus in both cases, the deflection of the bar itself is negligible.

APPENDIX BDETERMINATION OF CROSSHEAD BOUNCE CORRECTION FACTORIN TENSILE IMPACT TESTING

In tensile impact testing, upon contacting the anvil at the bottom of the swing of the pendulum, the crosshead bounces away with an initial velocity v_1 dependent upon the degree of elasticity of the contacting surfaces. In several cases, this rebound velocity has been measured to be about 1.88 m/s for steel crossheads (ASTM D1822 (69)).

After impact and rebound of the crosshead the specimen is pulled by two moving bodies, the pendulum with an energy of $MV^2/2$ and the crosshead with an energy of $mv^2/2$. When the specimen breaks, only that energy is recorded on the dial which is lost by pendulum. Therefore one must add the incremental energy contributed by the crosshead to determine the true energy used to break the specimen. This correction can be calculated as follows:

By definition

$$E = (M/2) (V^2 - v_2^2) \quad (B.1)$$

and

$$e = (m/2) (v_1^2 - v_2^2) \quad (B.2)$$

where:

$$M = \text{mass of pendulum} = 0.681 \text{ N} \cdot \text{s}^2/\text{m}$$

- m = mass of crosshead = $0.0805 \text{ N.S}^2/\text{m}$,
 V = maximum velocity of center of percussion
of crosshead of pendulum = 3.44 m/s ,
 V_2 = velocity of center of percussion at the time
when specimen breaks, m/s ,
 v_1 = crosshead velocity immediately after bounce
= 1.88 m/s ,
 v_2 = crosshead velocity at time when specimen
breaks, m/s ,
 E = energy read on pendulum dial, J ,
 e = energy contribution of crosshead or bounce
correction factor to be added to dial reading, J .

Also, once the rebound of the crosshead has occurred, the momentum of the system in the horizontal direction must remain constant.

$$MV - mv_1 = MV_2 - mv_2 \quad (\text{B.3})$$

Equations (B.1), (B.2) and (B.3) can be combined to eliminate

V_2 as:

$$e = m/2 \{v_1^2 - [v_1 - (M/m)(V - \sqrt{V^2 - (2E/M)})]^2\} \quad (\text{B.4})$$

For fixed values of V , M , m and v_1 , e can be plotted as a function

of E as shown in Figure (B.1) and hence the bounce correction factor can be read off for any value of e between 0 and $(m/2) v_1^2$. If the calculated value of e by equation (B.4) is higher than $(m/2) v_1^2$, the correction factor is taken as $m/2 v_1^2$ (ASTM D 1822 (69)).

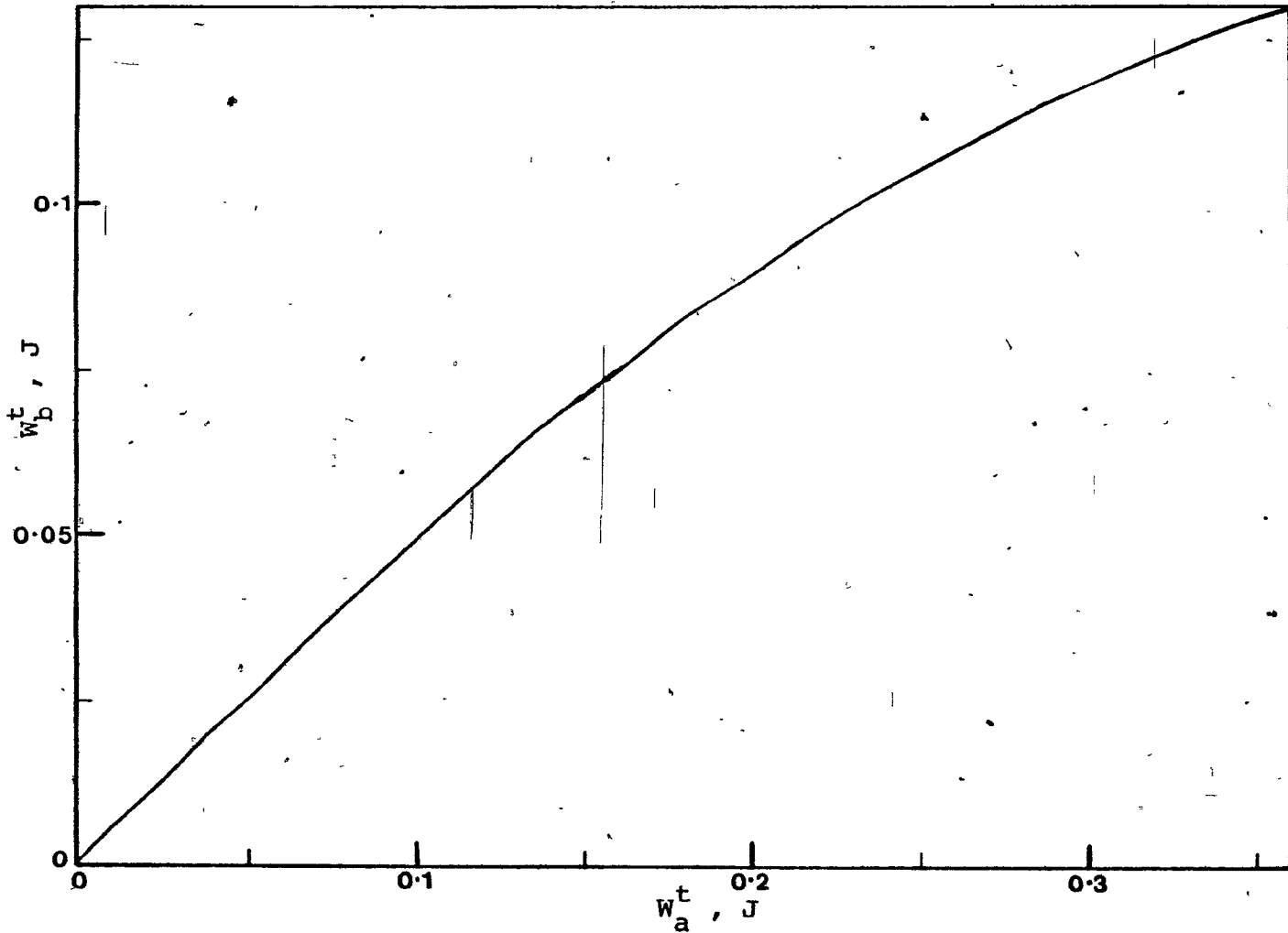


Figure (B.1). Crosshead Bounce Correction Factor for Tensile Impact Testing.

APPENDIX CCOMPUTER PROGRAMS USED FOR NUMERICAL CALCULATIONS(FORTRAN WITH WATFIV COMPILER)C.1 Moduli of Unidirectional Composite with Log-normal Fiber Length Distribution

The listing for the program is provided below. For given values of (\bar{z}/d) and s_z , the log-normal fiber length distribution is generated using the subroutine FIBD. Also, for given material parameters, E_L and E_T are calculated for different aspect ratios using subroutine RALMAX. Finally, the overall moduli \bar{E}_L and \bar{E}_T are computed for the previously described three methods of summation by Simpson's rule.

```

C   TO COMPUTE LONGITUDINAL AND TRANSVERSE MODULI FOR A
L   1 UNIDIRECTIONAL COMPOSITE WITH LOG-NORMAL
C   2 FIBER LENGTH DISTRIBUTION.
      DIMENSION EL(6,30),ET(6,30),ELL(6,5,30),ETL(6,5,30),
      1 ELP(6,5,30),ETP(6,5,30),ELS(6,5,30),ETS(6,5,30),
      2 SUM(15),FL(6,30),EM(7),SIG(5)
      REAL L,LM
      LM=0.3
      EF=10000000.
      D=0.01
      VF=0.2
      DO 101 K=1,4,1
      SIG(K)=(K-1.0)/10.0+0.15
      WRITE (6,4)SIG(K)
      4  FORMAT('1',10X,'SIG = ',F6.4)
      WRITE (6,5)
      5  FORMAT(14X,'FL',15X,'L')
      DO 101 J=1,21,1
      L=(J-1.0)/20.0
      CALL FIBD(SIG,FL,J,K,LM,L)
      WRITE (6,6)FL(K,J),L
      6  FORMAT(10X,F9.5,10X,F6.4)
      101 CONTINUE
      400 DO 100 I=1,5,1
      EM(I)=100000.*I
      WRITE (6,1)EM(I),VF
      1  FORMAT('1',10X,'EM = ',E9.2,10X,'VF = ',F6.4)
      WRITE (6,2)
      2  FORMAT(15X,'EL',18X,'ET',16X,'L')
      DO 100 J=1,21,1
      L=(J-1.)/20.0
      CALL RALMAX(EL,ET,L,I,J,D,EF,EM,VF)
      WRITE (6,3)EL(I,J),ET(I,J),L
      3  FORMAT(10X,E12.5,8X,E12.5,8X,F6.4)
      100 CONTINUE
      WRITE (6,8)
      8  FORMAT ('1',10X,'LONG. MODULUS',8X,'TRANS. MODULUS')
      DO 102 I1=1,5,1
      DO 102 K1=1,4,1
      DO 103 J1=1,21,1
      ELL(I1,K1,J1)=FL(K1,J1)*ALOG(EL(I1,J1))
      ETL(I1,K1,J1)=FL(K1,J1)*ALOG(ET(I1,J1))
      ELP(I1,K1,J1)=FL(K1,J1)*EL(I1,J1)
      ETP(I1,K1,J1)=FL(K1,J1)*ET(I1,J1)
      ELS(I1,K1,J1)=FL(K1,J1)/EL(I1,J1)
      ETS(I1,K1,J1)=FL(K1,J1)/ET(I1,J1)
      103 CONTINUE
      DO 199 N2=1,7,1
      SUM(N2) =0.0
      199 CONTINUE
      DO 104 J2=1,21,2

```

```

SUM(1)=SUM(1)+ELL(I1,K1,J2)*2.0
SUM(2)=SUM(2)+ETL(I1,K1,J2)*2.0
SUM(3)=SUM(3)+ELP(I1,K1,J2)*2.0
SUM(4)=SUM(4)+ETP(I1,K1,J2)*2.0
SUM(5)=SUM(5)+ELS(I1,K1,J2)*2.0
SUM(6)=SUM(6)+ETS(I1,K1,J2)*2.0
SUM(7)=SUM(7)+FL(K1,J2)*2.0
104 CONTINUE
DO 105 J3=2,20,2
SUM(1)=SUM(1)+ELL(I1,K1,J3)*4.0
SUM(2)=SUM(2)+ETL(I1,K1,J3)*4.0
SUM(3)=SUM(3)+ELP(I1,K1,J3)*4.0
SUM(4)=SUM(4)+ETP(I1,K1,J3)*4.0
SUM(5)=SUM(5)+ELS(I1,K1,J3)*4.0
SUM(6)=SUM(6)+ETS(I1,K1,J3)*4.0
SUM(7)=SUM(7)+FL(K1,J3)*4.0
105 CONTINUE
SUMA=(SUM(1)-ELL(I1,K1,1)-ELL(I1,K1,21))*0.05/3.0
SUMB=(SUM(2)-ETL(I1,K1,1)-ETL(I1,K1,21))*0.05/3.0
SUMC=(SUM(3)-ELP(I1,K1,1)-ELP(I1,K1,21))*0.05/3.0
SUMD=(SUM(4)-ETP(I1,K1,1)-ETP(I1,K1,21))*0.05/3.0
SUME=(SUM(5)-ELS(I1,K1,1)-ELS(I1,K1,21))*0.05/3.0
SUMF=(SUM(6)-ETS(I1,K1,1)-ETS(I1,K1,21))*0.05/3.0
SUMG=(SUM(7)-FL(K1,1)-FL(K1,21))*0.05/3.0
ELLO=EXP(SUMA/SUMG)
ETLO=EXP(SUMB/SUMG)
ELPO=SUMC/SUMG
ETPO=SUMD/SUMG
ELSO=SUME/SUMF
ETSO=SUMG/SUMF
WRITE(6,7)EM(I1),SIG(K1)
7 FORMAT ('OFOR EM = ',E9.2,'AND SIG = ',F6.4)
WRITE(6,9)ELLO,ETLO
9 FORMAT (10X,E10.4,11X,E10.4,8X,'BY LOG. ADDITION')
WRITE(6,10)ELPO,ETPO
10 FORMAT (10X,E10.4,11X,E10.4,8X,'BY DIRECT ADDITION')
WRITE(6,11)ELSO,ETSO
11 FORMAT (10X,E10.4,11X,E10.4,8X,'B

103 CONTINUE
VF=VF+0.2
IF (VF-0.8)400,400,401
401 STOP
END
SUBROUTINE RALMAX(EL,ET,P,I,J,D,EF,EM,VF)
DIMENSION EL(6,30),ET(6,30),EM(7)
IF (J.EQ.1)GO TO 200
AS=P/D
SA=D/P
ASP=2.0*AS+1.0
SAF=SA+2.0
ER=EF/EM(I)

```

```
EP=(ER-1.0)*VF
EL(I,J)=EM(I)*(1.0+ASP*EP/(ER+2.0*AS-EP))
ET(I,J)=EM(I)*(1.0+SAP*EP/(ER+SA+1.0-EP))
GO TO 201
200 EL(I,J)=EM(I)
ET(I,J)=EM(I)
201 RETURN
END
SUBROUTINE FIBD(SIG,FL,J,K,LM,S)
DIMENSION SIG(5),FL(6,30)
REAL LM,LML
IF (J.EQ.1)GO TO 300
PA=1.0+(SIG(K)/LM)**2
SD=SQRT(ALOG(PA))
LML=ALOG(LM)-0.5*SD**2
B=1.0/(SD*SQRT(2.0*3.14159))
C=ALOG(S)
R=-0.5*(C-LML)*(C-LML)
E=R/SD**2
FL(K,J)=(B/S)*EXP(E)
GO TO 301
300 FL(K,J)=0.0
301 RETURN
END
```

C.2 Moduli for Composites with Non-Homogeneous
Fiber Orientation Distribution

The values of mean aspect ratio, material properties and orientation parameter in the center and at the surface are defined in the beginning. Fiber orientation distribution is then computed for different values of c_l corresponding to elemental thicknesses. Corresponding composite moduli are computed using subroutines RALMAX and CLAST according to the method described in Section 4.2. The overall flexural and tensile moduli are then computed by integrating across the thickness using Simpson's rule.

```

//CE15RAMA JOB (CE15,000,010,0100,0000,20,,1)
// EXEC WATFIV
//GO.SYSIN DD *
#WATFIV ,TIME=100,PAGES=100
C FILE RAMA
C THIS PROGRAM IS FOR COMPUTING OVERALL LONGITUDINAL AND
C TRANSVERSE MODULI FOR A COMPOSITE IN WHICH ORIENTATION
C VARIES ACROSS THE THICKNESS IN A LINEAR WAY, THE CENTRAL
C PLANE BEING RANDOM AND PERFECT ORIENTATION AT THE SURFACE.
C *****
C FIBER DISTRIBUTION IN A PLANE
C *****
C ALL INTEGRATIONS ARE PERFORMED BY SIMPSON'S RULE
C *****
DIMENSION CL(25),DEG(40),RAD(40),VD(40),V(25,40),EX(40),
1EY(40),CLT11(40),CLT22(40),EXEM(40),EYEM(40),SUMA(25),
2SUMB(25),SUMC(25),SUMAF(25),SUMBF(25),SUMCF(25),EXSL(25),
3EYSL(25),PCD(25)
EF=10000000.
AS = 30.0
C VF=0.2
VF=0.0
EM = 500000.0
UM=0.3
UF=0.2
CLM1=1.0
CLM2 = 5.0
DO 101 I=1,21,1
CL(I)=CLM1 + (CLM2-CLM1)*(I-1.0)/20.0
DO 101 J=1,37,1
DEG(J)=(J-1.0)*2.5
RAD(J)=DEG(J)*3.14159/180.0
VD(J)=3.14159*((COS(RAD(J))/CL(I))**2+(SIN(RAD(J))*CL(I))**2)
V(I,J)=1.0/VD(J)
101 CONTINUE
201 CALL RAI,MAX(EL,ET,GLT,ULT,EF,EM,AS,VF,UM,UF)
WRITE (6,1)
1 FORMAT('1',10X,'GENERALISED RAYLEIGH-MAXWELL')
WRITE (6,2)EL,ET,GLT,ULT
2 FORMAT(10X,'EL = ',E12.5,10X,'ET = ',E12.5/10X,'GLT = '
1,E12.5,'ULT = ',F6.4)
ELDEM=EL/EM
ETDEM=ET/EM
WRITE (6,3)ELDEM,ETDEM
3 FORMAT(10X,'EL/EM = ',F6.4,14X,'ET/EM = ',F6.4)
WRITE (6,4)
4 FORMAT(///,'CLASSICAL THEORY WITH SYMMETRY')
WRITE (6,5)
5 FORMAT('0',5X,'EX',11X,'EX/EM',11X,'EY',11X,'EY/EM',11X,
1'ANG')
DO 100 I=1,37,1
CALL CLAST(RAD,EL,ET,ULT,GLT,I,CLT11,CLT22)
EX(I)=1.0/CLT11(I)-

```

```

EY(I)=1.0/CLT22(I)
EXEM(I)=EX(I)/EM
EYEM(I)=EY(I)/EM
WRITE (6,6)EX(I),EXEM(I),EY(I),EYEM(I),DEG(I)
6  FORMAT(E12.5,5X,F7.4,5X,E12.5,5X,F7.4,5X,F6.2)
100 CONTINUE
WRITE (6,11)
11  FORMAT('1',12X,'CL',15X,'EXL',18X,'EYL')
DO 200 I=1,21,1
SUMA(I)=0.0
SUMB(I)=0.0
SUMC(I)=0.0
DO 103 J=1,37,2
SUMA(I)=SUMA(I)+V(I,J)*ALOG(EX(J))*2.0
SUMB(I)=SUMB(I)+V(I,J)*ALOG(EY(J))*2.0
SUMC(I)=SUMC(I)+V(I,J)*2.0
103 CONTINUE
DO 104 J=2,36,2
SUMA(I)=SUMA(I)+V(I,J)*ALOG(EX(J))*4.0
SUMB(I)=SUMB(I)+V(I,J)*ALOG(EY(J))*4.0
SUMC(I)=SUMC(I)+V(I,J)*4.0
104 CONTINUE
SUMAF(I)=SUMA(I)-V(I,1)*ALOG(EX(1))-V(I,37)*ALOG(EX(37))
SUMBF(I)=SUMB(I)-V(I,1)*ALOG(EY(1))-V(I,37)*ALOG(EY(37))
SUMCF(I)=SUMC(I)-V(I,1)-V(I,37)
EXSL(I)=EXP(SUMAF(I)/SUMCF(I))
EYSL(I)=EXP(SUMBF(I)/SUMCF(I))
WRITE (6,7)CL(I),EXSL(I),EYSL(I)
7  FORMAT(BX,F8.3,8X,E13.6,8X,E13.6)
200 CONTINUE
C LOOP FOR THE FINAL INTEGRATION OVER THE THICKNESS
SUMFA=0.0
SUMFB=0.0
DO 105 I=1,21,2
PCD(I)=(I-1.0)/40.0
SUMFA=SUMFA + 2.0*EXSL(I)*PCD(I)**2.0
SUMFB=SUMFB + 2.0*EYSL(I)*PCD(I)**2.0
105 CONTINUE
DO 106 I=2,20,2
PCD(I)=(I-1.0)/40.0
SUMFA=SUMFA + 4.0*EXSL(I)*PCD(I)**2.0
106 CONTINUE
ELOVER=(SUMFA-EXSL(1)*PCD(1)**2.0-EXSL(21)*PCD(21)**2.0)/5.0
ETOVER=(SUMFB-EYSL(1)*PCD(1)**2.0-EYSL(21)*PCD(21)**2.0)/5.0
WRITE (6,8)
8  FORMAT('0THE OVERALL MODULI FOR THE COMPOSITE-FLEXURE')
WRITE (6,9)ELOVER,ETOVER,VF
9  FORMAT('0LONG. MODULUS = ',E12.5,8X,'TRANS. MODULUS = ',
1E12.5/'0FOR VOL. FRACTION = ',F6.4)
ELOEM=ELOVER/EM
ETOEM=ETOVER/EM
WRITE (6,10)ELOEM,ETOEM
10 FORMAT('0REDUCED LONG. MODULUS = ',F8.5/'0REDUCED TRANS.

```

```

1MODULUS = ',F8.5)
C LOOP FOR THE FINAL INTEGRATION - TENSION
SUMFA=0.0
SUMFB=0.0
DO 107 I=1,21,2
SUMFA=SUMFA+2.0*EXSL(I)
SUMFB=SUMFB+2.0*EYSL(I)
107 CONTINUE
DO 108 I=2,20,2
SUMFA=SUMFA+4.0*EXSL(I)
SUMFB=SUMFB+4.0*EYSL(I)
108 CONTINUE
ELOVET=(SUMFA-EXSL(1)-EXSL(21))/60.0
ETOVET=(SUMFB-EYSL(1)-EYSL(21))/60.0
WRITE (6,12)
12 FORMAT('0THE OVERALL MODULI FOR THE COMPOSITE-TENSION')
WRITE(6,13)ELOVET,ETOVET,VF
13 FORMAT('0LONG. MODULUS =',E12.5,8X,'TRANS. MODULUS =',E12.5/
1'0FOR VOL. FRACTION =',F6.4)
ELOEMT=ELOVET/EM
ETOEMT=ETOVET/EM
WRITE (6,14)ELOEMT,ETOEMT
14 FORMAT('0REDUCED LONG. MODULUS =',F8.5/
1'0REDUCED TRANS. MODULUS =',F8.5)
ELFT=ELOVER/ELOVET
ETFT=ETOVER/ETOVET
WRITE (6,15)ELFT,ETFT
15 FORMAT('0LONGITUDINAL - EF/ET =',F8.5/
1'0TRANSVERSE - EF/ET =',F8.5)
VF = VF+0.1
IF (VF-1.0)201,201,202
202 STOP
END.
C *****
C SUBROUTINE RALMAX
C *****
SUBROUTINE RALMAX(EL,ET,GLT,ULT,EF,EM,AS,VF,UM,UF)
SA=1.0/AS
ER=EF/EM
ES=(ER-1.0)*VF
GF=EF/(2.0*(1.0+UF))
GM=EM/(2.0*(1.0+UM))
GR=GF/GM
GS=(GR-1.0)*VF
EL=EM*(1.0+(2.0*AS+1.0)*ES/(ER+2.0*AS-ES))
ET=EM*(1.0+(SA+2.0)*ES/(ER+1.0+SA-ES))
ULT=UM*(1.0-VF)+UF*VF
GLT=GM*(1.0+(SA+2.0)*GS/(GR+1.0+SA-ES))
RETURN
END
C *****
C SUBROUTINE CLASSICAL THEORY
C *****

```

```
SUBROUTINE CLAST(RAD,EL,ET,ULT,GLT,I,CLT11,CLT22)
  DIMENSION RAD(40),CLT11(40),CLT22(40),CXY11(40),CXY22(40)
  1,CXY66(40),CXY16(40),CXY26(40),CXY61(40),CXY62(40),
  2CXY12(40),CXY21(40)
  RAD2=RAD(I)*2.0
  BRC=1.0/GLT-2.0*ULT/EL
  CXY11(I)=COS(RAD(I))*4/EL+SIN(RAD(I))*4/ET+
  1SIN(RAD2)**2*BRC/4.0
  CXY22(I)=SIN(RAD(I))*4/EL+COS(RAD(I))*4/ET+
  1SIN(RAD2)**2*BRC/4.0
  CXY66(I)=1/EL+2*ULT/EL+1/ET-COS(RAD2)**2*(1/EL+1/ET
  1-BRC)
  CXY12(I)=SIN(RAD2)**2*(1/EL+1/ET-BRC)/4.0-ULT/EL
  CXY21(I)=CXY12(I)
  CXY16(I)=SIN(RAD2)*(1/EL-BRC/2.0-SIN(RAD(I))*2*
  1(1/EL+1/ET-BRC))
  CXY61(I)=CXY16(I)
  CXY26(I)=SIN(RAD2)*(1/EL-BRC/2.0-COS(RAD(I))*2*
  1(1/EL+1/ET-BRC))
  CXY62(I)=CXY26(I)
  CLT11(I)=CXY11(I)-CXY16(I)**2/CXY66(I)
  CLT22(I)=CXY22(I)-CXY26(I)**2/CXY66(I)
  RETURN
  END
```

C.3 Key to Major Symbols Used in Computer Programs

<u>Symbol</u>		<u>Description</u>
<u>In Listing</u>	<u>In Text</u>	
AS	(z/d)	Fiber aspect ratio.
CL	C_{λ}	Orientation Parameter.
CLM1	-	C_{λ} in the center.
CLM2	-	C_{λ} at the surface.
CLT11 - CLT66	C_{ij}^{lt}	Components of compliance matrix $[C^{lt}]$.
CXY11 - CXY66	C_{ij}^{XY}	Components of compliance matrix $[C^{XY}]$.
EF	E_F	Fiber Young's modulus.
EM	E_m	Matrix Young's modulus.
EL, ET	E_L, E_T	Composite moduli in directions L, T.
EX, EY	E_x, E_y	Composite moduli in directions x, y.
ELLO, ETLO	\bar{E}_L, \bar{E}_T	Overall composite moduli by logarithmic summation (unidirectional).

<u>Symbol</u>		<u>Description</u>
<u>In Listing</u>	<u>In Text</u>	
ELPO , ETPO	\bar{E}_L, \bar{E}_T	Overall composite moduli by parallel summation (unidirectional).
ELSO , ETSO	\bar{E}_L, \bar{E}_T	Overall composite moduli by series summation (unidirectional).
ELOVER , ETOVER	E_l^f, E_t^f	Overall flexural moduli in directions l, t .
ELOVET , ETOVET	E_l^t, E_t^t	Overall tensile moduli in directions l, t .
ELFT , ETFT	$(E^f/E^t)_l, (E^f/E^t)_t$	Ratios of flexural to tensile moduli in directions l, t .
FL	$f(z)$	Fiber length distribution function.
L	\bar{z}	Fiber length.
LM	\bar{z}	Mean fiber length.
LML	\bar{X}	Parameter in log-normal distribution function.
SD	S_x	Parameter in log-normal distribution function.

<u>Symbol</u>		<u>Description</u>
<u>In Listing</u>	<u>In Text</u>	
SIG	S_z	Standard deviation of fiber length distribution.
\overline{VF}	v_f	Fiber volume fraction.

NOMENCLATURE

<u>Symbol</u>	<u>Description</u>
C_l	Orientation parameter in l direction.
C_t	Orientation parameter in t direction.
C_{LM}	Maximum value of C_l (at surface) for non-homogeneous orientation distribution.
$[C^{lt}]$	Compliance matrix with reference to directions l and t (symmetrical case).
$[C^{xy}]$	Compliance matrix with reference to directions x and y (nonsymmetrical case).
d	Fiber diameter.
E_C	Composite Young's modulus.
E_f	Fiber Young's modulus.
E_m	Matrix Young's modulus.
E_L	Young's modulus of unidirectional composite in direction L .
E_T	Young's modulus of unidirectional composite in direction T .
\overline{E}_L	Overall Young's modulus of unidirectional composite with a fiber length distribution in direction L .

<u>Symbol</u>	<u>Description</u>
\overline{E}_T	Overall Young's modulus of unidirectional composite with a fiber length distribution in direction T .
E_ℓ	Young's modulus in direction ℓ (symmetrical case with angle θ) .
E_t	Young's modulus in direction t (symmetrical case with angle θ) .
\overline{E}_ℓ	Young's modulus in direction ℓ for a fiber orientation distribution corresponding to a given value of C_ℓ .
\overline{E}_t	Young's modulus in direction t for a fiber orientation distribution corresponding to a given value of C_ℓ .
E_x	Young's modulus in direction x (non-symmetrical case with angle θ) .
E_y	Young's modulus in direction y (non-symmetrical case with angle θ) .
E_ℓ^f	Overall flexural modulus in direction ℓ for model in Section 4.3 .
E_t^f	Overall flexural modulus in direction t for model in Section 4.3 .

<u>Symbol</u>	<u>Description</u>
E_{ℓ}^t	Overall tensile modulus in direction ℓ for model in Section 4.3.
E_t^t	Overall tensile modulus in direction t for model in Section 4.3 .
$f(z)$	Fiber length distribution function.
F	Force for three-point bending.
G_f	Shear modulus for fibers.
G_m	Shear modulus for matrix.
G_{LT}	Shear modulus of unidirectional composite with reference directions L and T .
$G_{\ell t}$	Shear modulus of composite with reference directions ℓ and t (symmetrical case).
G_{xy}	Shear modulus of composite with reference directions x and y (non-symmetrical case).
h	Distance from the central plane in the model of Section 4.3 .
h_m	Half-thickness of a specimen in the model of Section 4.3 .
I	Moment of Inertia of cross-section of a specimen.

<u>Symbol</u>	<u>Description</u>
L	Direction of fiber orientation for a unidirectional composite.
l	Reference direction for symmetrical case (longitudinal).
M_f	Fiber mass fraction.
S	Span length in three-point bending test.
S_x	Polydispersity parameter in fiber length distribution function.
s_z	Standard deviation of fiber length distribution.
T	Transverse direction for unidirectional composite.
t	Reference direction for symmetrical case (transverse).
V_f	Fiber volume fraction.
$V(\theta)$	Fraction of fibers in direction $\theta \pm d\theta/2$ with respect to the reference direction.
\bar{X}	Parameter in fiber length distribution function.
W^I	Izod-type impact energy.
W^t	Tensile impact energy.

SymbolDescription \bar{x}

Parameter in fiber length distribution function.

 x, y

Reference directions for non-symmetrical case.

 z

Fiber length.

 \bar{z}

Mean fiber length.

Greek Symbols θ

Angle of fiber orientation direction with the reference direction.

 σ_L

Stress in direction L of unidirectional composite.

 σ_T

Stress in direction T of unidirectional composite.

 σ_x

Stress in direction x (non-symmetrical case with angle θ).

 σ_y

Stress in direction y (non-symmetrical case with angle θ).

 σ_c

Composite strength.

 σ_f

Fiber tensile strength.

 σ_m

Matrix tensile strength.

<u>Symbol</u>	<u>Description</u>
σ_l^t	Tensile strength in direction l .
σ_t^t	Tensile strength in direction t .
ϵ_L	Strain in direction L of unidirectional composite.
ϵ_T	Strain in direction T of unidirectional composite.
ϵ_x	Strain in direction x (non-symmetrical case with angle θ) .
ϵ_y	Strain in direction y (non-symmetrical case with angle θ) .
γ_{xy}	Shear strain in plane $x-y$ (non-symmetrical case with angle θ) .
μ_f	Fiber Poisson's ratio.
μ_m	Matrix Poisson's ratio.
μ_{LT}	Poisson's ratio of unidirectional composite with reference directions L and T .
μ_{lt}	Poisson's ratio of composite with reference directions l and t (symmetrical case with angle θ) .
μ_{xy}	Poisson's ratio of composite with reference directions x and y (nonsymmetrical case with angle θ) .

REFERENCES

- (1) J.-M. Charrier, "Basic Aspects of Structure-Properties Relationships for Composites", Polym. Eng. and Sci., 15, 10, 731-746 (1975).
- (2) W.V. Titow and B.J. Lanham, "Reinforced Thermoplastics", John Wiley and Sons, Inc., New York (1975).
- (3) D. Santrach, "Industrial Applications and Properties of Short Glass Fiber-Reinforced Plastics", Polymer Composites, 3, 4, 239-244 (1982).
- (4) J.E. Ashton, J.C. Halpin and P.H. Petit, "Primer on Composite Materials: Analysis", Ch. 5, Technomic, Stamford, Conn. (1969).
- (5) M. Takayanagi, H. Harima and Y. Iwata, Rep. Prog. Polym. Phys., Japan, 6, 121 (1963).
- (6) G.J. Weng and C.T. Sun, "Effect of Fiber Length on Elastic Moduli of Randomly Oriented Chopped Fiber Composites" in S.W. Tsai, ed., "Composite Materials: Testing and Design", Fifth Conference, ASTM STP 674, 149-162 (1979).
- (7) H.L. Cox, "The Elasticity and Strength of Paper and Other Fibrous Materials"- Brit. J. Appl. Phy., 3, 72-79 (1952).
- (8) R. Hill, "Theory of Mechanical Properties of Fiber - Strengthened Materials: III Self-Consistent Model", J. Mech. Phy. Solids, 13, 189-198 (1965).

- (9) J.C. Halpin and J.L. Kardos, "The Halpin-Tsai Equations: A Review", *Polym. Eng. and Sci.*, 16, 5, 344-352 (1976).
- (10) J.J. Hermans, "The Elastic Properties of Fiber Reinforced Materials when the Fibers are Aligned", *Proc. Konigl. Nederl. Akad. van Wetenschappen, Amsterdam*, B70, 1, 1-24 (1967).
- (11) L.E. Nielsen, "Generalized Equations for the Elastic Moduli of Composite Materials", *J. Appl. Phys.*, 41, 11, 4626-4627 (1970).
- (12) T.-W. Chou, S. Nomura and M. Taya, "Self Consistent Approach to the Elastic Stiffness of Short Fiber Composites", *J. Comp. Mat.*, 14, 178-188 (1980).
- (13) M. Manera, "Elastic Properties of Randomly Oriented Short Fiber-Glass Composites", *J. Comp. Mat.*, 11, 235-247 (1977).
- (14) T.S. Chow, "Review: The Effect of Particle Shape on Mechanical Properties of Filled Polymers", *J. Mat. Sc.*, 15, 1873-1888 (1980).
- (15) J.D. Eshelby, "The Determination of the Elastic Field of an Ellipsoidal Inclusion, and Related Problems", *Proc. Royal Soc. (London)*, A241, 376-396 (1957).
- (16) J. Cook, "The Elastic Constants of an Isotropic Matrix Reinforced with Imperfectly Oriented Fibers", *Brit. J. Appl. Phys. (J. Phys. D)*, 1, 2, 799-812 (1968).
- (17) R.H. Knibbs and J.B. Morris, "The Effects of Fiber Orientation on the Physical Properties of Composites", *Composites*, 5, 5, 209-218 (1974).

- (18) H. Krenchel, "Fiber Reinforcement", Akademisk, Forlag, Copenhagen (1964).
- (19) H. Fukuda and K. Kawada, "On Young's Modulus of Short Fiber Composites", Fiber Sci. and Tech. 7, 207-222 (1974).
- (20) M.A. Eisenberg, "Theory of Fabrication - Induced Anisotropy of Chopped - Fiber/Resin Panels", Fiber Sci. and Tech., 12, 83-95 (1979).
- (21) L. Nicolais, L. Nicodemo, P. Masi and A.T. Dibenedetto, "The Effect of Hot Drawing on the Properties of Short Fiber Reinforced Extruded Sheets", Polym. Eng. and Sci., 19, 14, 1046-1053 (1979).
- (22) A.C. Curtis, P.S. Hope and I.M. Ward, "Modulus Development in Oriented Short-Glass-Fiber-Reinforced Polymer Composites", Polymer Composites, 3, 3, 138-145 (1982).
- (23) J.-M. Charrier and K.D. Tran, "The Quantitative Characterization of the Structure of Short Fiber-Composites" (to be published).
- (24) J. M. Sudlow, "Mechanical Properties and Orientation in Short Fiber Composites", M.Eng. Thesis, McGill University (1972).
- (25) J.-M. Charrier, S.O. Padmanabhan and K.D. Tran, Paper in preparation.
- (26) R.N. Christensen and F.M. Waals, "Effective Stiffness of Randomly Oriented Fiber Composites", J. Comp. Mat., 6, 518-532 (1972).
- (27) J.C. Halpin and N.J. Pagano, "The Laminate Approximation for Randomly Oriented Fibrous Composites", J. Comp. Mat., 3, 720-724 (1969).

- (28) P.T. Loughlin, C.Y. Chen and C.L. Tucker, "Properties of Short Fiber Reinforced Polymers - II Mechanical Property Predictions", SPE 39th ANTEC, 61-63 (1981).
- (29) M.W. Darlington, B.K. Gladwell and G.R. Smith, "Structure and Mechanical Properties in Injection Molded Discs of Glass Fiber Reinforced Polypropylene", Polymer, 18, 1269-1274 (1977).
- (30) J.-M. Charrier and M.J. Sudlow, "Structure-Properties Relationships for Short-Fiber Composites", Fiber Sci. and Tech., 6, 249-266 (1973).
- (31) L.J. Cohen and J.P. Romualdi, "Stress, Strain and Displacement Fields in a Composite Material Reinforced with Discontinuous Fibers", J. Franklin Inst., 284, 6, 388-406 (1967).
- (32) J.J. Zybert, W.A. Rachinger, P.P. Phakey and H.J. Orams, "Theoretical Determination of Composite Material Elastic Compliances", Composites, 11, 175-180 (1980).
- (33) Z. Hashin, "Theory of Fiber Reinforced Materials", NASA Report, CR - 1974.
- (34) A. Kelly and W.R. Tyson, "The Principles of Fiber Reinforcement of Metals", J. Mech. Phy. and Solids, 7, 60-95 (1958).
- (35) W.H. Bowyer and M.G. Bader, "On the Reinforcement of Thermoplastics by Imperfectly Aligned Discontinuous Fibers", J. Mat. Sci., 7, 1315-1321 (1972).
- (36) M.G. Bader and W.H. Bowyer, "The Mechanical Properties of Thermoplastics Strengthened by Short Discontinuous Fibers", J. Phy. D: Appl. Phy., 5, 2215-2225 (1972).

- (37) F. Ramsteiner and R. Theysohn, "Tensile and Impact Strength of Unidirectional, Short Fiber-Reinforced Thermoplastics", *Composites*, 10, 2, 111-119 (1979).
- (38) V.B. Gupta and R.K. Mittal, "Some Studies on Short Glass Fiber-Reinforced Polypropylene", *Proceedings, IUPAC MACRO'82*, Amherst, Ma., 473 (1982).
- (39) C.T. Chen and C.T. Sun, "Stress Distribution along a Short Fiber in Fiber Reinforced Plastics", *J. Mat. Sci.*, 15, 931-938 (1980).
- (40) P.E. Chen, "Strength Properties of Discontinuous Fiber Composites", *Polym. Eng. and Sci.*, 11, 1, 51-56 (1971).
- (41) R.M. Barker and T.F. McLaughlin, "Stress Concentration near a Discontinuity in Fiber Composites", *J. Comp. Mat.*, 5, 492-502 (1971).
- (42) J.C. Halpin and J.L. Kardos, "Strength of Discontinuous Reinforced Composites: I Fiber Reinforced Composites", *Polym. Eng. and Sci.*, 18, 6, 496-504 (1978).
- (43) J.K. Lees, "A Study of the Tensile Strength of Short Fiber Reinforced Plastics", *Polym. Eng. and Sci.*, 8, 3, 195-201 (1968).
- (44) P.W. Jackson and D. Cratchley, "The Effect of Fiber Orientation on the Tensile Strength of Fiber-Reinforced Metals", 14, 49-64 (1966).

- (45) P.H. Petit and M.E. Waddoup, "A Method of Predicting the Non-linear Behavior of Laminated Composites", J. Comp. Mat., 3, 2-18 (1969).
- (46) Y.U. Chen, J.L. White and Y. Oyanagi, "A Fundamental Study of the Rheological Properties of GFRPE and PS Melts", J. Rheology, 22, 5, 507-520 (1978).
- (47) W.W. Chan, J.-M. Charrier, P. Vadnais and T. Varadi, "Flow of Short-Glass-Fiber-Filled Thermoplastics in Channels of Circular or Thin Rectangular Cross-Sections", Polymer Composites, 4, 1, 9-18 (1983).
- (48) L. G. Leal, "The Slow Motion of Slender Rod-like Particles in a Second Order Fluid", J. Fluid Mech., 69, 2, 305-337 (1975).
- (49) J.P. Bell, "Flow Orientation of Short Fiber Composites", J. Comp. Mat., 3, 244-253 (1969).
- (50) W.K. Lee and H.H. George, "Flow Visualization of Fiber Suspensions", Polym. Eng. and Sci., 18, 2, 146-156 (1978).
- (51) M. Takano, "Viscoelastic Effect on Flow Orientation of Short Fibers", ARPA Report, HPC 73-165 (1973).
- (52) L. Goettler, "Flow Orientation of Short Fibers in Transfer Molding", 25th SPE ANTEC, Section 14-A, Reinforced Plastics/Composite Division (1970).
- (53) D.C. Fuccella, "Glass Fiber Orientation in Injection Molded Thermoplastic Parts", 27th SPE ANTEC, Section 11F, Reinforced Plastics/Composite Division (1972).

- (54) M.W. Darlington, P.L. McGinley and G.R. Smith, "Structure and Anisotropy of Stiffness in Glass Fiber-Reinforced Thermoplastics", *J. Mat. Sci.*, 11, 870-886 (1976).
- (55) P.F. Bright and M.W. Darlington, "Factors Influencing Fiber Orientation and Mechanical Properties in Fiber-Reinforced Thermoplastics Injection Moldings", *Plastics and Rubber Processing and Applications*, 1, 2, 139-150 (1981).
- (56) P.F. Bright, R.J. Crowson and M.J. Folkes, "A Study of the Effect of Injection Speed on Fiber Orientation in Simple Moldings of Short Glass Fiber-Filled Polypropylene", *J. Mat. Sci.*, 13, 2497-2506 (1978).
- (57) M.J. Folkes, Short-Fiber-Reinforced Thermoplastics. John-Wiley and Sons, Somerset, N.J. (1982).
- (58) S.F. Xavier, D. Tyagi and A. Misra, "Influence of Injection Molding Parameters on the Morphology and Mechanical Properties of Glass Fiber-Reinforced Polypropylene Composites", *Polymer Composites*, 3, 2, 88-96 (1982).
- (59) C.M.R. Dunn and S. Turner, "The Characterization of Reinforced Thermoplastics for Industry and Engineering Uses", *Composite - Standards Testing and Design Conference Proceedings*, London (1974).
- (60) D.C. Taggart and R.B. Pipes, "Test Method Evaluation for Fiber-Reinforced Molding Materials", *Polymer Composites*, 1, 1, 56-61 (1980).

- (61) R.C. Stephenson, S. Turner and M. Whale, "The Load-Bearing Capacity of Short Fiber-Reinforced Thermoplastic Composites - A New Practical System of Evaluation", Polym. Eng. and Sci., 19, 3, 173-180 (1979).
- (62) J.-M. Charrier and V.V. Skatchkov, "Processing - Structure - Properties Relationships for Short Fiber Thermoplastic Composites", Proceedings, VII-th International Congress on Rheology, Gothenburg, Sweden, 542 (1976).
- (63) K.D. Tran, "Structure and Flow Properties of Glass Fiber-Filled Thermoplastics", M.Eng. Thesis, McGill University (1979).
- (64) S. Padmanabhan, "Integrated Rheological and Structural Investigation of Short Glass Fiber-Filled Thermoplastics", M.Eng. Thesis, McGill University (1980).
- (65) W.W. Chan, J.-M. Charrier, S. Padmanabhan and P. Vadnais, "Fluid Flow of Short Fiber-Filled Thermoplastics", SPE 39th ANTEC, 53-56 (1981).
- (66) D. Pouliot, "Fabrication and Testing of Short Fiber-Reinforced Composites", M.Eng. Thesis, McGill University (1978).
- (67) J.-M. Charrier and S.R. Doshi, "The Role of Structure in the Processing and the Properties of Short Fiber-Thermoplastic Composites", Proceedings, IUPAC MACRO'82, Amherst, Ma., 470 (1982).
- (68) Private Communication, G.M. Cannavo, Wilson-Fiberfil International, Evansville, Indiana.

- (69) Annual Book of ASTM Standards, "Plastics - General Test Methods; Nomenclature", Part 35, American Society for Testing and Materials, Philadelphia, Pa., (1978).
- (70) B.K. Daniels, N.K. Harakas and R.C. Jackson, "Short Beam Shear Tests of Graphite Fiber Composites", Fiber Sci. and Tech., 3, 187-208 (1971).
- (71) H.D. Wagner, G. Marom and I. Roman, "Analysis of Several Loading Methods for Simultaneous Determination of Young's and Shear Moduli in Composites", Fiber Sci. and Tech., 16, 61-65 (1982).